2012-6

Mathematical and Computational Modelling for Biosensors: A Modular Approach

Yupeng Liu
Technological University Dublin, yupeng.liu@tudublin.ie

DUBLIN INSTITUTE of TECHNOLOGY

Institiúid Teicneolaíochta Bhaile Átha Cliath

Mathematical and Computational Modelling for Biosensors: A Modular Approach

by

Yupeng Liu, B.Sc. M.Sc.

A thesis submitted for the degree of

Doctor of Philosophy (Ph.D.)

in the School of Mathematical Sciences,

Dublin Institute of Technology.

Supervisor: Dr. Dana Mackey

June 2012

Abstract

Biosensors are analytic devices which detect biochemical and physiological changes and represent an emerging technology for low-cost, rapid and simple-to-operate biomedical diagnostic tools. Biosensor design and functionality are based on well understood physical and chemical processes which can be easily translated into mathematical models involving ordinary and partial differential equations. Using mathematical and computational modelling techniques to characterize the biosensor response as a function of its input parameters in a wide range of physical contexts can guide the experimental work, thus reducing development time and costs.

This thesis is based on a close collaboration with Biochemistry researchers at the National Centre for Sensor Research (NCSR) and Biomedical Diagnostics Institute (BDI) at Dublin City University and the mathematical models we develop are relevant to ongoing experimental work in these centres relating to design optimization of biocatalytic and bioaffinity devices. Our approach is to use numerical solutions as a first step towards determining the accuracy of these models, since the simulations successfully reproduce the experimental outcomes; future work can then concentrate on a more detailed theoretical analysis.

Declaration

I certify that this thesis which I now submit for examination for the award of degree of Doctor of Philosophy (Ph.D.), is entirely my own work and has not been taken from the work of others, save and to the extent that such work has been cited and acknowledged within the text of my work.

This thesis was prepared according to the regulations for postgraduate study by research of the Dublin Institute of Technology and has not been submitted in whole or in part for another award in any other Institute.

The work reported on in this thesis conforms to the principles and requirements of the Institute's guidelines for ethics in research.

The Institute has permission to keep, lend or copy this thesis in whole or in part, on condition that any such use of the material of the thesis be duly acknowledged.

Signature: ..... Date: .....

Yupeng Liu

Acknowledgments

My first, and most earnest, acknowledgment must go to my supervisor Dr. Dana Mackey - I thank her for her patience, motivation, enthusiasm, and immense knowledge. Her guidance helped me in all the time of research and writing of this thesis. In every sense, none of this work would have been possible without her.

I would like to express my sincere gratitude to Dr. Chris Hills, Ms. Maev Maguire, Dr. Brendan Redmond for their support, friendship and confidence in me over the past years. My sincere thanks also goes to my collaborators Prof. Antony Killard from UWE at Bristol (formerly of Dublin City University), and his Ph.D. student Ms. Kyriaki Karagianni. It was a great pleasure working with them on this diverse and exciting project.

I would also like to acknowledge the Irish Research Council for Science, Engineering and Technology (IRCSET), Dublin Institute of Technology and Mathematics Applications Consortium for Science and Industry (MACSI) for their financial support of my doctoral research. Special thanks goes to MACSI: the postgraduate workshops and seminars have been a great help for my research.

A penultimate thank-you goes to my wonderful parents for always being there when I needed them most. My final, and most heartfelt, acknowledgment must go to Qi. Her support, encouragement, and companionship have turned my journey through Ph.D. studies into a pleasure.

Table of contents

Table of figures

Chapter 1

Introduction and Background

1.1 Introduction to Biosensors

Biosensors are analytical devices which detect biochemical and physiological changes and represent an emerging technology for low-cost, rapid and simple-to-operate biomedical diagnostic tools. The level of commercial development in biosensors is significant, and novel biosensors are continuously being developed to detect different analytes. For example, protein biomarkers are important indicators of the onset or existence of different diseases. Other important applications of biosensors are in detection of toxins and pollutants in air and water environments, food safety [1] and drug discovery [38]. The beneficial impact on society as a result of the availability of such systems to both personal health and environmental quality is immense. Therefore, investigating any strategy that could reduce development times and costs, reveal alternative system designs and subsequently increase the rate at which new devices are brought to the market, is of utmost importance. In particular, mathematical modelling and

simulation, the so-called "virtual experimentation" are relatively inexpensive and yet powerful tools for scientific analysis and prediction.

A biosensor is an analytical device which converts a biochemical reaction into a measurable signal using an optical or electrochemical transducer. The most important component of a biosensor is the biological recognition element, which can be an enzyme, and antibody, a strand of mucleic acid or even a whole cell or organ. Biosensors can be classified according to their transduction system; two important examples we encounter in this thesis are electrochemical and optical biosensors. They can also be classified according to the choice of the biological recognition element which divides them into two broad classes: biocatalytic and bioaffinity. Biocatalytic devices typically involve enzymes and rely on catalytic reactions that produce or consume electrons; for this reason such devices use electrochemical transducers. The affinity-based biosensors, such as immunosensors which rely on antibody-antigen binding use optical systems as transduction methods. Some performance criteria associated with biosensors are listed below [47]:

- **Specificity**. The specificity of a biosensor is it's ability to measure the concentration of analyte without interference from other components that might be present in the sample.

- **Accuracy**. The accuracy of a biosensor describes how well the measured concentrations agree with accepted reference values. The accuracy is determined from measurements made on standard samples in comparison either with the results of an independent reference assay or with quoted values for the standard.

- **Limit of detection**. The limit of detection (LOD) is the lowest analyte concentration that can be detected but not necessarily quantitated as an exact value.

- The **lower** (and **upper**) **limits of quantitation** are the lowest (and highest) analyte concentrations that can be measured with suitable precision and accuracy.

- **Linearity**. The linearity of an assay refers to the ability of the assay to obtain response values that are related to the analyte concentration by a defined mathematical function.

- **Range**. The range of an assay is the interval between (and including) the upper and lower limits of quantitation, i.e., the range within which the precision, accuracy and linearity are acceptable.

- **Sensitivity**. Sensitivity is defined as the assay response per unit analyte concentration. This is the slope of the standard curve for the assay.

1.1.1 Enzyme Biosensors

An enzyme biosensor, as shown in Figure 1.1, is an analytical device that combines an enzyme (as the biological sensing element) with a transducer (which may be amperometric, potentiometric, conductimetric, optical, or calorimetric, etc.) to produce a signal proportional to target analyte concentration. This signal can result from a change in proton concentration, release or uptake of gases, brought about by the reaction catalyzed by the enzyme. The transducer converts this signal into a mea-

surable response, such as current, potential, temperature change, or absorption of light through electrochemical, thermal, or optical means. This signal can be further amplified, processed, or stored for later analysis.

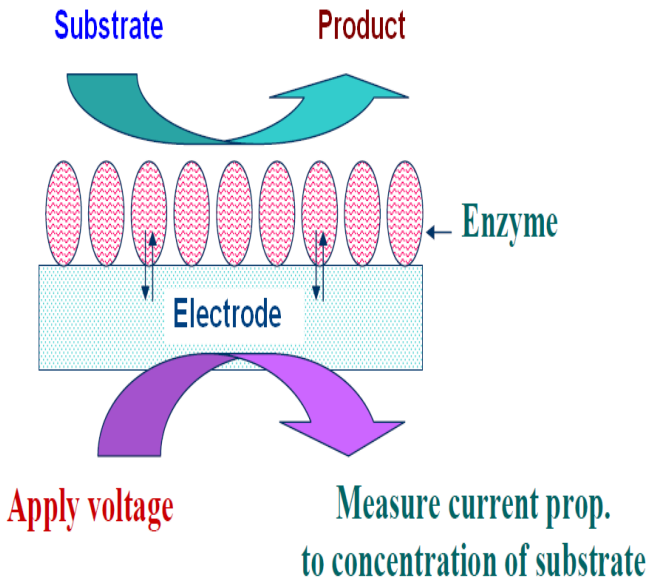

Figure 1.1 – Enzyme based biosensor.

Enzyme biosensors have been applied to detect various substrates, which are selectively oxidised or reduced in enzyme-catalyzed processes depending on the nature of the substrates and enzymes used (oxidases or reductases) to construct a sensor. Most enzyme biosensors modelled in this thesis use amperometric techniques [19]. Amperometry is the determination of the intensity of the current crossing an electrochemical cell under an imposed potential. This intensity is a function of the concentration of the electrochemically active species in the sample. Oxidation or reduction of a species is generally performed by a working electrode, and a second electrode acts as a reference. For example, a glucose-sensitive biosensor that uses glucose oxidase could

detect either the H_2O_2 produced by the enzymatic reaction, or the amount of oxygen consumed during the oxidation of glucose [10]. For the repeated use of enzymes, cells, antibodies, and other biologically active agents in analytical devices, numerous techniques for fixing them to carrier materials have been developed. **Immobilization**, particularly of enzymes, brings about a number of further advantages for their application in analytical chemistry. These are:

- in many cases the enzyme is stabilized;
- the enzyme-carrier complex may be easily separated from the sample, i.e., the latter is not contaminated by the enzyme preparation;
- the stable and largely constant enzyme activity render the enzyme an integral part of the analytical instrument [40].

1.1.2 Immunosensors

An immunosensor, is an affinity ligand-based biosensor in which the immunochemical reaction is coupled to a transducer. The fundamental basis of all immunosensors is the specificity of the molecular recognition of antigens by antibodies and their tendency to form a stable complex.

An **antigen** is a substance which has the ability to induce an immunological response, such as, for example, bacteria, viruses, allergens, etc. An **antibody** is a soluble protein produced by the body's immune system that circulates freely and exhibits properties that contribute specifically to immunity and protection against

foreign material [5]. The functionality of immunoassays relies on the following properties of antibodies (see [46]): their ability to bind to a wide range of natural and artificial chemicals, cells and viruses; exceptional specificity for certain analytes and finally, strength of binding. Since the binding between the antibody and antigen does not generate electrons, immunoassays often require the use of labelled materials in order to measure the amount of antigen or antibody present. A **label** is a molecule that will react as part of the assay, and in doing so produces a signal that can be measured in the solution. Examples of labels include radioactive compounds or enzymes, that can generate colour or create fluorescent or luminescent products that can be measured by optical or electronic equipment.

The measurement of the analyte using labels is broadly categorized into **competitive** and **non-competitive** methods. In competitive formats, unlabelled analyte in the test sample is measured by its ability to compete with labelled antigen for a limited number of antibody binding sites [14]. The unlabelled antigen blocks the ability of the labelled antigen to bind because that binding site on the antibody is already occupied. Thus, in a competitive immunoassay, less label measured in the assay means more of the unlabelled (test sample) antigen is present. The amount of antigen in the test sample is inversely related to the amount of label measured in the competitive format: i.e., as one increases, the other decreases. Competitive assays will be studied in Chapter 5 of this thesis.

Results can be either **qualitative** (for example, the pregnancy test provides a "positive" or "negative" result), but most often, in mathematical modelling we will

be concerned with **quantitative** results, which are provided as numerical results which give the compound concentration as a function of the (unlabelled) analyte in the sample taking into consideration the competitive/non-competitive nature of the device. These results are compared with experimental measurements which are often presented in the form of **calibration curves** (also known as **dose-response** curves). A calibration curve is constructed by measuring and plotting the biosensor response against a wide range of initial analyte concentrations and used for future estimations of the "dose" once the "response" is known.

The high affinity and specificity of avidin-biotin interactions have been exploited for various applications in immunology and assay preparation. Biotin is a vitamin (vitamin H) that is present in small amounts in all living cells and is critical for a number of biological processes, while avidin is a biotin-binding protein that is believed to function as an antibiotic in the eggs of birds and reptiles. The avidin-biotin system is modelled in Chapter 5, where it is coupled to a bi-enzyme electrode.

1.2 Measuring Concentrations and Basic Chemical Kinetics

Any quantitative study of solutions requires that we know the amount of solute dissolved in a solvent or the concentration of the solution. Chemists employ several different concentration measures, each one having advantages and limitations. The

use of the solution generally determines how we express its concentration. There are four concentration units defined: percent by weight, mole fraction, molarity, and molality. The concentration unit used in this thesis is molarity (M).

A **mole** is the amount of substance that contains as many atoms, molecules, ions, or any other entities as there are atoms in exactly 12g of carbon-12. It has been determined experimentally that the number of atoms per mole of carbon-12 is

$$N_A = 6.0221367 \times 10^{23} \text{ mol}^{-1},$$

which is known as the **Avogadro constant**. The **molar mass** of a substance is the mass in grams or kilograms of one mole of the substance. In many calculations, molar masses are more conveniently expressed as kg/mol [11].

Molar concentration or **molarity** is defined as the number of moles of solute dissolved in one litre (L) of solution; that is,

$$\text{molarity} = \frac{\text{number of moles of solute}}{\text{L of solution}}.$$

Thus, molarity has units moles per litre (mol/L). By convention, we use square brackets [ ] to represent molarity. It is one of the most commonly employed concentration measures. The advantage of using molarity is that it is generally easier to measure the volume of a solution using precisely calibrated volumetric flasks than to weigh the solvent. Its main drawback is that it is temperature dependent, because the volume of a solution usually increases with increasing temperature. Another drawback is that molarity does not tell one the amount of solvent present [11].

A solution of concentration 1 mol/L is also denoted as 1 molar (1 M). In the numerical simulations throughout the thesis we often use the International System units of mol/m^3 where

$$1 \text{ mol/m}^3 = 10^{-3} \text{ M} = 1 \text{ mM}.$$

To understand the mechanism of a reaction or reactions, or to experimentally determine the rate of a reaction or reactions and its/their dependence on different parameters, the study of chemical kinetics is essential. Consider the simple reaction

$$P \longrightarrow Q,$$

and let the concentrations of P and Q at times t_1 and t_2 be $[P]_1$, $[P]_2$ and $[Q]_1$, $[Q]_2$, where $t_2 > t_1$. Then the reaction rate over the time interval $t_2 - t_1$ can be expressed as

$$\text{reaction rate } = \frac{[P]_2 - [P]_1}{t_2 - t_1} = -\frac{\Delta[P]}{\Delta t},$$

since $[P]_2 < [P]_1$. Alternatively, the rate of reaction can be expressed in terms of the product Q as

$$\text{reaction rate } = \frac{[Q]_2 - [Q]_1}{t_2 - t_1} = \frac{\Delta[Q]}{\Delta t},$$

since $[Q]_2 > [Q]_1$. In practice, the quantity of interest is not the rate over a certain time interval, but the instantaneous reaction rate, where Δt approaches zero, which is given by

$$\text{reaction rate } = -\frac{d[P]}{dt} = \frac{d[Q]}{dt}.$$

This rate has the units of M/s, where M (molarity), has the units moles per liter (mol/L). For more complicated reactions, the rate of change of the reactant and the

product may not equal each other. For example, the reaction

$$2P \longrightarrow Q,$$

(in which two molecules of P combine to yield one molecule of Q) has the rate expressed as

$$\text{reaction rate } = -\frac{1}{2}\frac{d[P]}{dt} = \frac{d[Q]}{dt},$$

since the disappearance of the reactant is twice as fast as the product. In general, for a reaction

$$aA + bB \longrightarrow cC + dD, \tag{1.1}$$

where $[A]$, $[B]$, $[C]$ and $[D]$ denote the concentration of the reactants and products at time t, the rate of the reaction is given by

$$\text{reaction rate } = -\frac{1}{a}\frac{d[A]}{dt} = -\frac{1}{b}\frac{d[B]}{dt} = \frac{1}{c}\frac{d[C]}{dt} = \frac{1}{d}\frac{d[D]}{dt}.$$

The relationship between the chemical reaction rate and the concentrations of the different reactants is complicated and must be determined experimentally. For the general equation (1.1), the reaction rate can usually be expressed as

$$\text{reaction rate } \propto [A]^a[B]^b$$

which gives the equation

$$\text{reaction rate } = k[A]^a[B]^b, \tag{1.2}$$

which is known as **rate law** or **law of mass action**. The proportionality constant k is known as the **rate constant**. The rate law states that at any given time, t, the reaction rate is proportional to the concentrations of A and B raised to some powers.

Note that the rate law is defined in terms of the reactant concentrations, but the rate constant, k, for a given reaction does not depend on the concentrations of the reactants. Expressing the rate of a reaction by using the rate law enables us to define the **order of a reaction**. In equation (1.2), we say that the reaction is of order a with respect to A and of order b with respect to B, which gives an overall reaction order of $(a + b)$. The order of a reaction specifies the empirical dependence of the rate on concentrations. It may be zero, an integer, or a non-integer.

In what follows, mathematical descriptions in the form of differential equations are given for the law of mass action in the context of several simple reactions.

First-order reactions

The simplest possible reaction involves the irreversible conversion of a substance X to Y as in

$$X \longrightarrow Y. \tag{1.3}$$

The law of mass action can be written as

$$\frac{dx}{dt} = -kx,$$

where k is the rate constant of the reaction, and x denotes the concentration of the reactant X. This is a first-order reaction since its rate only depends on the first power of the concentration. In reality, most reactions are not as simple as irreversible reactions since, with accumulation of product, the reverse reaction becomes important. These reactions are named reversible reactions, where the equilibrium does not lie far

to one side. For example,

$$X \underset{k_{-1}}{\overset{k_1}{\rightleftarrows}} Y, \tag{1.4}$$

where k_{-1} is the dissociation rate constant. It has the rate equation

$$\frac{dx}{dt} = -k_1 x + k_{-1} y = -\frac{dy}{dt},$$

where y denotes the concentration of Y.

As stated above, most reactions are not as simple as irreversible reactions since, with accumulation of product, the reverse reaction becomes important. These reactions are named reversible reactions, where the equilibrium does not lie far to one side. Consider the reaction

$$A \underset{k_{-1}}{\overset{k_1}{\rightleftarrows}} B, \tag{1.5}$$

whose rate of reaction is given by

$$\text{reaction rate } = \frac{d[A]}{dt} = -k_1[A] + k_{-1}[B].$$

If we consider the rate equation at equilibrium, we obtain the equilibrium constant k_1/k_{-1}. The relationship between reaction rates and equilibria is rooted in a principle of great importance in chemical kinetics. The **principle of microscopic reversibility** states that, at equilibrium, the rates of the forward and reverse processes are equal for every elementary reaction occurring. This means that the process $A \longrightarrow B$ is exactly balanced by $B \longrightarrow A$.

Second-order reactions

Many biochemical reactions are not of first-order, but are of second or higher order. Simple examples of second-order irreversible reactions are

$$2X \xrightarrow{k} Y$$

and

$$X + Y \xrightarrow{k} Z.$$

The rate of such reactions is proportional to the second power of the concentration, or product of concentrations, given by

$$\frac{dy}{dt} = -\frac{1}{2}\frac{dx}{dt} = kx^2$$

and

$$\frac{dz}{dt} = -\frac{dx}{dt} = -\frac{dy}{dt} = kxy$$

respectively, where z denotes the concentration of Z. Similarly, a simple example of second-order reversible reactions is

$$X + Y \underset{k_{-1}}{\overset{k_1}{\rightleftarrows}} Z,$$

which has the corresponding rate equation of

$$\frac{dz}{dt} = -\frac{dx}{dt} = -\frac{dy}{dt} = k_1xy - k_{-1}z.$$

Note that, reaction rates are expressed in mole/litre/second (M/s). The first-order rate constants have the dimension of time^{-1} (s^{-1}) and the second-order rate constants have the dimension of concentration^{-1} $\times$ time^{-1} (M^{-1}·s^{-1}); zero-order rate constants have the dimension of concentration $\times$ time^{-1} [28].

1.3 Enzyme-Substrate Kinetics: The Michaelis-Menten Model

Enzyme catalysis is one of the most fascinating areas in the study of chemical kinetics. The phenomenon of enzyme catalysis usually results in a very large increase in reaction rate in the order of 10^6 to 10^{18} and high specificity. Specificity means that an enzyme molecule is capable of selectively catalyzing certain reactants, called **substrates**, while discriminating against other molecules. An enzyme usually contains one or more active sites, where reactions with substrate take place. The specificity of enzymes for substrates varies from molecule to molecule. In the 1890s the German chemist, Emil Fischer, (1852-1919) proposed a lock-and-key theory of enzyme specificity. According to Fischer, the active site can be assumed to have a rigid structure, similar to a lock. A substrate molecule then has a complementary structure and functions as a key. The binding of substrate to enzyme results in a distortion of the substrate into the conformation of the transition state. At the same time, the enzyme undergoes a change in conformation to fit the substrate. This explains the flexibility and the phenomenon of cooperativity of the protein. Cooperativity means that the binding of a substrate to an enzyme with multiple binding sites can alter the substrate's affinity for enzyme binding at its other sites.

1.3.1 The Michaelis-Menten Model

Enzyme reactions do not follow the law of mass action directly. The rate of the reaction only increases to a certain extent as the concentration of substrate increases. The maximum reaction rate is reached at high substrate concentrations due to enzyme saturation. This is in contrast to the law of mass action, which states that the reaction rate increases as the concentration of substrate increases [25].

The simplest model that explains the kinetic behaviour of enzyme reactions is the classic 1913 model of Michaelis and Menten [33] which is widely used in biochemistry for many types of enzymes. The Michaelis-Menten model is based on the assumption that the enzyme binds the substrate to form an intermediate complex which then dissociates to form the final product and release the enzyme in its original form. The schematic representation of this two-step process is given by

$$E + S \underset{k_{-1}}{\overset{k_1}{\rightleftarrows}} C \xrightarrow{k_2} E + P, \tag{1.6}$$

where k_1, k_{-1} and k_2 are constant parameters associated with the rates of the reaction. The double arrow symbol $\rightleftarrows$ indicates that the reaction is reversible while the single arrow $\rightarrow$ indicates that the reaction is irreversible. Based on the principles of mass action and conservation of mass, the dynamics of different species in the Michaelis-Menten model can be described by the following system of ordinary

differential equations

$$\frac{dS}{dt} = -k_1 ES + k_{-1} C, \tag{1.7}$$

$$\frac{dE}{dt} = -k_1 ES + (k_2 + k_{-1}) C, \tag{1.8}$$

$$\frac{dC}{dt} = k_1 ES - (k_2 + k_{-1}) C, \tag{1.9}$$

$$\frac{dP}{dt} = k_2 C, \tag{1.10}$$

with initial conditions:

$$E(0) = E_0, \quad S(0) = S_0, \quad C(0) = 0, \quad P(0) = 0.$$

Note that

$$\frac{dE}{dt} + \frac{dC}{dt} = 0$$

in system of equations (1.7)-(1.10), and hence $E + C = E_0$. This conservation law will be used extensively throughout our models, and expresses the fact that the enzyme only exists in two forms during the reaction: free enzyme and complex-bound enzyme. We can obtain a second conservation law $S + C + P = S_0$ from equations (1.7)-(1.10) by the fact that

$$\frac{dS}{dt} + \frac{dC}{dt} + \frac{dP}{dt} = 0.$$

Then the system of equations reduces to only two equations, which are given in terms of the substrate concentration, S, and the complex concentration, C, namely

$$\frac{dS}{dt} = -k_1 (E_0 - C) S + k_{-1} C, \tag{1.11}$$

$$\frac{dC}{dt} = k_1 (E_0 - C) S - (k_2 + k_{-1}) C, \tag{1.12}$$

with initial conditions

$$S(0) = S_0, \quad C(0) = 0. \tag{1.13}$$

In constructing the Michaelis-Menten model, the following simplifying assumptions are usually made [33]:

- The concentration of substrate vastly exceeds the concentration of enzyme. This means that the free concentration of substrate is very close to the concentration that is added, and that substrate concentration is constant throughout the assay.
- Neither substrate nor product acts as an allosteric modulator to alter the enzyme velocity.
- Binding of substrate to one enzyme binding site does not influence the affinity or activity of an adjacent site.
- There is negligible spontaneous creation of product without enzyme.

1.3.2 The Quasi-Steady-State Approximation

In the original Michaelis-Menten model [33], it was assumed that the substrate concentration, S, is in instantaneous equilibrium with the enzyme-substrate complex concentration, C, which gives

$$k_1 ES = k_{-1} C.$$

Then, by using the initial condition, $E + C = E_0$, we find that

$$C = \frac{E_0 S}{K_s + S},$$

where $K_s = k_{-1}/k_1$. If we let V denote the velocity of the reaction, then the rate at which the product is formed is given by

$$V = \frac{dP}{dt} = k_2 C = \frac{k_2 E_0 S}{K_s + S} = \frac{V_{max} S}{K_s + S},$$

where

$$V_{max} = k_2 E_0 \tag{1.14}$$

is the maximum reaction velocity, attained when the enzyme is saturated with substrate [25].

An alternative analysis of an enzymatic reaction was proposed by Briggs and Haldane in [7], and forms the basis for most modern descriptions of enzyme reactions. Their assumption is that the rates of formation and breakdown of the complex are essentially equal at all times, except at the beginning of the reaction, when the formation of the complex is very fast. Thus, we have $dC/dt \approx 0$. It is simple to determine the velocity of the reaction with this assumption. From (1.12) we obtain the complex concentration, C, in terms of the substrate concentration, S, as

$$C = \frac{k_1 E_0 S}{k_{-1} + k_2 + k_1 S} = \frac{E_0 S}{K_M + S}. \tag{1.15}$$

This expression for C does not satisfy the initial conditions specified before, namely $C(0) = 0$ and $S(0) = S_0$, as we get

$$C(0) = \frac{E_0 S_0}{S_0 + K_M} \neq 0.$$

If we insert equation (1.15) into equation (1.11), we obtain

$$\frac{dS}{dt} \approx -k_2 C = -\frac{k_2 E_0 S}{K_M + S}. \tag{1.16}$$

Since the enzyme is traditionally considered to be present in small amounts compared with the substrate ($E_0 \ll S_0$) the assumption is that the substrate concentration effectively does not change during this initial transient stage. In this case, the

(approximate) dynamics are governed by equation (1.16) with the initial condition $S(0) = S_0$. This is known as the **quasi-steady-state approximation**.

Mathematical studies of the quasi-steady-state approximation typically involve an elementary singular perturbation analysis of the Michaelis Menten equations (1.11) and (1.12), where a small parameter, ε, introduced by non-dimensionalisation is $\varepsilon = E_0/S_0$ [25], [18]. In this framework, the initial rapid formation of enzyme-substrate complex can be modelled as a boundary layer near $t = 0$ while the quasi-steady-state approximation corresponds to the outer solution.

The quasi-steady-state approximation gives an expression for the velocity of the reaction which is useful for practical applications. Equation (1.16) implies that

$$V = \frac{dP}{dt} = -\frac{dS}{dt} = \frac{k_2 E_0 S}{K_M + S} = \frac{V_{max} S}{K_M + S}, \tag{1.17}$$

where V_{max} is defined in (1.14) and

$$K_M = \frac{k_{-1} + k_2}{k_1}, \tag{1.18}$$

is referred to as the **Michaelis constant**. Note that K_M has concentration units and this constant can be easily determined from experimental data if we notice that, setting

$$S = K_M,$$

equation (1.17) implies

$$V = \frac{V_{max}}{2}.$$

This allows us to interpret K_M as the substrate concentration at which the velocity of the reaction is half-maximal and it indicates how efficiently an enzyme selects its

substrate and converts it to product. The lower the value of K_M, the more effective the enzyme is at low substrate concentrations, and K_M is unique for each enzyme-substrate pair. Consequently, K_M values are useful for comparing the activities of two enzymes that act on the same substrate or for assessing the ability of different substrates to be recognized by a single enzyme. For practical purposes, it is also useful to know how fast the enzyme operates after it has selected and bound its corresponding substrate; that is, how fast does the complex proceed to the product and free enzyme. This property is characterized by the **catalytic constant**

$$k_{cat} = \frac{V_{max}}{E_0},$$

and in the Michaelis-Menten scheme, we have $k_{cat} = k_2$. Thus, k_{cat} is the rate constant of the reaction when the enzyme is saturated with substrate (i.e., when $C \approx E_0$, $V_0 \approx V_{max}$, where V_0 is the initial velocity of the reaction); we have already seen this relationship in equation (1.14). k_{cat} is also known as the enzyme's **turnover number** because it is the number of catalytic cycles that each active site undergoes per unit time. It is a first-order rate constant and therefore has units of s^{-1} [25].

A useful method for experimental determination of the constants K_M and V_{max} is given by the **Lineweaver-Burk** plot. This method consists of plotting the linear relationship

$$\frac{1}{V} = \frac{K_M}{V_{max}} \cdot \frac{1}{[S]} + \frac{1}{V_{max}} \tag{1.19}$$

which is obtained from equation (1.17) and gives the reciprocal of the reaction velocity, $1/V$, as a function of $1/[S]$. Once velocity measurements are made for a range of substrate concentrations (both higher and lower than K_M) and the straight line

is plotted, V_{max} and K_M can be easily determined from the observation that the intercept on the vertical axis is $1/V_{max}$ while the intercept on the horizontal axis is $-1/K_M$; see Figure 1.2.

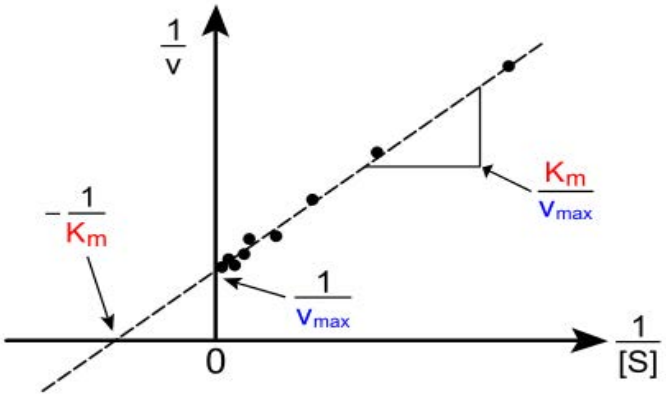

Figure 1.2 – A Lineweaver-Burk Plot.

"The Improved Euler method" is used to solve the system of equations (1.7)-(1.10) and the numerical solution is shown in Figure 1.3. The equations have been non-dimensionalised so that the four unknown functions have similar orders of magnitude (note, for example, that the initial non-dimensional values of enzyme and substrate are both 1).

1.3.3 Reversible Michaelis-Menten Kinetics

The classical Michaelis-Menten reaction scheme (1.6) assumes that the complex dissociation step is irreversible. In reality, there will be some degree of reversibility in product formation in many chemical reactions. Thus, a more realistic model for the

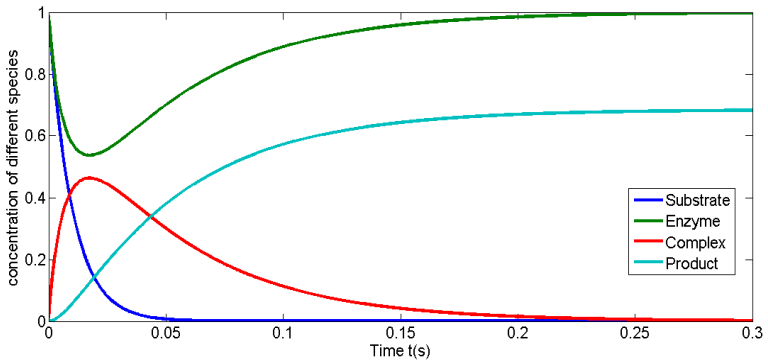

Figure 1.3 – Relative concentrations of reactants and product of the standard Michaelis-Menten kinetics. Typical values for constants used in this simulation are shown in Table 1.1.

Description	***Constant***	***Value***
Reaction rate constants (m^3/mol·s):	k_1	10^2
	k_3	10^2
Reaction rate constants (s^{-1}):	k_{-1}	10^{-1}
	k_{-2}	10^{-2}
	k_{-3}	10^{-1}
	k_2	10^3
	k_4	10
Initial concentrations:		
Total enzyme (mol/m^2)	e_0	1
Substrate (mol/m^3=mM)	S_0	1

Table 1.1 – Typical values for constants.

Michaelis-Menten kinetics would be

$$E + S \underset{k_{-1}}{\overset{k_1}{\rightleftarrows}} C \underset{k_{-2}}{\overset{k_2}{\rightleftarrows}} E + P, \tag{1.20}$$

where k_{-2} is another reaction rate constant. The dynamics of the system are described by the following system of nonlinear differential equations by using the law of mass action:

$$\frac{dS}{dt} = -k_1 ES + k_{-1} C, \tag{1.21}$$

$$\frac{dE}{dt} = -k_1 ES + (k_2 + k_{-1})C - k_{-2} EP, \tag{1.22}$$

$$\frac{dC}{dt} = k_1 ES - (k_2 + k_{-1})C + k_{-2} EP, \tag{1.23}$$

$$\frac{dP}{dt} = k_2 C - k_{-2} EP, \tag{1.24}$$

with initial conditions $E(0) = E_0$, $S(0) = S_0$, $C(0) = 0$ and $P(0) = 0$. The reversible model was also analyzed in [44] where a dynamical systems analysis revealed that this model yields qualitatively similar results to those of the standard Michaelis-Menten model. The only difference consists in slightly different values for the steady-states (such as, for example, $C^* = 0$ in the standard model, while $C^* = O(\varepsilon)$ in the reversible model, where $\varepsilon = E_0/S_0$). For later analysis in this thesis, we will always work with the standard model, as these small variations are not worth the inconvenience of dealing with an extra term and having to specify another experimental constant, k_{-2}.

1.3.4 Cascade Reactions

A cascade reaction is a sequence of biochemical reactions which have the property that the product of one reaction is a reactant in the following reaction. We will focus, in particular, on a cascade scheme which consists of two enzyme-substrate reactions described by the Michaelis-Menten kinetic models, namely,

$$E_1 + S_1 \underset{k_{-1}}{\overset{k_1}{\rightleftarrows}} C_1 \xrightarrow{k_2} E_1 + S_2, \qquad E_2 + S_2 \underset{k_{-3}}{\overset{k_3}{\rightleftarrows}} C_2 \xrightarrow{k_4} E_2 + P, \tag{1.25}$$

where E_1 is the first enzyme, E_2 is the second enzyme, S_1 is the first substrate, S_2 is the second substrate in the second reaction and also the product of the first reaction, C_1 and C_2 are the complexes and P is the final product, while k_1, k_{-1}, k_2, k_3, k_{-3} and k_4 are constant parameters which represent the rate of the reactions. This system will be studied in more detail in Chapter 4.

The differential equations governing the behavior of the relevant chemical species are:

$$\frac{dS_1}{dt} = -k_1 E_1 S_1 + k_{-1} C_1, \tag{1.26}$$

$$\frac{dE_1}{dt} = -k_1 E_1 S_1 + (k_2 + k_{-1}) C_1, \tag{1.27}$$

$$\frac{dC_1}{dt} = k_1 E_1 S_1 - (k_2 + k_{-1}) C_1, \tag{1.28}$$

$$\frac{dS_2}{dt} = k_2 C_1 - k_3 E_2 S_2 + k_{-3} C_2, \tag{1.29}$$

$$\frac{dE_2}{dt} = -k_3 E_2 S_2 + (k_4 + k_{-3}) C_2, \tag{1.30}$$

$$\frac{dC_2}{dt} = k_3 E_2 S_2 - (k_4 + k_{-3}) C_2, \tag{1.31}$$

$$\frac{dP}{dt} = k_4 C_2. \tag{1.32}$$

Typical initial conditions are:

$$E_1(0) = E_1^0, \quad E_2(0) = E_2^0, \quad S_1(0) = S_0, \quad S_2(0) = 0,$$
$$C_1(0) = 0, \quad C_2(0) = 0, \quad P(0) = 0,$$

and we can also write the following conservation laws

$$E_1 + C_1 = E_1^0,$$
$$E_2 + C_2 = E_2^0,$$
$$S_1 + C_1 + S_2 + C_2 + P = S_0.$$

The numerical simulation result of the cascade Michaelis-Menten model is shown in Figure 1.4. (Again, the numerical integration was performed on a scaled version of equations (1.26)-(1.32) which is why the initial values of enzymes and first substrate are 1.)

Chapter 4 deals with an experimental problem involving a cascade reaction, in which the two enzymes are immobilized on an electrode at the bottom of a flow cell. It is assumed that the two enzymes fully cover the surface of the electrode and it is only the total concentration, E, that can be measured experimentally, rather than the individual concentrations, E_1^0 and E_2^0. Hence, we let

$$E = E_1^0 + E_2^0, \text{ and } \zeta = \frac{E_1^0}{E_2^0}, \tag{1.33}$$

which gives

$$E_1^0 = \frac{E\zeta}{1+\zeta}, \text{ and } E_2^0 = \frac{E}{1+\zeta}.$$

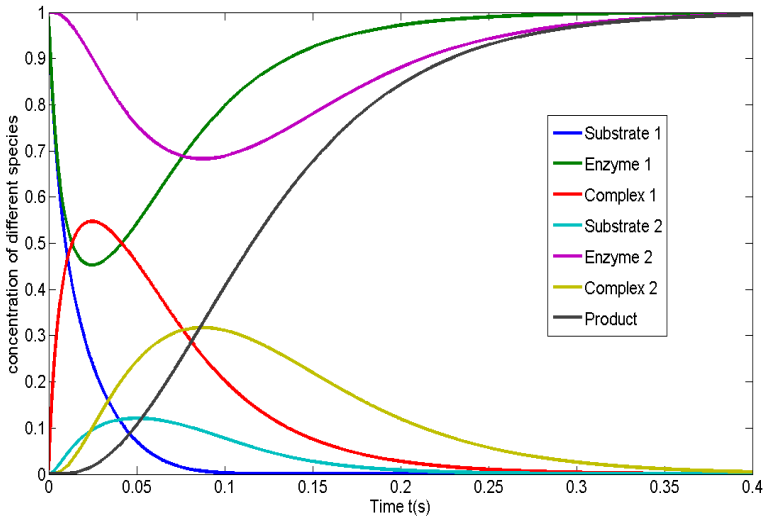

Figure 1.4 – Relative concentrations of reactants and product of the cascade reactions. Typical values for constants used in this simulation are shown in Table 1.1.

1.4 Measuring Electrode Currents

The measured current is accepted as a response of the electrochemical biosensor in physical experiments. The anodic current depends upon the flux of the product at the electrode surface. In the case of amperometry, the biosensor current is also directly proportional to the area of the electrode surface. The anodic current $i_A(t)$ of the amperometric biosensor at time t can be obtained explicitly from the Faraday and the Fick laws [43],

$$i_A(t) = n_e F A D_p \frac{\partial P}{\partial x}|_{x=0}, \tag{1.34}$$

where n_e is the number of electrons involved in a charge transfer, A is the electrode surface area and F is the Faraday constant, which has a value of

$$F = 96,485 \text{ C/mol}, \tag{1.35}$$

and D_p is the diffusion constant. Due to the direct proportionality, the current is normalized with the area of that surface. Consequently, the density $i(t)$ of the biosensor current at time t is expressed as

$$i(t) = \frac{i_A}{A} = n_e F D_p \frac{\partial P}{\partial x}|_{x=0}. \tag{1.36}$$

As $t \to \infty$, we have

$$I = \lim_{t\to\infty} i(t), \tag{1.37}$$

where I is taken as the density of the steady state biosensor current.

In an enzyme electrode, the enzyme catalyzed reaction occurs in a localized region at, or close to, the electrode surface. Consequently there is an interplay and interaction between the enzyme kinetics and mass transport of material to and from the electrode surface, [12]. In this project, mass transport obeys Fick's first and second laws. Fick's first law describes the relationship between flux and concentration gradient while the second law describes the rate of change of the concentration with time in terms of a second order partial differential equation.

1.5 Mathematical Modelling Techniques

It is stated in [48] that *Mathematical modelling, the process of describing scientific phenomena in a mathematical framework, brings the powerful machinery of mathematics—its ability to generalize, to extract what is common in diverse problems, and to build effective algorithms—to bear on characterisation, analysis, and*

prediction in scientific problems. Mathematical models lead to "virtual experiments" whose real-world analogues would be expensive, dangerous, or even impossible; they obviate the need to actually crash an airplane, spread deadly virus, or witness the origin of the universe. Mathematical models help to clarify relationships among a system's components as well as their relative significance. Through modelling, speculations about a system are given a form that allows them to be examined qualitatively and quantitatively from many angles; in particular, modelling allows the detection of discrepancies between theory and reality.

Biosensors are analytic devices which are well-suited to mathematical and computational modelling as they rely on continuous physical and chemical processes, such as reaction kinetics and transport of analytes which can be readily expressed as systems of ordinary and partial differential equations. Numerical integration of such equations will allow us to calculate the concentrations of relevant reactants at any point in space and time, which gives a unique insight into the functionality of the sensing platforms, not easily obtained from experiments alone.

Diffusion and Convection-diffusion equations

Biosensor models are based on transport of various analytes and we denote a typical concentration by $C(x, y, z, t)$, where x, y, z are spatial coordinates and t is time. The main transport partial differential equations are reviewed below for the case of three spatial variables, although in this thesis we will only consider one and two-dimensional

models. We can write the following conservation equation

$$\frac{d}{dt}\int\int\int_D CdV = -\int\int_S F \cdot dS \tag{1.38}$$

for any surface S enclosing a region D, where F is the flow rate of analyte. This equation says that the net rate of change of the amount of C in D equals the flux of F through S. The minus sign comes from the convention that $dS = ndS$ is chosen so that n points outward, so that the flux is positive when the analyte is flowing out through S. Using the divergence theorem, the equation above can be written in differential form as

$$\frac{\partial C}{\partial t} = -div\mathbf{F}. \tag{1.39}$$

In the case of diffusion alone, when the analyte is not moved by fluid motion, Fick's law states that

$$\vec{F} = -k\nabla C, \tag{1.40}$$

which means that the flow points in the direction of $-\nabla C$, so the analyte moves from regions of higher concentrations to regions of lower concentrations. The proportionality constant k is known as the diffusion coefficient or diffusivity of the analyte. Combining Fick's law with equation (1.40) we get

$$\frac{\partial C}{\partial t} = k\nabla^2 C = k\left(\frac{\partial^2 C}{\partial x^2} + \frac{\partial^2 C}{\partial y^2} + \frac{\partial^2 C}{\partial z^2}\right), \tag{1.41}$$

which is known as the **diffusion equation or heat equation**. If the analyte is also connected by the fluid sample (as in the case of Fluid Injection Analysis experiments studied in Chapters 3 and 4) then the flow rate is expressed as

$$\vec{F} = C\vec{v}, \tag{1.42}$$

which means that the entire quantity of C at a given point is moved by the velocity vector $\vec{v}$. The convection equation is the

$$\frac{\partial C}{\partial t} = -div(C\vec{v}). \tag{1.43}$$

For an incompressible flow, such as water, we have $div(\vec{v}) = 0$ and the convection equation takes the more familiar form

$$\frac{\partial C}{\partial t} + \vec{v} \cdot \nabla C = 0. \tag{1.44}$$

Combining the effects of diffusion with convection yields

$$\frac{\partial C}{\partial t} + \vec{v} \cdot \nabla C = k\nabla^2 C, \tag{1.45}$$

which is known as the **convection-diffusion** (or **advection-diffusion**) equation.

Non-dimensionalisation and Scaling

After a mathematical model of a continuous physical system, which may consist of, say, a set of differential equations and associated initial and boundary conditions, has been created, we try to obtain the solutions for this model. Generally, there are two kinds of solutions: exact analytical solutions and approximate solutions. Exact solutions are obtained by solving equations analytically. Approximate solutions are obtained by applying some type of approximation to an equation or a system of equations and solving the resulting system. In order to obtain an approximate solution, a useful approach is to non-dimensionalise the system. This has the advantage of reducing the number of independent variables in a system and also removing the various units involved in it. Since real-life problems are often very difficult to

analyze rigorously, one way to simplify analysis is to apply some kind of asymptotic reduction, based on the idea that we can neglect certain terms which are small compared with others in the system. After the process of non-dimensionalisation, we end up with equations with dimensionless variables, rather than equations with a large number of physical parameters and variables all with dimensional units. The science of non-dimensionalisation lies in the choice of scales. There is no standard way to do the scaling - the main principle is to balance the terms in the equation by choosing self-consistent scales, since the purpose is to make the largest dimensionless parameter numerically of order one in the attained properly scaled equations. Note that the process of rescaling may be necessary if the scaling causes inconsistency of the differential equation. Normally, to check for the consistency of the system, we use the approximate solution just obtained to evaluate the order of magnitude of the neglected terms, so as to ensure that they are indeed relatively small. For a more detailed reference on scaling refer to [29] and [37].

1.6 Numerical Approximation using Finite Difference Techniques

The idea behind finite-difference methods is to replace the partial derivatives occurring in partial differential equations by approximations based on Taylor series expansions of functions near the points of interest. For example, the partial derivative

$\partial u/\partial t$ may be replaced by the approximation

$$\frac{\partial u(x,t)}{\partial t} = \frac{u(x,t+\Delta t) - u(x,t)}{\Delta t}. \tag{1.46}$$

This is called a **finite-difference approximation** because it involves small, but not infinitesimal, differences of the function u. This particular finite-difference approximation is called a **forward difference**, since the differencing is in the forward t direction; only the values of u at t and $t+\Delta t$ are used. We can also define **backward differences** using the formula

$$\frac{\partial u(x,t)}{\partial t} = \frac{u(x,t) - u(x,t-\Delta t)}{\Delta t}. \tag{1.47}$$

When applied to the diffusion equation, forward- and backward- difference approximations for $\partial u/\partial t$ lead to **explicit** and **fully implicit** finite-difference schemes, respectively.

For second partial derivatives, such as $\partial^2 u/\partial x^2$, we can define a symmetric finite-difference approximation as the forward difference of backward-difference approximation to the first derivative. We obtain the **symmetric central-difference** approximation

$$\frac{\partial^2 u(x,t)}{\partial x^2} = \frac{u(x+\Delta x,t) - 2u(x,t) + u(x-\Delta x,t)}{\Delta x^2}. \tag{1.48}$$

To continue with the finite-difference approximation to the diffusion equation we divide the x-axis into equally spaced **nodes** a distance Δx apart, and the t-axis into equally spaced nodes a distance Δt apart. This divides the (x,t) plane into a mesh, where the **mesh points** have the form $(n\Delta x, m\Delta t)$. We then concern ourselves only

with the values of $u(x,t)$ at mesh points $(n\Delta x, m\Delta t)$. We write

$$u_n^m = u(n\Delta x, m\Delta t) \tag{1.49}$$

for the value of $u(x,t)$ at the mesh point $(n\Delta x, m\Delta t)$. For example, the general diffusion equation

$$\frac{\partial u(x,t)}{\partial t} = \frac{\partial^2 u(x,t)}{\partial x^2}, \tag{1.50}$$

can be approximated by

$$\frac{u_n^{m+1} - u_n^m}{\Delta t} = \frac{u_{n+1}^m - 2u_n^m + u_{n-1}^m}{\Delta x^2}, \tag{1.51}$$

which can be rearranged to give the difference equations

$$u_n^{m+1} = \alpha u_{n+1}^m + (1-2\alpha)u_n^m + \alpha u_{n-1}^m, \tag{1.52}$$

where

$$\alpha = \frac{\Delta t}{\Delta x^2}. \tag{1.53}$$

If, at time step m, we know u_n^m for all values of n we can explicitly calculate u_n^{m+1}. This is why this method is called explicit. It can be shown (see, for example, [41]) that this method is stable if $0 < \alpha \leq \frac{1}{2}$ and unstable if $\alpha > \frac{1}{2}$. Hence, to ensure that the explicit method converges we need to choose a sufficiently small time step, so that

$$\Delta t \leq \frac{1}{2}(\Delta x)^2. \tag{1.54}$$

Implicit finite-difference methods are used to overcome the stability limitations imposed by the restriction $0 < \alpha \leq \frac{1}{2}$, which applies to the explicit method. Implicit methods allow us to use a large number of x-mesh points without having to take

extremely small time steps.

One of the best known implicit schemes is the Crank-Nicolson Method, which is essentially an average of the implicit and explicit methods, and has the form

$$\frac{u_n^{m+1} - u_n^m}{\Delta t} = \frac{1}{2}\left(\frac{u_{n+1}^m - 2u_n^m + u_{n-1}^m}{\Delta x^2} + \frac{u_{n+1}^{m+1} - 2u_n^{m+1} + u_{n-1}^{m+1}}{\Delta x^2}\right). \tag{1.55}$$

Rearranging, we obtain the system of difference equations

$$u_n^{m+1} - \frac{1}{2}\alpha\left(u_{n-1}^{m+1} - 2u_n^{m+1} + u_{n+1}^{m+1}\right) = u_n^m + \frac{1}{2}\alpha\left(u_{n-1}^m - 2u_n^m + u_{n+1}^m\right), \tag{1.56}$$

where, as before, $\alpha = \Delta t/\Delta x^2$. Note that u_n^{m+1}, u_{n-1}^{m+1} and u_{n+1}^{m+1} are now determined implicitly in terms of all the u_n^m, u_{n+1}^m and u_{n-1}^m. This system of equations is then solved using the techniques of LU decomposition and SOR (Successive Order Relaxation). It can be shown that the Crank-Nicolson method is both stable and convergent for all values of $\alpha > 0$.

1.7 Outline of Thesis

This thesis is motivated by a collaboration with the National Centre for Sensor Research (NCSR) and the Biomedical Diagnostics Institute (BDI) at Dublin City University. We use mathematical and computational modelling techniques to characterize the biosensor response as a function of its input parameter in a wide range of physical contexts; it can guide experiments and therefore reduce development times and costs. Several models of varying complexity are proposed in answer to experimental problems, usually concerned with optimizing design parameters for biosensors. One main concern is to simplify the models as much as possible, without the loss of important

information from the original problem.

Chapter 1 provides some background material, which includes the motivation for studying biosensors as well as an elementary description of their structure and functionality. This chapter also includes an introduction to basic chemical kinetics and the well-known Michaelis-Menten model for enzyme-substrate interactions.

In Chapter 2, we describe a method for accurate determination of kinetic rate constants for an immobilized enzyme, based on experimental procedure and statistical analysis. We then present three simple problems involving immobilized horseradish peroxidase (HRP) and diffusion of its substrate, hydrogen peroxide, to the reaction site. The models consist of diffusion equations with reaction boundary conditions. The experimental work was conducted in parallel with the mathematical and computational modelling, using precisely determined physical constants, and the two sets of data are then compared.

Chapter 3 introduces mathematical models for antigen-antibody interactions which are relevant to immunosensing devices. We first look at the kinetics of the binding reaction in a direct assay (which is modelled by a system of ordinary differential equations) and then study the effects of transport. Two simple problems are presented, namely the diffusion of an analyte in a small cell (which is a simplified model for a pregnancy testing device) and transport of analyte by convection in a flow channel (which is relevant to the BIACORE device). In both these problems, the other reactant is surface-bound.

In Chapter 4, we investigate the problem of optimizing the design of a bi-enzyme biosensor by binding the ratio of two immobilized enzymes which maximizes signal amplitude. This problem represents a necessary first step towards modelling the enzyme-channelling immunoassay.

In Chapter 5, we construct a model for a biosensor based on the same enzyme coupling in order to detect the immunological reaction between avidin and biotin. This time we consider a combination of avidin and HRP immobilized on an electrode and a fluid sample containing biotin and GOX-labelled biotin. The specific avidin-biotin interaction brings the biotin-GOX conjugate close to the immobilized HRP on the electrode surface, using a constant biotin-GOX concentration and increasing the concentration of free biotin, we can construct theoretical calibration curves for biotin determination.

Finally, a summary of the work from the previous chapters is given, and further suggestions on modelling biosensor problems are made.

Chapter 2

Enzyme Substrate Interactions with Free and Immobilized Enzyme

This chapter investigates the electrochemical response of an immobilized enzyme and introduces concepts which will be used extensively in Chapters 4 and 5. We present an experimental and theoretical method for accurate determination of Michaelis-Menten kinetic rate constants (K_M, k_{cat}, and V_{max}) for immobilized horseradish peroxidase (HRP), followed by three simple examples where the experimental work was conducted in parallel with the mathematical and numerical modelling. There is good agreement between the results of these procedures if precisely determined physical constants are used for the simulations.

2.1 Determination of Rate Constants for Free and Immobilized Enzymes

Immobilized enzymes are used extensively in the manufacturing of electrochemical biosensors as well as in other scientific fields. In order to characterize the efficiency of the deposited biological molecule and understand its reaction mechanism it is necessary to determine the kinetic rate constants. However, the calculation of these constants requires a precise experimental determination of the amount of enzyme immobilized on the solid surface. In this section we summarize a method for accurate determination of real kinetic rate constants based on the Michaelis-Menten model. The experimental work was performed by our collaborators at NCSR and the results of this collaboration can be found in [24].

Recall that the Michaelis-Menten kinetic scheme is given by

$$E + S \underset{k_{-1}}{\overset{k_1}{\rightleftarrows}} C \xrightarrow{k_{cat}} E + P, \tag{2.1}$$

and the associated mathematical model was presented in Section 1.3.1 (note that $k_{cat} = k_2$). We now review some of the kinetic constants in this scheme and their significance. Recall that the Michaelis-Menten constant K_M is defined as the concentration of substrate at which the rate of the enzyme reaction reaches half of its maximum value V_{max}. The constant k_{cat} is the catalytic turnover number of the enzyme. This represents the number of substrate molecules that are converted into product by an enzyme molecule in a time unit when the enzyme is fully saturated by the substrate. As discussed in Section 1.3.1, if the total amount of the active enzyme

is known and the maximum catalytic rate (V_{max}) is calculated, the catalytic turnover number of the enzyme can be calculated from the equation

$$V_{max} = \frac{k_{cat}}{K_M}[E_t], \tag{2.2}$$

where $[E_t]$ represents the concentration of enzyme at time t. The **specificity constant**, k_{cat}/K_M, measures how fast the enzyme binds the substrate and how fast it converts it to product. This is a very useful kinetic constant as it reflects the specificity of an enzyme for a particular substrate.

The enzyme used for this problem is horseradish peroxidase (HRP), which belongs to the family of heme peroxidases and its catalytic activity has been extensively studied (see [21], [34]). Although it is well known that HRP follows an irreversible ping-pong mechanism [14], the Michaelis-Menten scheme has been used extensively before [21] and found to be a good approximation under certain conditions. HRP is immobilized on a screen printed carbon electrode modified with electropolymerised polyaniline/polyvinylsulphonate (PANI/PVS), and its kinetics with the substrate hydrogen peroxide (H_2O_2) is monitored using amperometric I-t curve methods. We refer the reader to [24] for more details regarding the experimental procedures.

In this study, linear regression analyses were performed using well-known scientific graphing and data analysis software such as Microsoft Excel and SigmaPlot. Values of the standard deviation, relative standard deviation, confidence intervals and confidence limits as well as significance tests are determined for the experimental data derived. As in most scientific literature, the error bars presented in the graphs

represent the calculated standard deviations about the mean value of the replicates. However, standard deviations only give a measure of the spread of a set of results about their mean value and do not indicate the way in which the results are distributed. Therefore, confidence intervals are graphed to illustrate the precision of the results obtained. The 99% confidence limit is chosen for this work to increase the level of certainty that the true value lies on that interval. Relative standard deviations or standard errors calculated are used for comparing the precision of the results. These are important in calculations requiring error propagation which cannot be shown by the confidence intervals or standard deviations. In experimental procedures where the final result depends on the many variables calculated before, systematic errors as well as random errors are most likely to affect the true value estimation. In order to decide if the difference between the measured and standard amounts can be accounted for by these random errors a simple significance test can be employed. The significance of differences in the values of parameters determined for distinct populations of electrodes is calculated using Analysis of Variance (ANOVA) in Excel with $\alpha = 0.01$ taken to indicate statistical significance level.

We note again that an essential step towards determining rate constants for immobilized enzymes consists of finding the relationship between the solution concentration of enzyme and the resulting mass on the electrode. The procedure presented in [24] (which was based on previous work in [34]) uses a linear regression analysis of two colorimetric calibration assays with the enzyme in solution and immobilized enzyme

and the following equation is obtained

$$\text{Mass of immobilized enzyme} = 0.00098[\text{HRP}] - 5.26844 \times 10^{-6}, \qquad (2.3)$$

where [HRP] represents solution concentration (measured in mg/ml). The correlation between the solution concentration and the amount of immobilized enzyme is plotted in Figure 2.1. Note that this equation is only valid for the linear region of the assay (the full equation presented in [34] shows a logarithmic dependence of immobilized mass on solution concentration) and that the linear region usually depends on experimental factors.

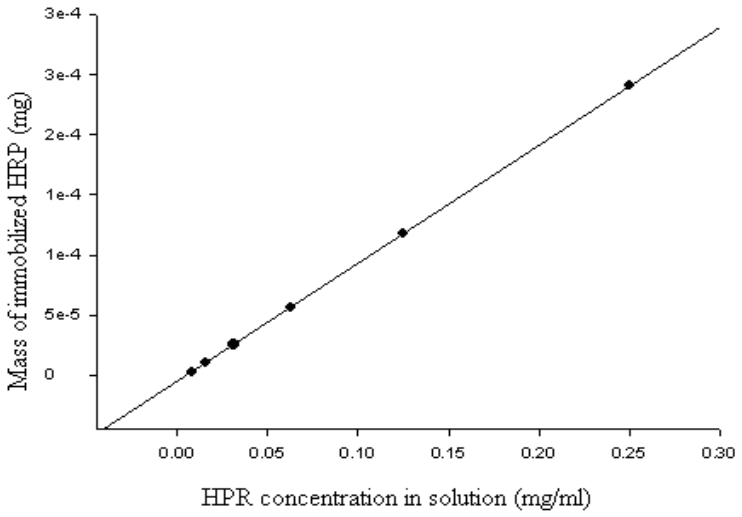

Figure 2.1 – Correlation between the concentration of horseradish peroxidase in solution and the mass of the enzyme immobilized on the electrode surface.

GraphPad prism software [35] was used to perform the non-linear regression analysis. For the best-fit graph, the enzyme kinetics and Michaelis-Menten options were

selected, so the polynomial equation used, namely,

$$Y = \frac{B_{max} \cdot X}{k_d + X}, \tag{2.4}$$

had the same form as the Michaelis-Menten equation (see (2.5) below). The goal of nonlinear regression is to find the best-fit values of the parameters; these were reported automatically with the best-fit curve and are presented in Table 2.1.

	K_M (mM)	V_{max} (mM/s)	k_{cat} (s^{-1})	R^2
Lineweaver-Burk plot	3.59 ($\pm$0.73)	0.0066 ($\pm$0.0012)	2899 ($\pm$560)	0.9876
Eadie-Hofstee plot	2.87($\pm$0.51)	0.0060($\pm$0.0006)	2643($\pm$264)	0.9143
Hanes plot	2.31($\pm$0.28)	0.0052($\pm$0.0003)	2291($\pm$132)	0.9926
Non-linear	2.52($\pm$1.09)	0.0058($\pm$0.0010)	2537($\pm$441)	0.9696

Table 2.1 – Calculated kinetic constants of a hydrogen peroxide reaction with horseradish peroxidase in buffer solution (pH= 6.8) (in parentheses are the standard errors).

In order to determine the enzyme rate constants K_M, k_{cat} and maximum velocity V_{max}, linearized models have been used such as Lineweaver-Burk (which was presented in Section 1.3.2) or alternative methods such as Eadie-Hofstee and Hanes plots. These models transform the Michaelis-Menten equation

$$V = \frac{V_{max} S}{K_M + S} \tag{2.5}$$

into a form that can be graphed as a straight line. Non-linear regression analysis, for instance, gives good quality results as it fits the best curve in the experimental

data using all the repetition values and not the mean values, and it does not involve any enlargement of the experimental errors. However, these methods require good balancing of the parameters and computational software and that is why most people generally continue to analyze their data using the linear methods. Therefore, all these different methods are used to calculate the solution phase rate constants of horseradish peroxidase and all of these results are presented in Table 2.1. All the values from the linear methods were calculated using linear regression analysis with 99% confidence intervals. The non-linear regression analysis results were calculated using 95% confidence intervals. The data presented in Table 2.1 and Figure 2.2, especially the R^2 and standard error values, indicate that the linear regression line is close to the mean experimental values and calculated values for Michaelis-Menten constants and catalytic turnovers derive a good level of precision since the standard errors are acceptable. The calculation is performed manually using the regression equation and its errors. Hanes and Eadie-Hofstee values are close to the values calculated by the non-linear regression analysis. Additionally, the calculated standard error values for both the Hanes and Eadie-Hofstee methods are lower than the Lineweaver-Burk method. These two methods were considered to have good accuracy and precision compared with the Lineweaver-Burk method. Our values are $K_M = 2.522$ mM and $V_{max} = 0.0058$ mM/s for hydrogen peroxide as the substrate, and are within the range of previously reported values and this allowed verification of the experimental procedure for the calculation of the rate constants and also confirmed the values which were proven by statistical analysis to show acceptable precision.

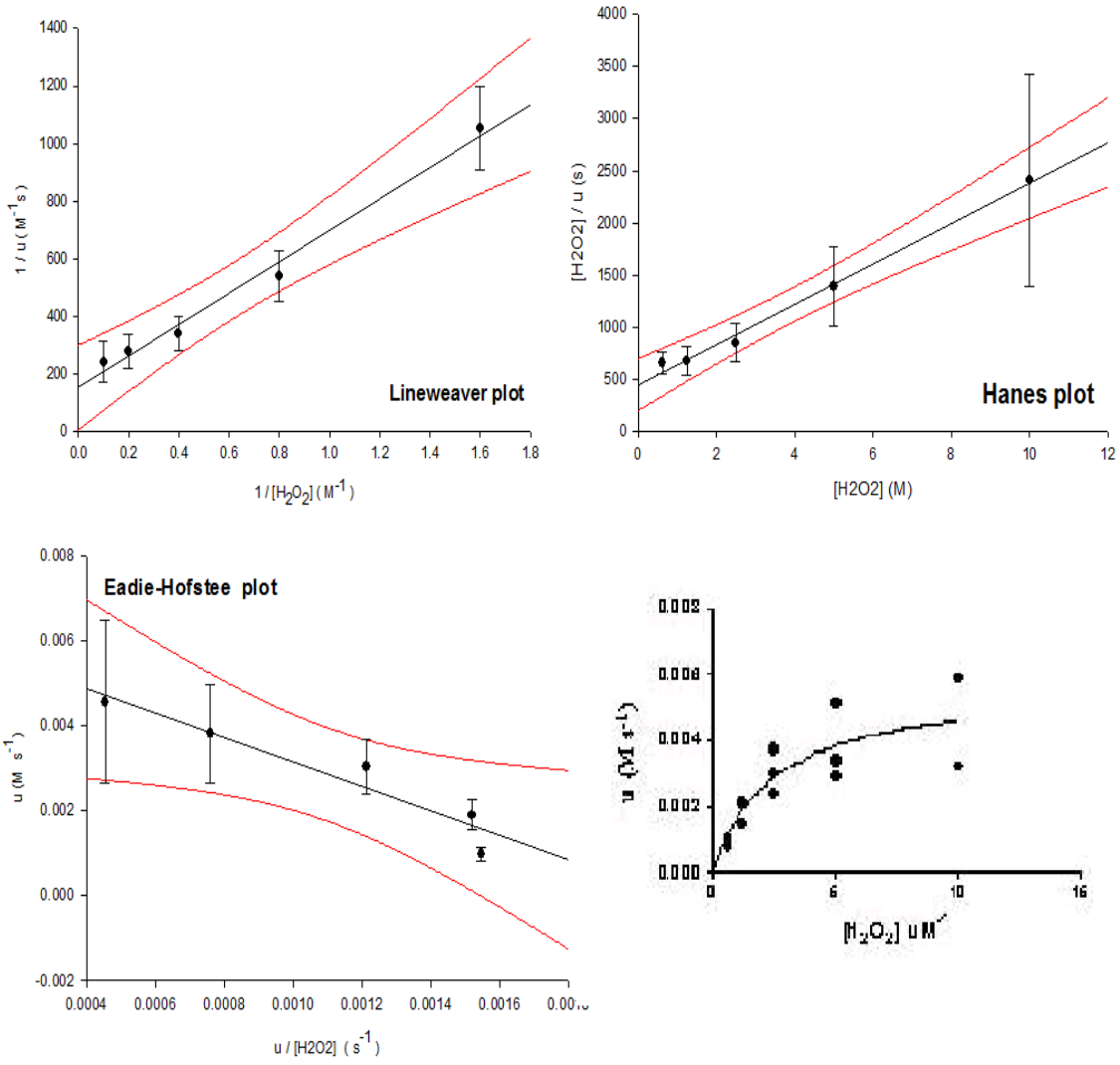

Figure 2.2 – Linearized and non-linearized treatments for calculation of the Michaelis-Menten rate constants ($n = 3$, $p = 0.01$). (a) Lineweaver plot: the reciprocal of reaction rate is plotted against the reciprocal of the concentration of the substrate; (b) Hanes plot: the ratio of the concentration of the substrate over the reaction rate is plotted over the concentration of the substrate; (c) Eadie-Hofstee plot: the reaction rate is plotted against the ratio of the reaction rate over the substrate concentration; (d) Non-linear regression fit.

Measurement of the theoretical enzyme surface concentration:

The enzyme surface concentration has units of mol/L which is derived from the equation

$$I = \frac{nFAL[E_t]k_{cat}K_s[S]}{[S] + K_sK_M}. \tag{2.6}$$

So after calculating the mass of the enzyme immobilized at the electrode surface with equation (2.3), the mass has to be converted into a concentration with a volume defined by the area of the electrode and the height of an enzyme monolayer. Assuming that the enzyme forms a monolayer on the electrode surface and that molecules form a uniform close packed structure, an approximate volume can be calculated by multiplying the electrode surface area ($A = 7.07 \times 10^{-6}$ m^2) with the enzyme's molecule diameter (5.2×10^{-9} m). The volume is calculated to be 3.7×10^{-14} m^3. Consequently, all the enzyme surface concentrations were calculated and the results are shown in Table 2.2.

The number of enzyme molecules which would form a monolayer on the defined electrode area, assuming a flat two-dimensional surface and employing a hexagonal close-packing sphere model, are calculated to be 9.5×10^{12} molecules. Nevertheless, this type of theoretical calculation of the molecules can overestimate the real number which forms a monolayer during immobilization.

S (mg/ml)	E (mM)	k_{cat} (s^{-1})	K_M (mM)	k_{cat}/K_M $(s^{-1}$ $(mM)^{-1})$
0.01	2.825	45.514	0.168	270.92
0.025	12.066	15.460	0.501	30.85
0.05	27.149	21.155	0.735	28.78
0.075	42.776	8.625	0.779	11.07
0.1	57.555	11.080	0.610	18.16
0.125	73.486	27.940	6.443	4.34
0.25	148.773	45.725	6.873	6.65

Table 2.2 – Typical values of solution HRP (S) and immobilized enzyme (E) concentrations and reaction constants.

2.2 A Model for Free Enzyme Diffusion

In this section we present a mathematical model for an enzyme-substrate reaction taking place while the reactants are free to diffuse inside a small cell. As usual, the reaction follows the Michaelis-Menten scheme

$$E + S \underset{k_{-1}}{\overset{k_1}{\rightleftarrows}} C \xrightarrow{k_{cat}} E + P. \tag{2.7}$$

Since the reaction takes place throughout the whole cell, it would be difficult (both experimentally and theoretically) to measure the electrical signal generated. This problem is therefore of little practical interest for biosensing applications but is included here for completeness. We assume that diffusion is one-dimensional so the physical domain is modelled as the interval $[0, L]$.

We model the situation where the enzyme is initially distributed uniformly throughout the cell, while the substrate is introduced at a given concentration near the top of the cell. The mathematical model consists of the following reaction-diffusion equations

$$\frac{\partial[E]}{\partial T} = D_e\frac{\partial^2[E]}{\partial X^2} + (k_{-1}+k_{cat})[C] - k_1[E][S], \tag{2.8}$$

$$\frac{\partial[S]}{\partial T} = D_s\frac{\partial^2[S]}{\partial X^2} + k_{-1}[C] - k_1[E][S], \tag{2.9}$$

$$\frac{\partial[C]}{\partial T} = D_c\frac{\partial^2[C]}{\partial X^2} - (k_{-1}+k_{cat})[C] + k_1[E][S], \tag{2.10}$$

$$\frac{\partial[P]}{\partial T} = D_p\frac{\partial^2[P]}{\partial X^2} + k_{cat}[C], \tag{2.11}$$

where $E(x,t)$, $S(x,t)$, $C(x,t)$ and $P(x,t)$ represent the concentration of enzyme, substrate, complex and product respectively at time t and position x, and D_s, D_p, D_e and D_c are the diffusion constants of the reaction. These equations are supplemented by zero-flux boundary conditions at both ends of the diffusion cell, namely;

$$\frac{\partial S}{\partial x}(L,t) = \frac{\partial P}{\partial x}(L,t) = \frac{\partial E}{\partial x}(L,t) = \frac{\partial C}{\partial x}(L,t) = 0,$$
$$\frac{\partial S}{\partial x}(0,t) = \frac{\partial P}{\partial x}(0,t) = \frac{\partial E}{\partial x}(0,t) = \frac{\partial C}{\partial x}(0,t) = 0,$$

with initial conditions as described above,which are;

$$E(x,0) = E_0, \quad \text{for all } x \in [0,L], \tag{2.12}$$

$$S(x,0) = \begin{cases} S_0, & x = L \qquad (2.13a) \\ 0, & \text{otherwise,} \qquad (2.13b) \end{cases}$$

$$C(x,0) = P(x,0) = 0. \tag{2.14}$$

The system of equations described above is solved numerically using a standard finite difference scheme. Numerical values for all parameters are shown in Table 2.3 and the

time evolution of the concentration profiles for all reactants and products is shown in Figures 2.3, 2.4, 2.5 and 2.6. Note that values for the kinetic constants K_M and k_{cat} are chosen in accordance with our results presented in Section 2.1 (see Table 2.1).

Description	***Constant***	***Value***
Diffusion layer depth (m)	L	14×10^{-3}
Diffusion constants (m^2/s):		
Substrate	D_s	1.5×10^{-9}
Enzyme	D_p	7.05×10^{-11}
Complex	D_e	7.05×10^{-11}
Product	D_c	2.3×10^{-9}
Reaction rate constant ($m^3/mol{\cdot}s$)	k_1	10^2
Reaction rate constants (s^{-1})	k_{-1}	10^{-1}
Constant s^{-1}	k_{cat}	45.7
Michaelis-Menten constant (mM)	K_M	2.52
Initial concentrations:		
Total enzyme (mol/m^2)	E_0	7.768×10^{-7}
Substrate (mol/m^3=mM)	S_0	0.25

Table 2.3 – Typical values for constants.

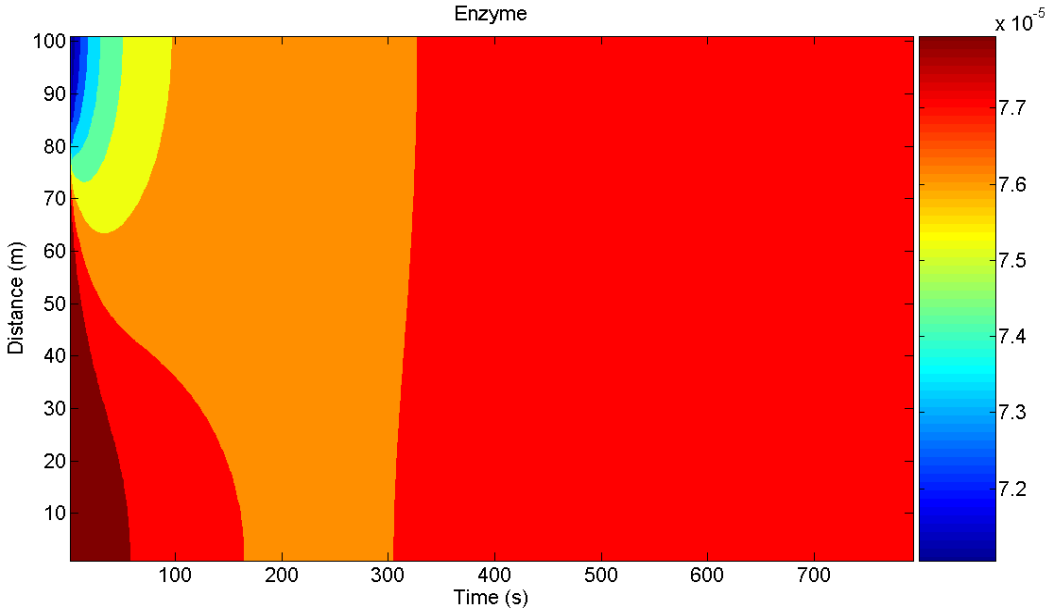

Figure 2.3 – Time evolution of enzyme.

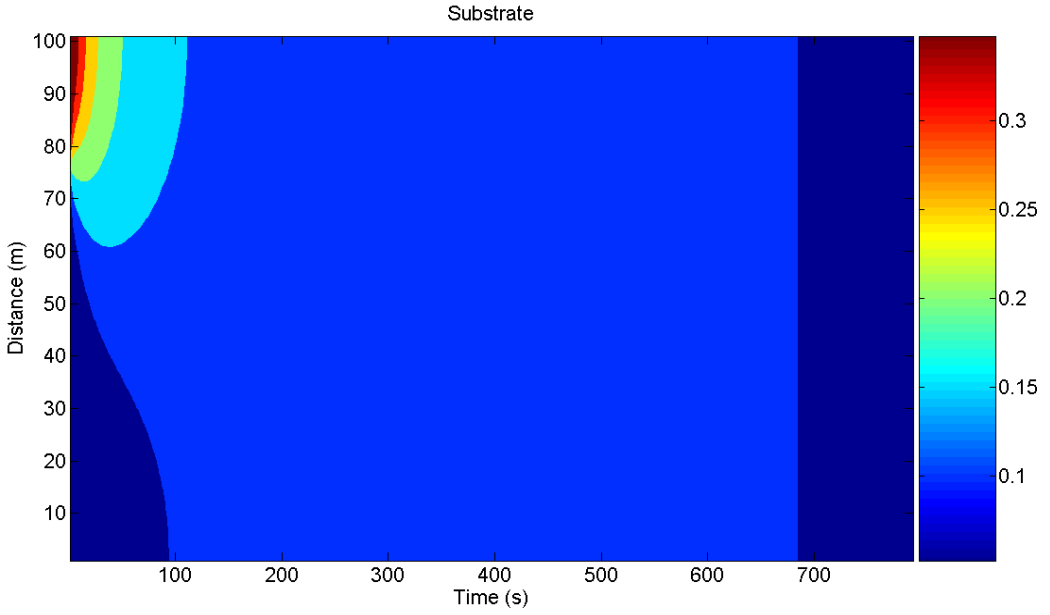

Figure 2.4 – Time evolution of substrate.

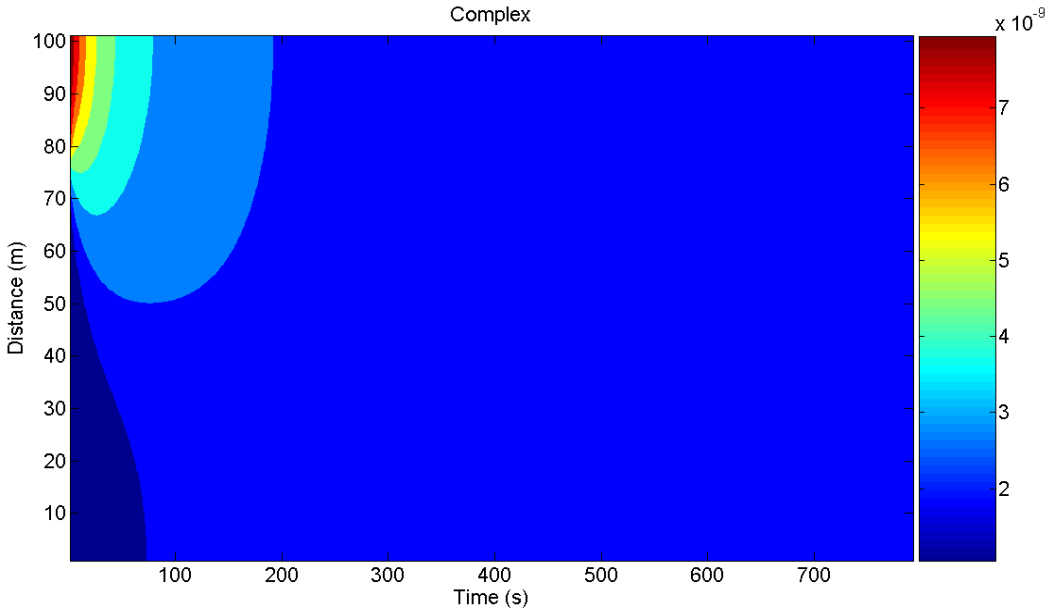

Figure 2.5 – Time evolution of complex.

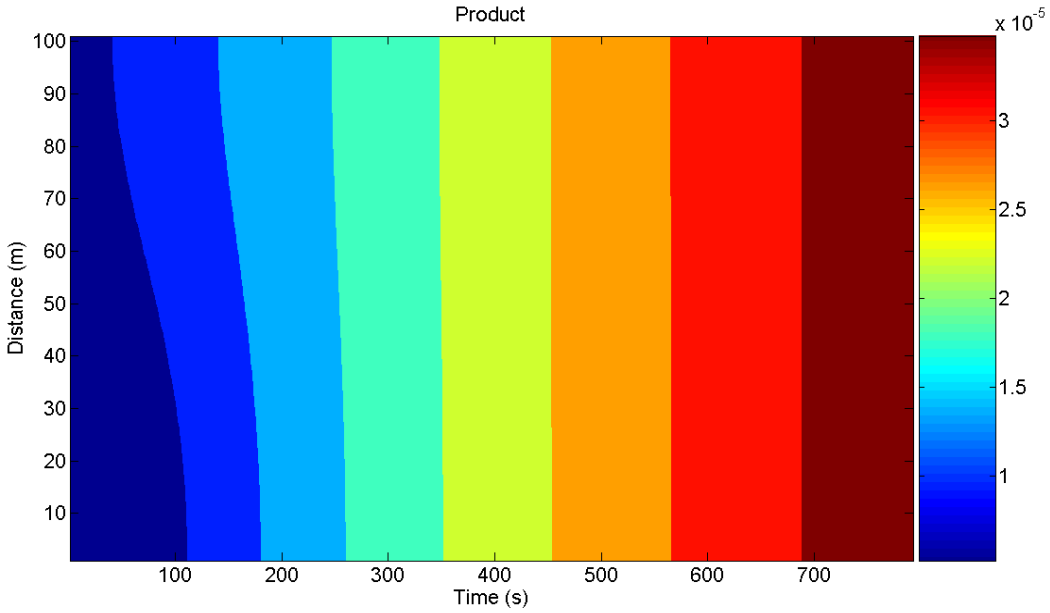

Figure 2.6 – Time evolution of product.

2.3 Modelling Experimental Configurations Involving Immobilized Enzymes

In this section we assume that enzyme is immobilized on the surface of an electrode, which is placed at the bottom of a cell. We are going to examine three models corresponding to three experiments carried out in this setting, with different initial conditions. In all three experiments, the physical processes taking place are diffusion of substrate through the cell, followed by reaction of substrate with the immobilized enzyme at the electrode. The enzyme-substrate interaction is modelled by the Michaelis-Menten scheme (2.7) and is an example of a so-called surface-volume reaction, which involves a free moving species and an immobilized one. Note that the complex once formed, is also surface-bound, while the product P is free to diffuse. As usual, we assume the rate of formation of product at the electrode is proportional to the current measured experimentally.

We assume the enzyme forms a monolayer on the electrode, so that all reactions occur at the lower boundary of the diffusion domain. For simplicity we also assume the model to be one-dimensional, where the spatial variable measures distance from the electrode, $x = 0$ corresponds to the electrode boundary while $x = L$ is the upper cell surface. The following notations are used:

- $E(t)$: enzyme concentration;
- $S(x,t)$: substrate concentration;
- $C(t)$: complex concentration;

- $P(x,t)$: final product concentration.

The mathematical model consists of the following diffusion equations for substrate and product plus boundary conditions of reactive type at the electrode (i.e., at $x = 0$):

$$\frac{\partial S}{\partial t} = D_s \frac{\partial^2 S}{\partial x^2}, \quad 0 \le x \le L, \quad t \ge 0, \tag{2.15}$$

$$\frac{\partial P}{\partial t} = D_p \frac{\partial^2 P}{\partial x^2}, \quad 0 \le x \le L, \quad t \ge 0, \tag{2.16}$$

$$D_s \frac{\partial S}{\partial x}(0,t) = k_1 ES - k_{-1} C, \tag{2.17}$$

$$D_p \frac{\partial P}{\partial x}(0,t) = k_{cat} C(0,t), \tag{2.18}$$

$$\frac{dE}{dt} = -k_1 ES + (k_{-1} + k_{cat})C, \tag{2.19}$$

$$\frac{dC}{dt} = k_1 ES - (k_{-1} + k_{cat})C. \tag{2.20}$$

In addition, we have the enzyme conservation law $E + C = E_0$, where E_0 is the initial concentration of enzyme. The boundary conditions at $x = L$ and initial conditions will be different for each of the three experiments we shall consider and they will be specified later.

2.3.1 Experiment 1: Finite Substrate Addition

The first experiment assumes that a finite amount of substrate is added to the cell at time $t = 0$, at a point close to the free surface as shown in Figure 2.7. We model this situation by adding initial conditions

$$S(x,0) = \begin{cases} S_0, & \text{if } x = L \\ 0, & \text{otherwise,} \end{cases}$$

$$E(0) = E_0, \quad C(0) = 0, \quad P(x,0) = 0, \tag{2.21}$$

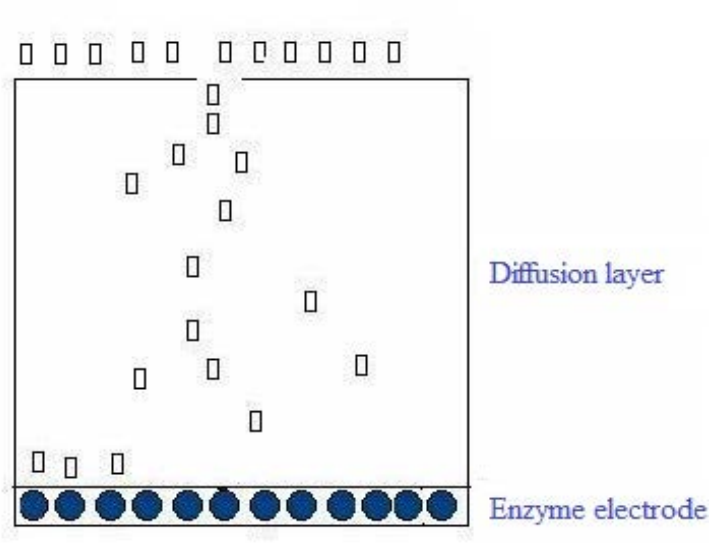

Figure 2.7 – A schematic representation of Experiment 1, where substrate is introduced at a single point in the cell.

and boundary conditions

$$D_s \frac{\partial S}{\partial x}(L,t) = 0, \quad D_p \frac{\partial P}{\partial x}(L,t) = 0, \tag{2.22}$$

to the generic diffusion equations and boundary conditions (2.15)-(2.20). Zero-flux boundary conditions are assumed at the free surface since no chemical species can leave the solution. A standard finite difference method is used to solve the system of equations (2.15)-(2.20) and some numerical solutions are shown in Figures 2.8 and 2.9. We use the numerical values displayed in Table 2.4.

Figure 2.8 illustrates the time evolution of the two spatially dependent species, product and substrate. (The values on the vertical axis represent distance from the electrode.) Figure 2.9 shows the time evolution of the current intensity as a

Description	***Constant***	***Exp. 1***	***Exp. 2***	***Exp. 3***
Diffusion layer depth (m)	L	14×10^{-3}	14×10^{-3}	14×10^{-3}
Diffusion constants (m^2/s)				
Substrate	D_s	1.5×10^{-9}	1.5×10^{-9}	1.5×10^{-9}
Product	D_p	2.3×10^{-9}	2.3×10^{-9}	2.3×10^{-9}
Reaction rate constant (m^3/mol·s)	k_1	10^2	10^2	10^2
Reaction rate constants (s^{-1})	k_{-1}	10^{-1}	10^{-1}	10^{-1}
	k_{cat}	45.7	27.9	45.7
Michaelis-Menten constant (mM)	K_M	6.78	6.44	6.78
Initial concentrations				
Total enzyme (mol/m^2)	E_0	7.87×10^{-7}	3.768×10^{-7}	7.87×10^{-7}
Substrate (mol/m^3=mM)	S_0	$0.1 - 0.5$	$0.05 - 0.25$	$0.1 - 0.5$

Table 2.4 – Typical values for constants.

function of time, from numerical integration of the mathematical model (left) and experimental measurements (right). The maximum values of these curves are then plotted as functions of the substrate concentrations in Figure 2.10.

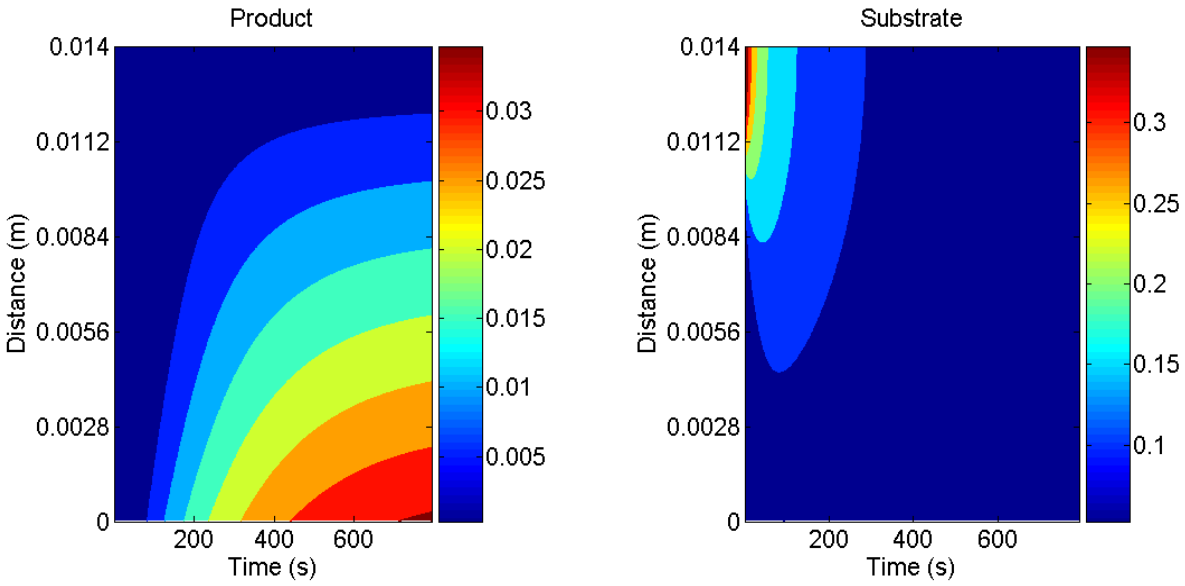

Figure 2.8 – Product and substrate concentration gradients in Experiment 1.

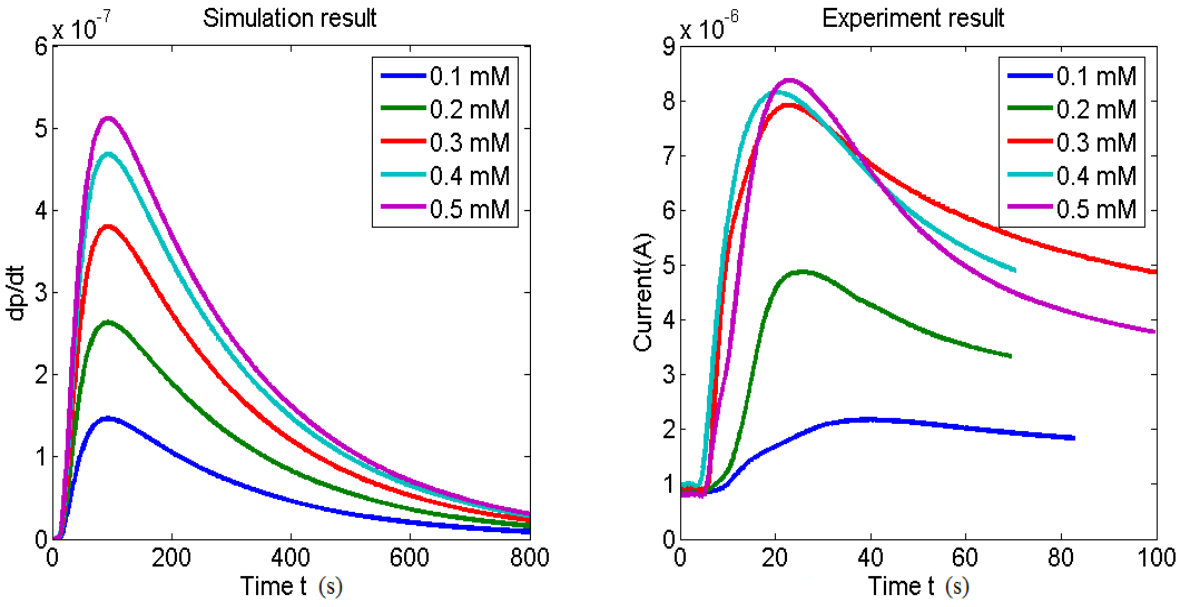

Figure 2.9 – Current profile as a function of time for different substrate concentrations (Experiment 1).

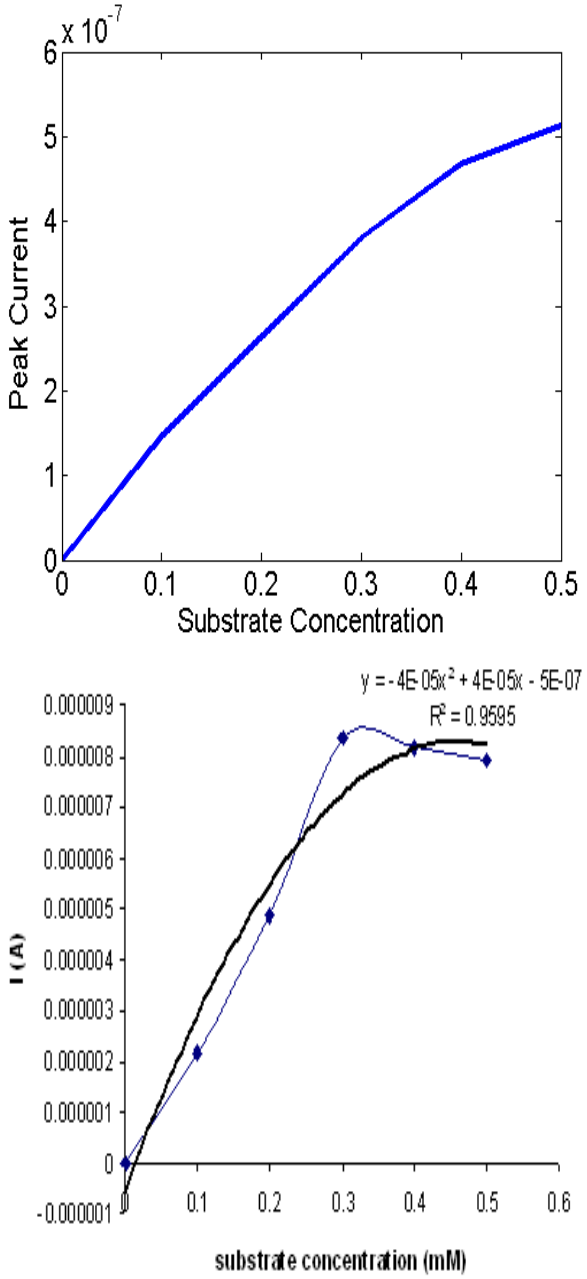

Figure 2.10 – Comparison between the simulation results (top) and experimental data (bottom) for recorded peak current intensity as a function of substrate concentration (Experiment 1).

2.3.2 Experiment 2: Uniformly Distributed Substrate

The second experiment assumes that a finite amount of substrate is uniformly distributed into the cell at time $t = 0$ as shown in Figure 2.11. In this experimental

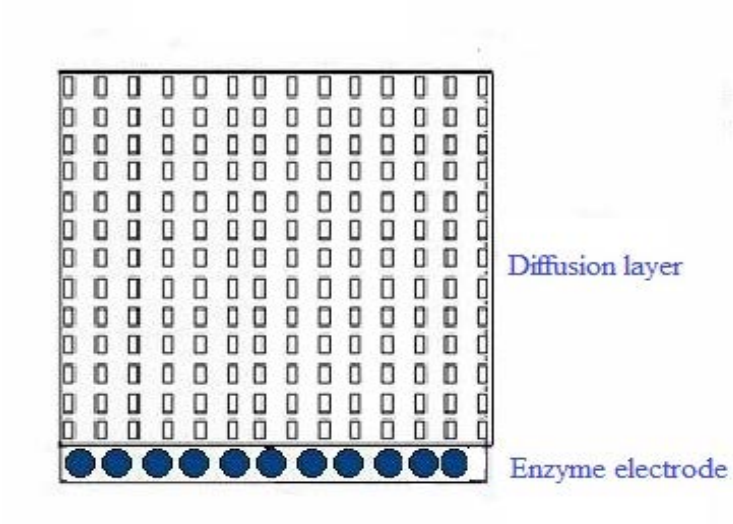

Figure 2.11 – A schematic representation of Experiment 2, where substrate is uniformly distributed.

setting, the substrate and enzyme are initially separated by a thin board but after removing the board, they react with each other and product is formed. We model this situation using the following initial and boundary conditions:

$$E(0) = E_0, \quad S(x,0) = S_0, \quad C(0) = 0, \quad P(x,0) = 0, \tag{2.23}$$

$$D_s \frac{\partial S}{\partial x}(L,t) = 0, \quad D_p \frac{\partial P}{\partial x}(L,t) = 0. \tag{2.24}$$

Once again, we use the numerical values displayed in Table 2.4. Figure 2.12 shows the time evolution of product and substrate concentrations throughout the cell (in this simulation, we use $S_0 = 1$.). Again, Figure 2.13 shows a comparison between the

simulation results and experimental data for the time evolution of recorded current intensity, while Figure 2.14 plots the maximum values of these currents as functions of initial substrate concentration.

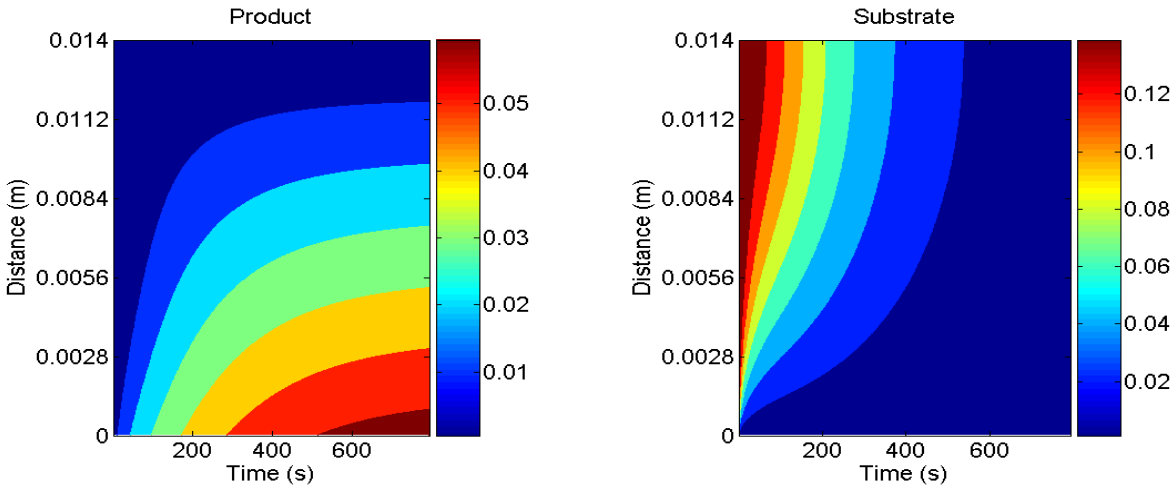

Figure 2.12 – Product and substrate concentration gradients in Experiment 2.

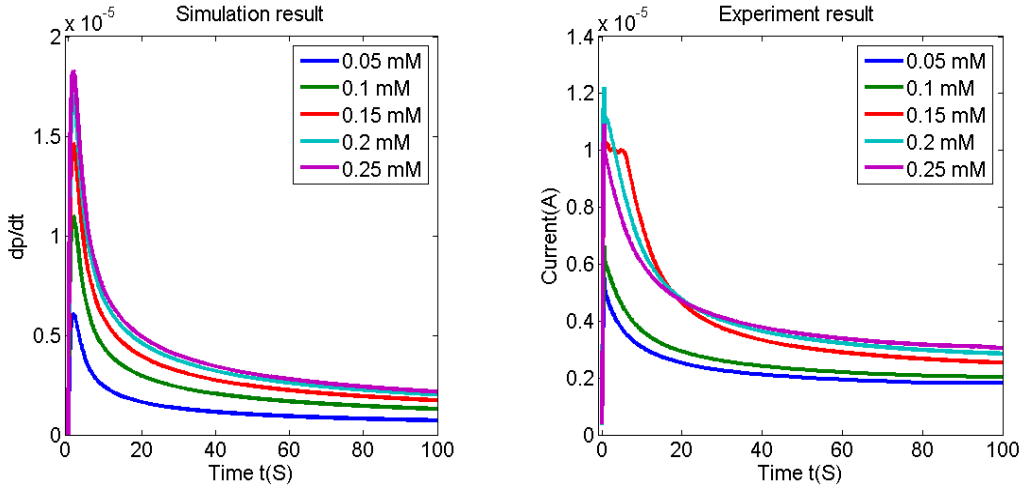

Figure 2.13 – Current profile as a function of time for different substrate concentrations (Experiment 2).

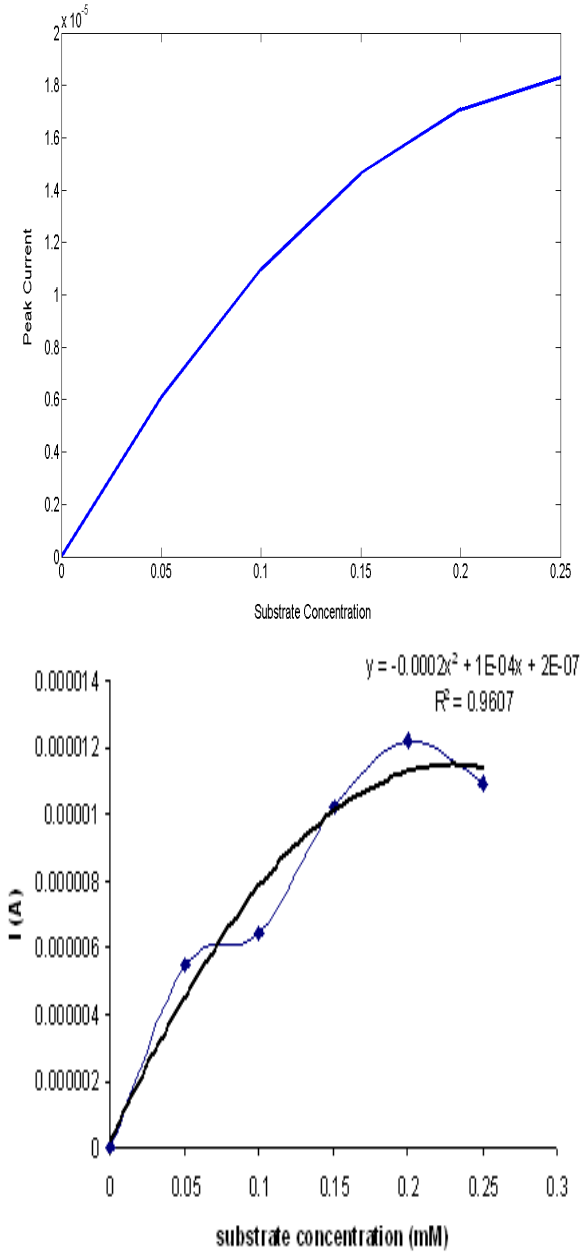

Figure 2.14 – Comparison between the simulation results (top) and experimental data (bottom) for recorded peak current intensity as a function of substrate concentration (Experiment 2).

2.3.3 Experiment 3: Flow Injection Analysis

The third experiment is a flow injection analysis (FIA) as shown in Figure 2.15, where

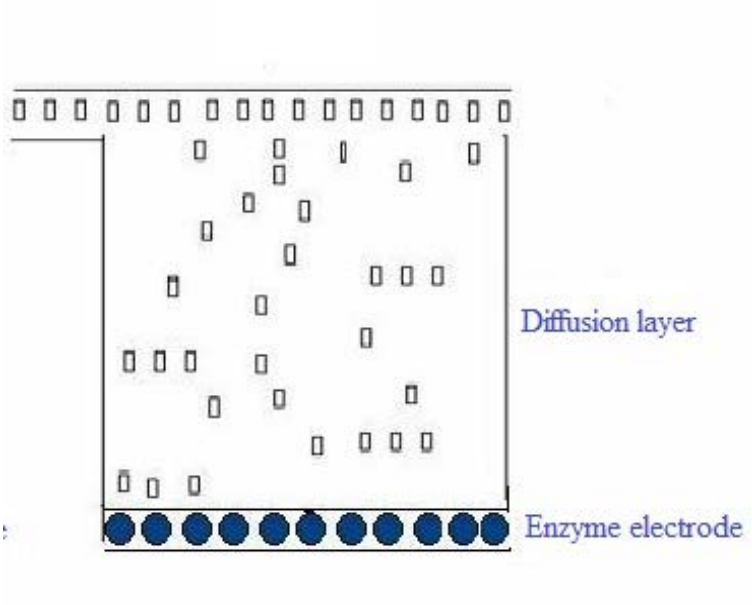

Figure 2.15 – A schematic representation of Experiment 3, a flow injection analysis.

substrate solutions of different concentrations are passed over the electrode and the corresponding currents are recorded. In this section we do not model the flow effect and the existence of the convective zone is only reflected by the boundary conditions imposed at the top of the diffusion layer. A more detailed analysis of a similar experiment, which includes modelling diffusion and convection, is given in Chapter 4. The system of equations (2.15)-(2.20) are now supplemented by the following initial conditions and surface boundary conditions:

$$S(x,0) = \begin{cases} S_0, & \text{if } x = L \\ 0, & \text{otherwise,} \end{cases}$$

$$E(0) = E_0, \quad C(0) = 0, \quad P(x,0) = 0, \tag{2.25}$$

$$S(L,t) = S_0, \quad P(L,t) = 0. \tag{2.26}$$

These boundary conditions express the fact that the substrate concentration at the top of the diffusion layer is kept constant by the flow, while the product is continuously flushed away, so its surface concentration is zero. The numerical values for all constants used in simulations of Experiment 3 can be found in Table 2.4. Figure 2.16 shows the time evolution of product and substrate concentrations throughout the cell. Figure 2.17 shows the time evolution of the recorded current as calculated from the numerical simulations (left) and measured experimentally (right). The reason why the curves are different in the two pictures is that, at the time when the experimental work was carried out, a continuous flow of substrate through the cell could not be achieved so a finite amount of H_2O_2 was used instead. As a consequence, the current profile reaches a peak and then decays (once the flow of substrate is diminished) in contrast with the model simulation where due to a constant concentration of substrate, the signal steady state is maintained. However, if we compare the maximum values of these signals, Figure 2.18 shows a reasonable similarity between simulation and experiment.

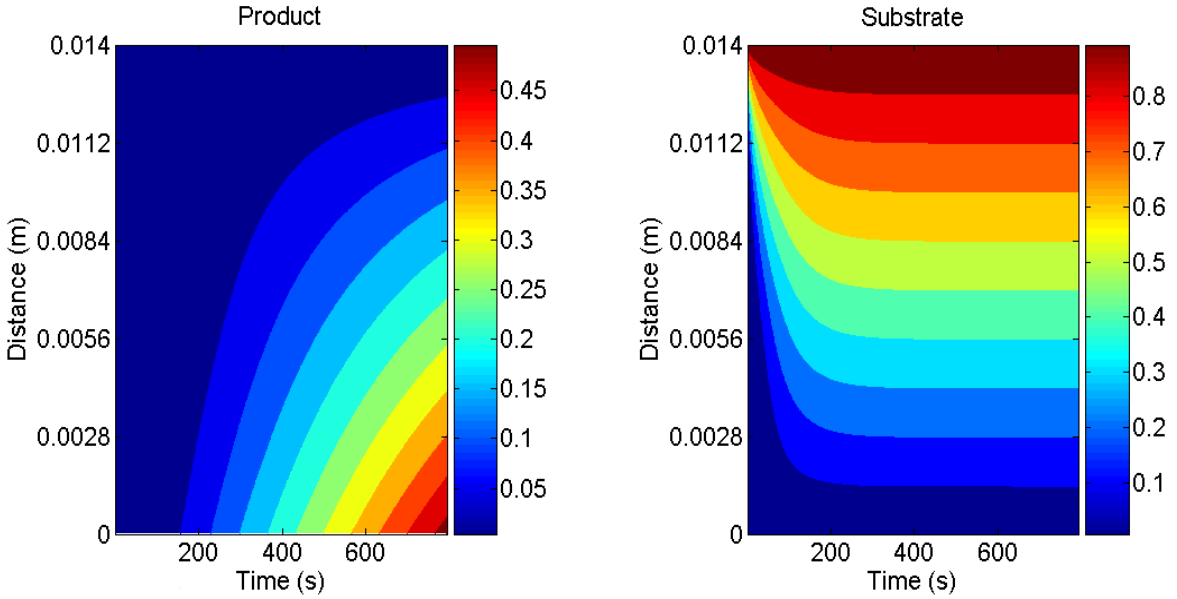

Figure 2.16 – Product and substrate concentration gradients in Experiment 3.

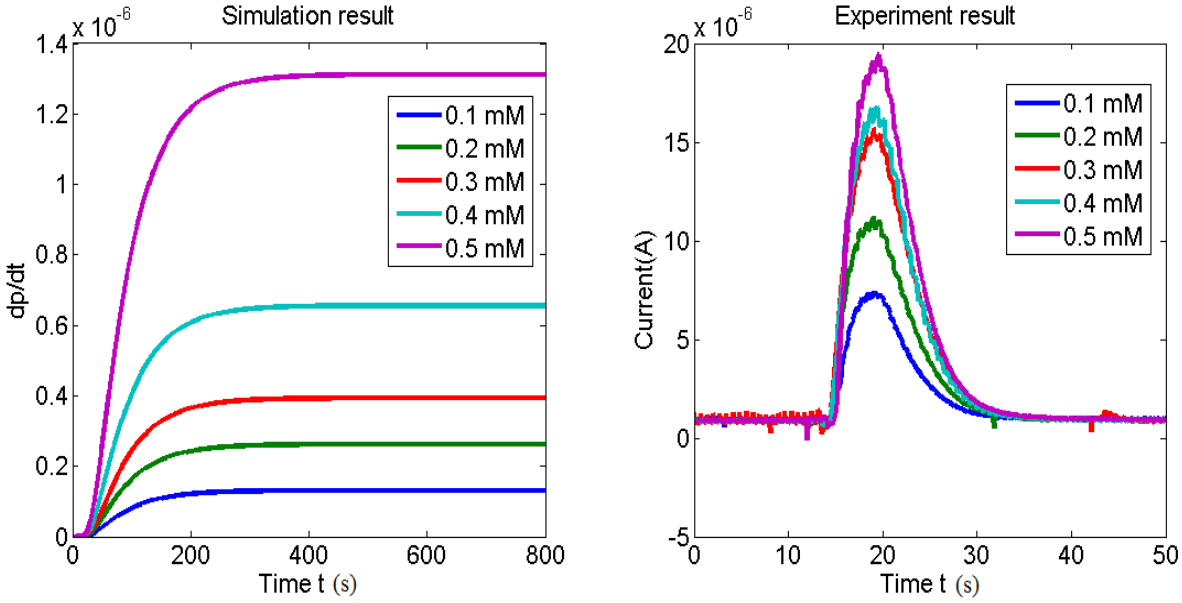

Figure 2.17 – Current profile as a function of time for different substrate concentrations (Experiment 3).

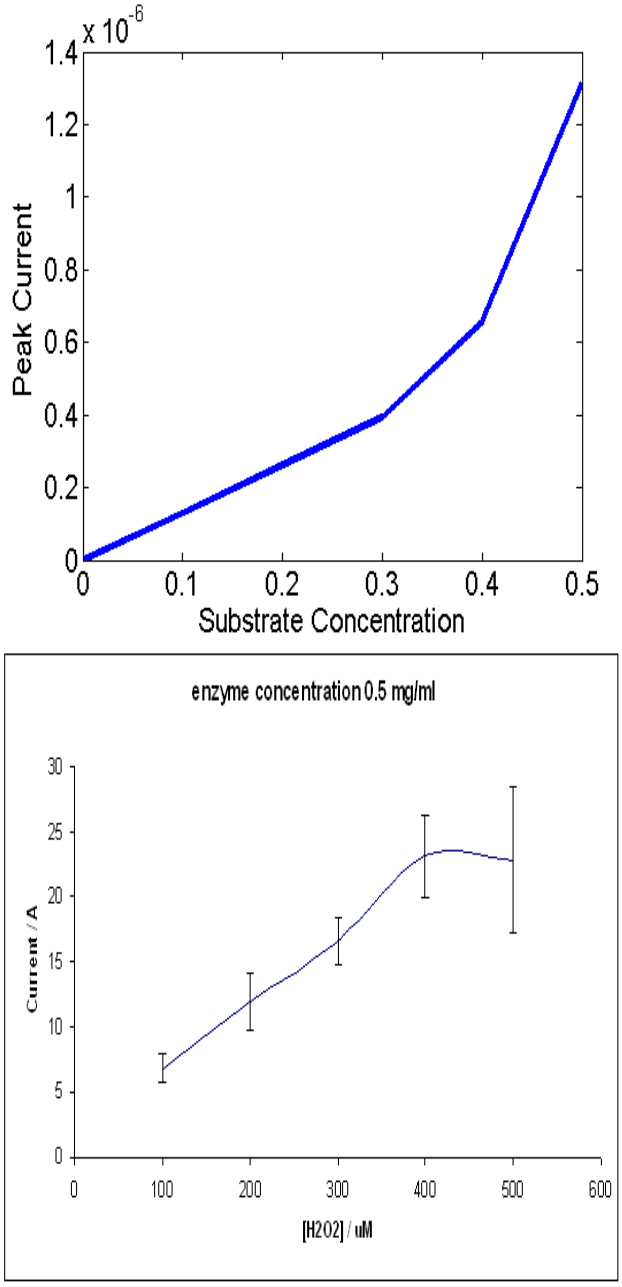

Figure 2.18 – Comparison between the simulation results (top) and experimental data (bottom) for recorded peak current intensity as a function of substrate concentration (Experiment 3).

2.4 Conclusions

We presented a method for determining Michaelis-Menten kinetic constants (K_M, k_{cat} and V_{max}) for horseradish peroxidase immobilized at a conduction polymer-modified electrode, based on experimental work and statistical analysis. It was found that, in general, immobilized enzyme is much less efficient at converting substrate than enzyme in solution. Possible explanations include conformational changes of the enzyme during deposition or obstruction of its active sites at the polymer-enzyme interface.

The mass of immobilized enzyme was correlated with concentrations derived from solution-phase enzyme assays and the results presented in Table 2.1 indicated that this mass has a significant impact on the rate constants. It was also found that the enzyme efficiency is greater at lower enzyme loadings, possibly because enzyme activity is negatively influenced by adjacent molecules on the immobilization surface.

We then presented three simple experimental problems and related mathematical models. The immobilized enzyme concentration was carefully matched with kinetic rate constant values, for both experimental work and numerical simulations. The results show good agreement.

Chapter 3

Biomolecular Interactions

Biomolecular interactions are central to understanding disease mechanisms and devising safe and effective drugs. In this chapter we introduce mathematical models for antibody-antigen interactions which are relevant to immunosensors. We look at the kinetics of the binding reaction in a direct assay and then study two problems where the antibody is bound to a surface while the antigen is transported by diffusion alone in a small cell or convected in the BIACORE device. The BIACORE modelling framework introduced here will be relevant to the flow injection experiment discussed in Chapter 4.

3.1 Kinetics of Antibody-Antigen Interactions

As mentioned in Section 1.1.2, immunosensors involve a binding reaction between an analyte and at least one antibody (see Figure 3.1). We begin this chapter by analyzing the kinetics of this simple reaction which lies at the heart of all (direct,

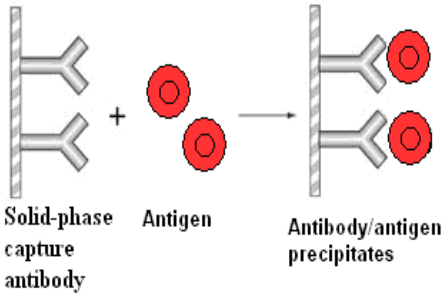

Figure 3.1 – Antibody-antigen interactions.

competitive or sandwich) immunoassays.

The antibody-antigen interactions can be expressed symbolically by the following reaction equation

$$A + B \underset{k_{-1}}{\overset{k_1}{\rightleftarrows}} P, \tag{3.1}$$

where A represents the antigen, B represents the antibody, and P represents the product of antibody and antigen. Reaction (3.1) has a forward (association) reaction rate of k_1 and a backward (dissociation) reaction rate of k_{-1}, where the forward reaction rate is very large (approximately 1000 times bigger than the reaction rate constant k_1 in the Michaelis-Menten kinetics) while the backward reaction is very slow and is therefore often neglected. This fact reflects the high affinity between antigen and its corresponding antibody.

The dynamics of the system are described by the following system of ordinary differential equations

$$\frac{dA}{dt} = -k_1AB + k_{-1}P, \tag{3.2}$$

$$\frac{dB}{dt} = -k_1AB + k_{-1}P, \tag{3.3}$$

$$\frac{dP}{dt} = k_1AB - k_{-1}P, \tag{3.4}$$

with initial conditions $A(0) = A_0$, $B(0) = B_0$ and $P(0) = 0$, where A_0 and B_0 are constants. Note that in the system of equations (3.2)-(3.4),

$$\frac{dA}{dt} + \frac{dP}{dt} = 0 \quad \text{and} \quad \frac{dB}{dt} + \frac{dP}{dt} = 0;$$

these together with the initial conditions give the associated conservation laws,

$$A + P = A_0, \quad B + P = B_0. \tag{3.5}$$

Since the equilibrium values A^*, B^* and P^* can be measured experimentally, we can determine that

$$\frac{k_1}{k_{-1}} = \frac{P^*}{A^*B^*}.$$

Using the above conservation laws, equations (3.2)-(3.4) can be reduced to a single equation in terms of P and is given as follows,

$$\frac{dP}{dt} = k_1(A_0 - P)(B_0 - P) - k_{-1}P. \tag{3.6}$$

The equilibrium value, P^*, is given by the smaller root of the quadratic equation

$$P^2 - P(A_0 + B_0 + \frac{k_{-1}}{k_1}) + A_0B_0 = 0, \tag{3.7}$$

since we must select the root that satisfies $P^* < \min(A_0, B_0)$. This gives the equilibrium product, P^*, as a function of initial antigen concentration A_0 (where B_0 is fixed)

and plotting this relationship will produce an increasing calibration curve which is the characteristic of direct assays.

3.2 A Diffusion Model for Antibody-Antigen Interactions

In this section we present a model for a simple experiment where the two species antibody and antigen are contained within a small cell, which we represent mathematically as a one-dimensional spatial domain. More specifically, we consider the case where the antibody is immobilized on a surface while the antigen is free to diffuse. The interaction of the two species is governed by an equation of type (3.1). A similar problem was presented in [22] and [23], where it was presented as a simplified analysis (ignoring competitive effects) of a Fluorescence Capillary-Fill Device, a type of pregnancy test studied in [3]. The time evolution of the antigen concentration, $A(x,t)$, can be described by the diffusion equation

$$\frac{\partial A}{\partial t} = D\frac{\partial^2 A}{\partial x^2}, \quad x \in (0,L), \quad t \geq 0, \tag{3.8}$$

where $x = 0$ represents the immobilization surface while $x = L$ is the free surface of the cell. We assume that, initially, the antigen is uniformly distributed throughout the cell; hence

$$A(x,0) = A_0. \tag{3.9}$$

The boundary conditions are:

$$\frac{\partial A}{\partial x}(L,t) = 0, \tag{3.10}$$

$$D\frac{\partial A}{\partial x}(0,t) = k_{-1}P(t) - k_1 A(0,t)B(t), \tag{3.11}$$

where $B(t)$ is the concentration of immobilized antibody and $P(t)$ is the concentration of product. Note that we also have the kinetic equations

$$\frac{dB}{dt} = -\frac{dP}{dt} = k_{-1}P(t) - k_1 A(0,t)B(t), \tag{3.12}$$

with initial conditions

$$B(0) = B_0, \quad P(0) = 0. \tag{3.13}$$

This model can be written solely in terms of $A(x,t)$ by using the antigen conservation law

$$\int_0^L A(x,t)dx + P(t) = \text{constant}, \tag{3.14}$$

which gives

$$P(t) = A_0 L - \int_0^L A(x,t)dx. \tag{3.15}$$

A similar conservation law for antibody gives

$$B(t) + P(t) = \text{constant}, \tag{3.16}$$

hence

$$B(t) = B_0 - P(t) = B_0 - A_0 L + \int_0^L A(x,t)dx. \tag{3.17}$$

Substituting $B(t)$ and $P(t)$ into our original model, yields:

$$\frac{\partial A}{\partial t} = D\frac{\partial^2 A}{\partial x^2}, \tag{3.18}$$

$$A(x,0) = A_0, \tag{3.19}$$

$$\frac{\partial A}{\partial x}(L,t) = 0, \tag{3.20}$$

$$D\frac{\partial A}{\partial x}(0,t) = k_{-1}P(t) - k_1 A(0,t)(B_0 - P(t)), \tag{3.21}$$

$$P(t) + \int_0^L A(x,t)dx = A_0 L. \tag{3.22}$$

The model can be non-dimensionalised by introducing the variables

$$\bar{x} = \frac{x}{L}, \quad \bar{t} = \frac{Dt}{L^2}, \quad a(\bar{x},\bar{t}) = \frac{LA(x,t)}{B_0}, \quad b(\bar{t}) = \frac{B(t)}{B_0}, \quad p(\bar{t}) = \frac{P(t)}{B_0}. \tag{3.23}$$

As a consequence, equations (3.8) to (3.13) become

$$\frac{\partial a}{\partial t} = \frac{\partial^2 a}{\partial x^2}, \quad x \in (0,1), \quad t \geq 0, \tag{3.24}$$

$$\frac{\partial a}{\partial x}(1,t) = 0, \tag{3.25}$$

$$\frac{\partial a}{\partial x}(0,t) = \alpha p(t) - \beta a(0,t)b(t), \tag{3.26}$$

$$\frac{\partial b}{\partial t}(t) = -\frac{\partial p}{\partial t}(t) = \alpha p(t) - \beta a(x,t)b(t), \tag{3.27}$$

where

$$\alpha = \frac{k_{-1}L^2}{D}, \quad \beta = \frac{k_1 L B_0}{D}, \tag{3.28}$$

with initial conditions

$$a(x,0) = a_0 = \frac{A_0 L}{B_0}, \quad b(0) = 1, \quad p(0) = 0, \tag{3.29}$$

where we have dropped the bars for convenience. The equations (3.18) to (3.22)

become

$$\frac{\partial a}{\partial t} = \frac{\partial^2 a}{\partial x^2}, \quad x \in (0,1), \quad t \geq 0, \tag{3.30}$$

$$\frac{\partial a}{\partial x}(1,t) = 0, \tag{3.31}$$

$$\frac{\partial a}{\partial x}(0,t) = \alpha p(t) - \beta a(0,t)[1-p(t)], \tag{3.32}$$

$$p(t) + \int_0^1 a(x,t)dx = a_0. \tag{3.33}$$

A detailed mathematical analysis of this model for antibody-antigen interactions is given in [30] and [31] for the purpose of proving existence and uniqueness of solutions. It is also shown that the diffusion equation and associated boundary conditions for $A(x,t)$ can be written in an equivalent form as a system of coupled Volterra integro-differential equations involving the unknown functions

$$\phi_1(t) = a(0,t), \tag{3.34}$$

$$\phi_2(t) = \int_0^1 a(x,t)dx, \tag{3.35}$$

which are then solved numerically. We now give a numerical solution for this model by integrating equations (3.8)-(3.13) directly using a finite difference scheme. The parameter values used in this numerical simulation are supplied by our BDI/NCSR collaborators and are shown in Table 3.1. Note that the ratio between the association and dissociation rates, k_1/k_{-1} is of order 10^5 $\mathrm{m}^3/\mathrm{mol}$, which is consistent with literature values for generic biomolecular interactions.

Figure 3.2 shows the antigen concentration as a function of time and distance from the reaction boundary. Figure 3.3 shows the time evolution of the bound product for different values of the initial antigen concentration; the steady-states obtained in

Description	***Constant***	***Value***
Diffusion layer depth (m)	L	2×10^{-3}
Diffusion constant (m^2/s)	D_s	1.5×10^{-9}
Reaction rate constant ($m^3/mol{\cdot}s$)	k_1	10^2
Reaction rate constant (s^{-1})	k_{-1}	10^{-3}
Initial concentrations:		
Antibody (mol/m^2)	B_0	3.768×10^{-7}
Antigen (mol/m^3=mM)	A_0	$0 - 10^{-3}$

Table 3.1 – Typical values for constants.

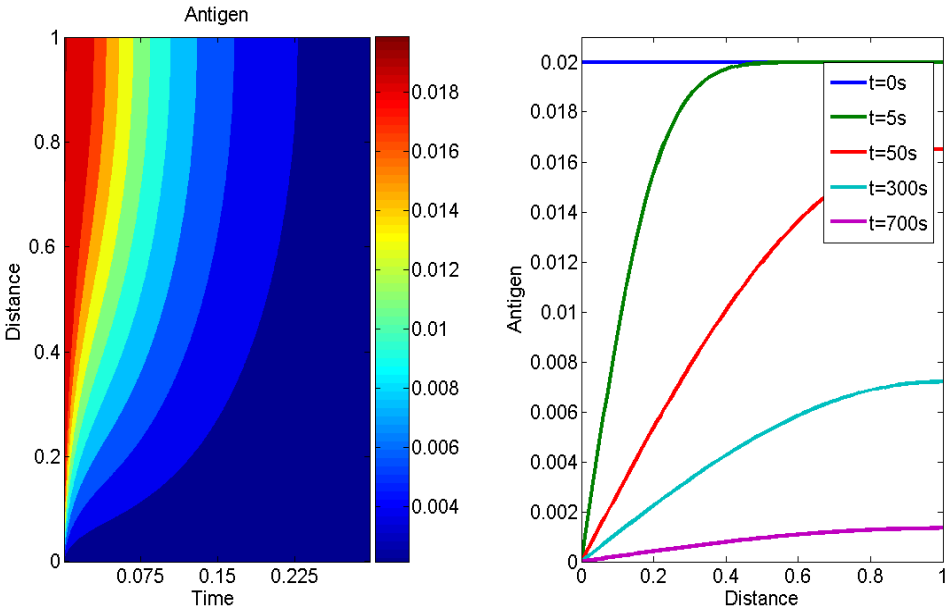

Figure 3.2 – Time evolution of the antigen concentration gradient across the cell.

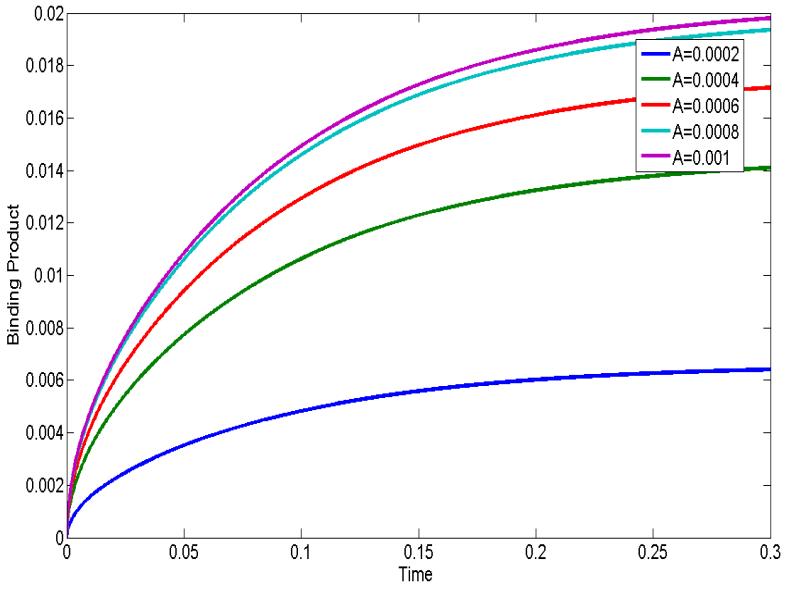

Figure 3.3 – Dependence of binding product on time for different A_0.

the simulation are subsequently used for constructing the calibration curve shown in Figure 3.4. Finally, Figure 3.5 shows the time evolution of the functions $\phi_1(t)$ (the antigen concentration at the reactive surface) and $\phi_2(t)$ (the total amount in the cell); these profiles are similar to those obtained in [22].

3.3 Mathematical Modelling for BIACORE

One of the most widely used optical biosensors is the BIACORE instrument which is used for real-time determination of reaction rates for biomolecular interactions. The operation of this instrument is based on an optical phenomenon called Surface Plasmon Resonance (SPR) to monitor the interaction between a surface-bound molecule (called the ligand) and an analyte contained in a solution sample which is passed over the surface. The SPR response is a measure of the refractive index at the surface

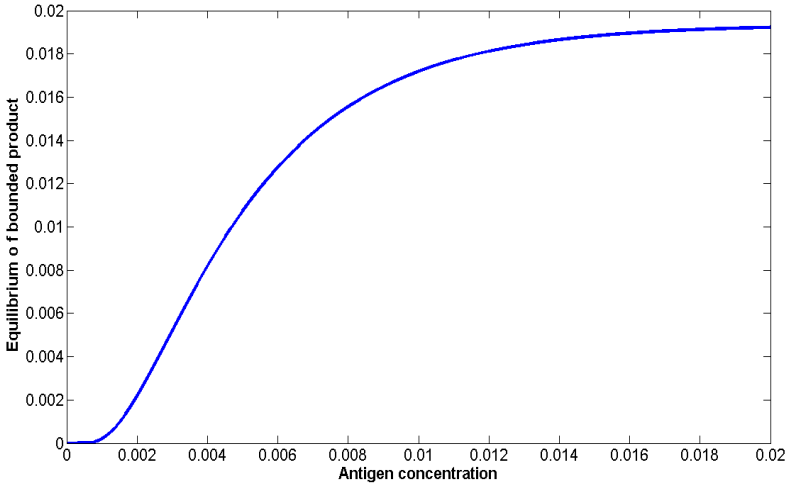

Figure 3.4 – Calibration curve for antigen.

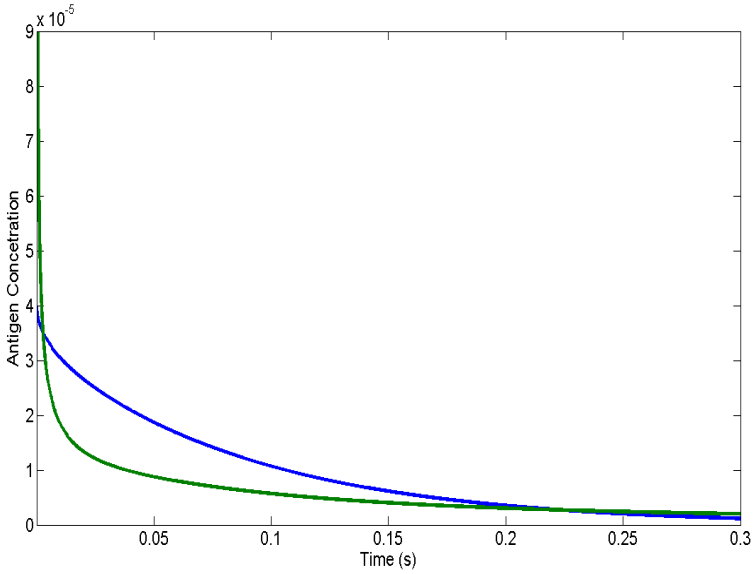

Figure 3.5 – Time evolution of the functions $\phi_1(t)$ (blue curve) and $\phi_2(t)$ (green curve).

of the sensor chip and is therefore directly related to the concentration of analyte bound to the ligand. The BIACORE system cannot be used for experiments which involve the two reactants mixed together in the solution. However, many biochemical

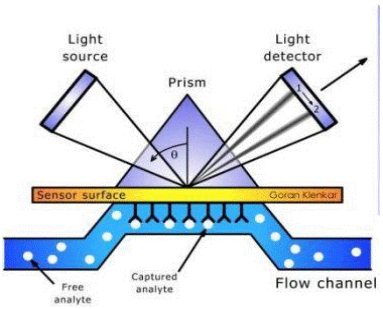

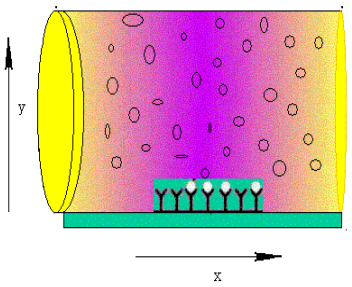

Figure 3.6 – (a) BIACORE. (b) BIACORE flow channel.

reactions occur between an immobilized reactant and another which is floating freely in solution. (See [15] for a list of examples.)

The BIACORE device consists of a flow channel through which one of the reactants (the analyte) is convected from an inlet position, usually represented in the model as $x = 0$. The other reactant (the receptor) is immobilized on a sensor surface on the top of the channel. The time evolution of the binding of these reactants is monitored and the data is used for the determination of the rate constants. We use the coordinate system shown in Figure 3.6 (b) where the x-axis is parallel to the flow and the y-axis is perpendicular to the sensor surface. The channel coordinates are given by $0 \leq x \leq l$, $0 \leq y \leq h$, and we assume that the cross section is rectangular. Standard dimensions for the BIACORE system are $l = 0.24$ cm, $w = 0.05$ cm and $h = 0.005$ cm (see [39]).

We assume that the analyte is convected by a standard two-dimensional Poiseuille flow so that the velocity profile is parabolic for $0 \leq x \leq l$, equal to zero at the top ($y = h$) and bottom ($y = 0$) boundaries, and maximal and equal to v_c in the centre

$(y = h/2)$. The velocity $v(y)$ at a height y above the sensor surface is given by

$$v(y) = 4v_c(\frac{y}{h})(1 - \frac{y}{h}). \tag{3.36}$$

We also make the assumption that the fluid flow is not affected by the presence of the analyte so the velocity field is given independently of the analyte concentration equations. In practical contexts it is often the **volumetric flow rate, Q,** that is measured experimentally and used to estimate the fluid velocity. The volumetric flow rate is defined as the volume of fluid which passes through a cross section of the channel per unit time and has SI units of m^3/s. It can therefore be calculated using the formula

$$Q = \int\int_A \vec{v} \cdot \vec{n}\ dA, \tag{3.37}$$

where A is the cross-sectional area of the flow channel and $\vec{n}$ is the unit normal to this cross section. In the rectangular geometry described above, this surface integral can be evaluated to yield a relationship between the volumetric flow rate Q and fluid velocity v_c as follows

$$\begin{aligned} Q &= \int_0^w \int_0^h v(y)\ dydz, \\ &= w \cdot \frac{4v_c}{h^2} \int_0^h y(h-y)\ dy, \\ &= \frac{2hwv_c}{3}. \end{aligned} \tag{3.38}$$

As the typical flow rates in the BIACORE system range from 1 to 100 ml/min (see, for example, [39]), the formula above yields values for the average velocity v_c between 6 and 600 cm/min.

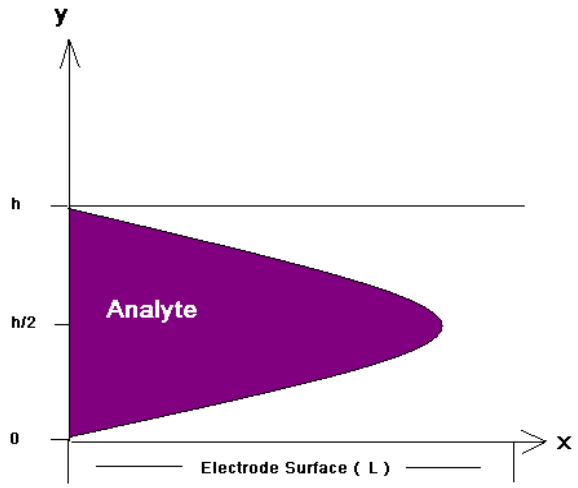

Figure 3.7 – Parabolic flow of analyte.

There have been many modelling strategies for BIACORE presented in the literature, ranging from simple compartmental models to integro-differential equations (see, for example, [16], [39] and [32]). Such mathematical models give analysts an improved understanding of the biomolecular interactions and transport processes and are often used to obtain theoretical approximations for the underlying rate constants. In what follows, we present a partial differential equation model for BIACORE, which describes transport by diffusion and convection, with associated boundary conditions for describing the reactive surface. We make the simplifying assumption that the reaction between the convected antigen and the immobilized antibody is confined to the surface of the flow channel, unlike some previous studies (for example, [39]) where the reactive zone is modelled as a separate layer of finite depth which is characterized by a different set of equations. It is also assumed that the antibodies are uniformly distributed on the sensor surface and that the height of the channel does not influence the binding kinetics. In the flow channel, the free analyte $A(t, x, y)$ is transported by

diffusion and convection, which is governed by the following equation

$$\frac{\partial A}{\partial t} = D(\frac{\partial^2 A}{\partial x^2} + \frac{\partial^2 A}{\partial y^2}) - 4v_c(\frac{y}{h})(1 - \frac{y}{h})\frac{\partial A}{\partial x}. \tag{3.39}$$

At the top of the channel ($y = h$) we have the zero-flux boundary condition

$$\frac{\partial A(t, x, y)}{\partial y} = 0, \text{ at } y = h. \tag{3.40}$$

At the sensor surface ($y = 0$) the analyte reacts with the immobilized antibody (according to the kinetic scheme (3.1)) as reflected in the following boundary condition

$$D\frac{\partial A(t, x, y)}{\partial y} = k_1 A(t, x, 0)B(t, x) - k_{-1}P(t, x), \text{ at } y = 0, \tag{3.41}$$

where $P(t, x)$ is the concentration of bound analyte-receptor complex on the cell surface and $B(t, x) = B_0 - P(t, x)$ is the free surface receptor concentration. B_0 is the total receptor concentration, which is constant with respect to both position and time.

The boundary conditions in the flow direction are specified at $x = 0$ and $x = L$, which are the end points of the reacting zone. Typical entrance and exit boundary conditions for such continuous flow problems are given by the Danckwerts equations (see [13])

$$D\frac{\partial A}{\partial x} = v(A - A_0), \quad \text{at } x = 0, \tag{3.42}$$

where A_0 is (known) upstream analyte concentration, and

$$\frac{\partial A}{\partial x} = 0, \quad \text{at } x = L. \tag{3.43}$$

These boundary conditions are essentially flux balance equations (see [36] for more detailed discussion) with the exit condition (3.43) suggesting that the analyte concentration in the flow is uniform beyond the reacting zone. The initial condition reflects

the fact that, at $t = 0$, there is no antigen in the flow channel, i.e.,

$$A(x, y, 0) = 0. \tag{3.44}$$

To nondimensionalise equations (3.39)-(3.43), we use similar scalings to those in Section 4.1, namely,

$$a = \frac{A}{A_0}, \quad p = \frac{P}{B_0}, \quad b = \frac{B}{B_0}, \quad \bar{x} = \frac{x}{l}, \quad \bar{y} = \frac{y}{h}, \quad \bar{t} = \frac{tD}{h^2},$$

which gives the following system (the bars have been omitted for simplicity)

$$\frac{\partial a}{\partial t} = \varepsilon^2 \frac{\partial^2 a}{\partial x^2} + \frac{\partial^2 a}{\partial y^2} - Pe \cdot y(1-y)\frac{\partial a}{\partial x}, \quad (x, y) \in (0, 1) \times (0, 1), \quad t \geq 0, \tag{3.45}$$

$$\frac{\partial a}{\partial y}(x, 1, t) = 0, \tag{3.46}$$

$$\frac{\partial a}{\partial y}(x, 0, t) = Da \cdot a(1-p) - \kappa p, \tag{3.47}$$

$$\frac{\partial a}{\partial x}(0, y, t) = v^*(a-1), \tag{3.48}$$

$$\frac{\partial a}{\partial x}(1, y, t) = 0, \tag{3.49}$$

$$a(x, y, 0) = 0, \tag{3.50}$$

where

$$\varepsilon = \frac{h}{l}, \quad Pe = \frac{4h^2}{D}\frac{v_c}{l}, \quad Da = \frac{h^2}{D}k_1 A_0, \quad \kappa = \frac{h^2 k_{-1}}{D}, \quad v^* = \frac{vl}{D}. \tag{3.51}$$

The dimensionless parameter, Pe, is called the Peclét number and measures the ratio of a characteristic diffusion time to a characteristic convection time. Typical BIACORE experiments have relatively large Peclét numbers, $Pe = O(10^2)$ or $O(10^3)$, which reflects the fact that in these experiments convection effects dominate diffusion effects. Another key parameter is the Damköhler number, Da, which represents the

ratio of the reaction rate to the diffusion rate.

The Crank-Nicolson method is used to solve the system of partial differential equations and boundary conditions (3.45)-(3.50) as described in Section 1.6. As we now deal with two spatial variables, we take a rectangular grid with grid spacing Δx in the x-direction and Δy in the y-direction, with $x_i = x_0 + i\Delta x$, $y_i = y_0 + i\Delta y$ and $t_n = n\Delta t$ (for all $i = 0, 1, 2 \ldots, ny$, $n = 0, 1, 2, \ldots$) and take $X = x_0 + nx\Delta x$, $Y = y_0 + ny\Delta y$. Then equation (3.45) is discretized as

$$\begin{aligned}\frac{a_{i,j,n+1} - a_{i,j,n}}{\Delta t} &= \frac{\varepsilon^2}{2}\left(\frac{a_{i-1,j,n+1} - 2a_{i,j,n+1} + a_{i+1,j,n+1}}{\Delta x^2} + \frac{a_{i-1,j,n} - 2a_{i,j,n} + a_{i+1,j,n}}{\Delta x^2}\right) \\ &+\frac{1}{2}\left(\frac{a_{i,j-1,n+1} - 2a_{i,j,n+1} + a_{i,j+1,n+1}}{\Delta y^2} + \frac{a_{i,j-1,n} - 2a_{i,j,n} + a_{i,j+1,n}}{\Delta y^2}\right) \\ &-\frac{F_y}{2}\left(\frac{a_{i+1,j,n+1} - a_{i-1,j,n+1}}{2\Delta x} + \frac{a_{i+1,j,n} - a_{i-1,j,n}}{2\Delta x}\right), \end{aligned} \tag{3.52}$$

where $F_y = Pe \cdot y_i(1 - y_i)$.

We let

$$S_x = \varepsilon\Delta t/\Delta x^2, \quad S_y = \Delta t/\Delta y^2, \quad C_x = F_y\Delta t/\Delta x,$$

which simplifies equation (3.52) to

$$\begin{aligned}(1 + S_x + S_y)a_{i,j,n+1} - \left(\frac{S_x}{2} + \frac{C_x}{4}\right)a_{i-1,j,n+1} \\ - \left(\frac{S_x}{2} - \frac{C_x}{4}\right)a_{i+1,j,n+1} - \frac{S_y}{2}a_{i,j-1,n+1} - \frac{S_y}{2}a_{i,j+1,n+1} \\ = (1 - S_x - S_y)a_{i,j,n} + \left(\frac{S_x}{2} + \frac{C_x}{4}\right)a_{i-1,j,n} \\ + \left(\frac{S_x}{2} - \frac{C_x}{4}\right)a_{i+1,j,n} + \frac{S_y}{2}a_{i,j-1,n} + \frac{S_y}{2}a_{i,j+1,n}. \end{aligned} \tag{3.53}$$

Description	***Constant***	***Value***
Flow cell length (m)	l	2.4×10^{-3}
Flow cell width (m)	h	5×10^{-4}
Diffusion constants (m^2/s)	D_s	6.7×10^{-10}
Reaction rate constants ($m^3/mol{\cdot}s$)	k_1	10^2
Reaction rate constants (s^{-1})	k_{-1}	10^{-3}
Initial concentrations:		
Antibody (mol/m^2)	B_0	3.768×10^{-7}
Analytes (mol/m^3=mM)	A_0	$0 - 10^{-3}$
Flow velocity (m/s)	v_0	10^{-4}

Table 3.2 – Typical values for constants.

Similarly, we can discretize the boundary conditions (3.46)-(3.50), and solve the system numerically. The concentration profile of the free analyte $a(x, y, t)$ in the flow channel is shown in Figure 3.8 for the case of diffusion-dominated transport ($v = 0$). The effect of convection on the antigen concentration is illustrated in Figure 3.9, where we take $v = 10^{-4}$ m/s. Note that the parabolic profile becomes asymmetric due to the depletion of antigen at the reactive lower boundary of the channel. Finally, the concentration of bound product $p(x, t)$ is calculated from equation (3.47) and plotted in Figure 3.10. As expected, this concentration rises initially and reaches a saturation value when all the available binding sites have been occupied.

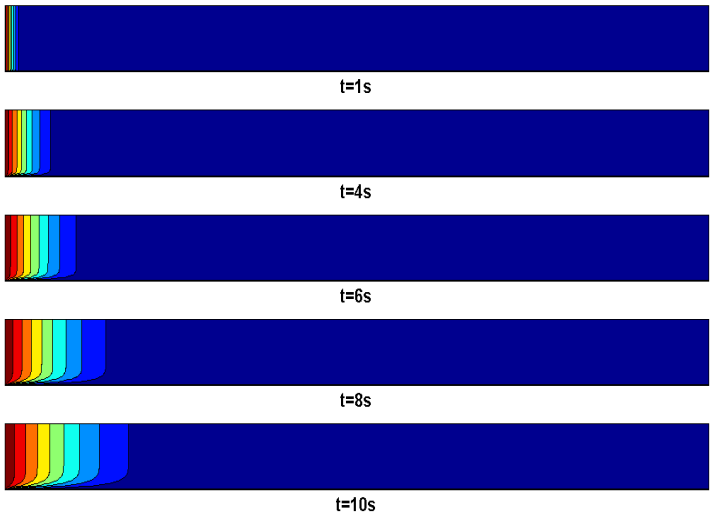

Figure 3.8 – Antigen concentration profile for $v = 0$.

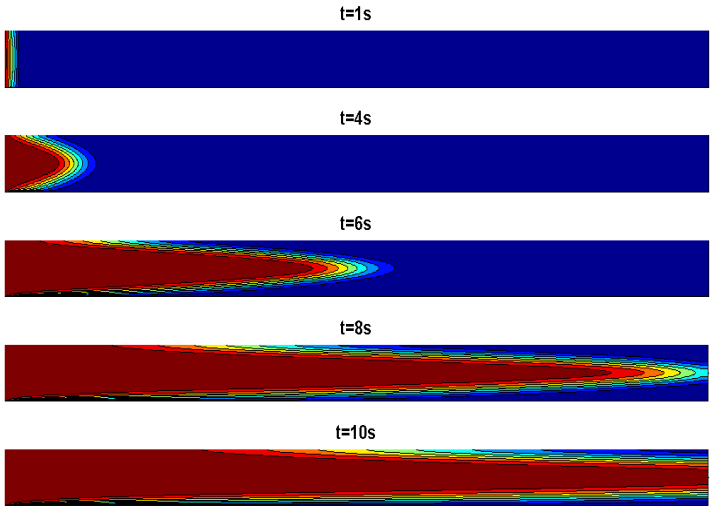

Figure 3.9 – Antigen concentration profile for $v = 10^{-4}$ m/s.

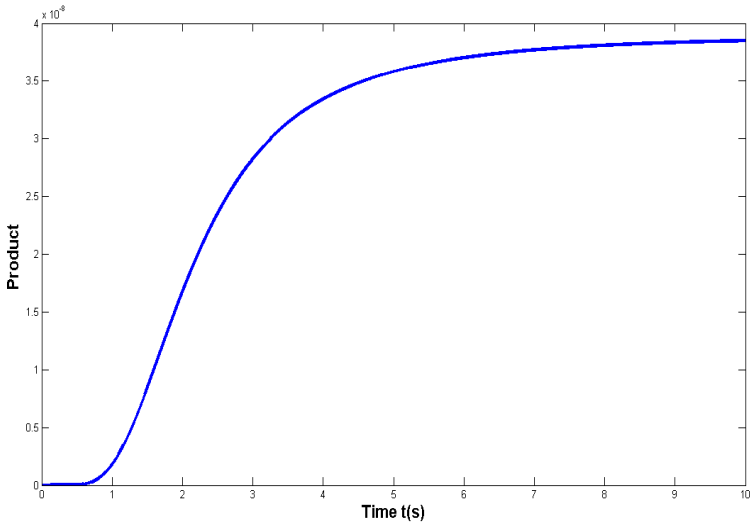

Figure 3.10 – Product at position $\bar{x} = 0.05$ cm.

3.4 Conclusions

In this chapter, we presented examples of mathematical models which incorporate the binding kinetics of antibody-antigen interactions. Specifically, we considered first the case where the two species are contained within a small cell (represented mathematically as a one-dimensional spatial domain) where the antibody is immobilized on a surface and the antigen is free to diffuse. The resulting mathematical model can be used to derive the dependence of the binding product on initial analyte which can then generate a theoretical calibration curve for the assay under consideration. Secondly, a modelling strategy was presented for the BIACORE device, which deals with the reaction between an immobilized ligand and a mobile analyte which is transported by diffusion and convection. This model is useful for illustrating the behaviour of a flow injection analysis (FIA) experiment (which will be discussed again in Chapter 4) and introduces relevant fluid dynamics concepts as well as design parameters.

Chapter 4

An Optimization Problem for a Bi-enzyme Electrode

In this chapter we investigate the problem of optimizing the design of a bi-enzyme biosensor by finding the ratio of two immobilized enzymes which maximizes signal amplitude. A new convection-diffusion model is proposed here as a generalization to existing models and, after comparing numerical solutions, a discussion is given regarding the best modelling strategy.

4.1 Experiment Configuration

The problem we study here is motivated by a series of experiments conducted at the NCSR (DCU) over the past few years by a group of researchers interested in building a biosensing platform based on a bi-enzyme electrode (see, for example, [2]). Optimizing the ratio of the two immobilized enzymes is a necessary first step towards

modelling an enzyme-channelling immunoassay and we study the full problem in the next chapter.

This study investigates a model biosensor system which consists of two enzymes immobilized onto an electrode modified with the conducting polymer PANI/PVS (polyaniline/polyvinyl-sulphonate). The first enzyme, glucose oxidase (GOX), catalyzes the oxidation reaction of glucose to gluconic acid, with production of hydrogen peroxide (H_2O_2). The second enzyme, horseradish peroxidase (HRP), is oxidised by hydrogen peroxide and then subsequently reduced by electrons provided by the electrode, as shown in the scheme below

$$\beta\text{-D-glucose} + O_2 + H_2O \overset{\text{glucose}}{\underset{\text{oxidase}}{\longrightarrow}} \text{gluconic acid} + H_2O_2, \tag{4.1}$$

$$H_2O_2 + \text{HRP} \longrightarrow \text{Compound} + H_2O, \tag{4.2}$$

$$\text{Compound} + 2\text{e}^- + H^+ \longrightarrow \text{HRP} + H_2O. \tag{4.3}$$

The use of bi-enzyme systems has brought considerable advantages to the development of amperometric biosensors. Cascade schemes, where an enzyme is catalytically linked to another enzyme, can produce signal amplification and therefore increase the biosensor efficiency. When using oxidase/peroxidase bi-enzyme systems, the detection principle switches from an electrochemical oxidation to a reduction process that happens at much lower potentials and improves the selectivity of the device. HRP and GOX have very different kinetic characteristics which have been studied extensively. Their substrates and products are produced at different rates and so obtaining the optimum performance will depend on the correct ratio of the two enzymes.

Horseradish peroxidase (HRP) and glucose oxidase (GOX) were immobilized together in one step on the polymer-modified electrode. Different solutions containing the two enzymes were prepared at ratios HRP/GOX ranging from 1:7 to 7:1, maintaining a total concentration of 0.8 mg/ml, and used to immobilize the enzymes on the electrode. For more details of the immobilization procedure, we refer the reader to [2] or [31]. After the immobilization, the electrode is inserted in a flow-cell and an amperometric flow-injection analysis is carried out. Glucose standard solutions at concentrations between 0.5 and 20 mM are then passed over the electrode and the signals recorded. The flow injection system is illustrated in Figure 4.1 (reproduced with permission from [2]) and shows a peristaltic pump, which creates a constant flow of the reagents over the sensor surface, and a potentiostat interfaced with a PC which records amperometric measurements.

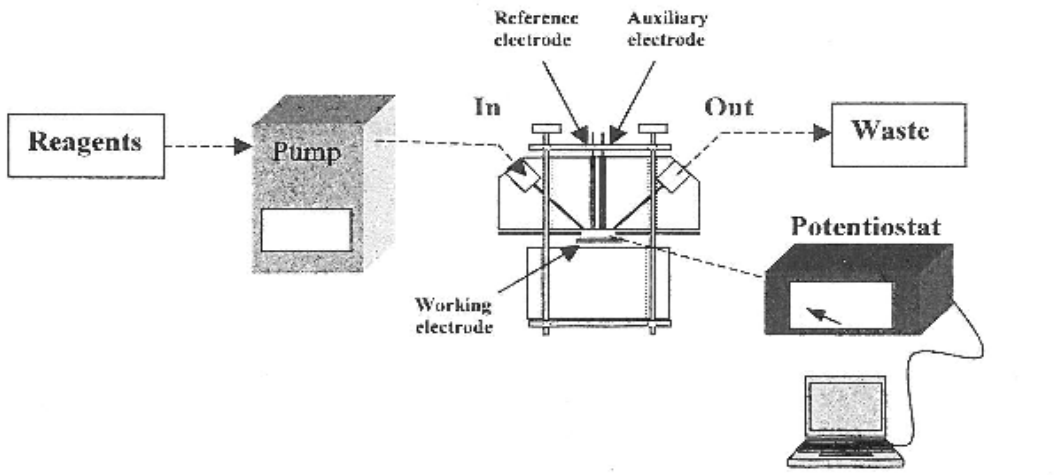

Figure 4.1 – Experimental set-up for FIA experiments.

Figure 4.2 (reproduced with permission from [2]) shows a typical amperogram recording after passing the glucose solutions over the electrode. The mass ratios HRP/GOX in the solutions used for the immobilization can be more conveniently expressed as molar ratios in order to visualise approximately the relative molecular distribution on the electrode surface of the two enzymes. Figure 4.3 (also reproduced from [2]) shows a comparison between all the sensitivities of the electrodes with different molar ratios HRP/GOX. It can be clearly seen that the electrode prepared with HRP/GOX at a molar ratio of 1:1 yields the highest sensitivity.

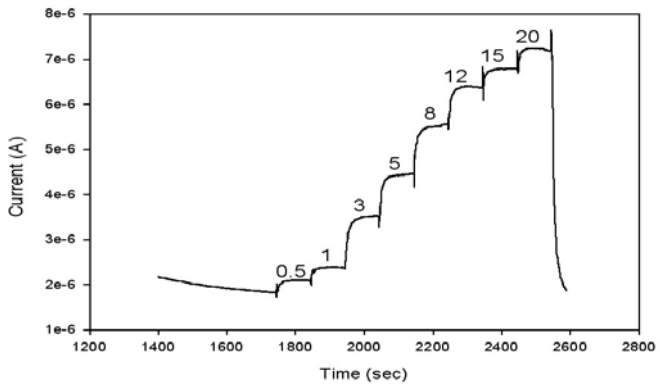

Figure 4.2 – Amperometric responses of a HRP/GOX bi-enzyme electrode to a range of glucose concentrations between 0.5 and 20 mM at −0.1 V vs. Ag/AgCl.

It is known that the GOX enzyme used in the experiments has an activity of 1.7 U/mol protein while the activity of HRP is 5.7 U/mol protein. [1] Therefore HRP is approximately three times more active than GOX and so, it is expected that a

[1] One unit U of an enzyme is defined as the amount which catalyzes the transformation of one μ mol of substrate per minute. The enzyme specific activity is a measure of the purity of the enzyme preparation and is defined as number of enzyme units per mass, U/mg or molar mass, U/mol.

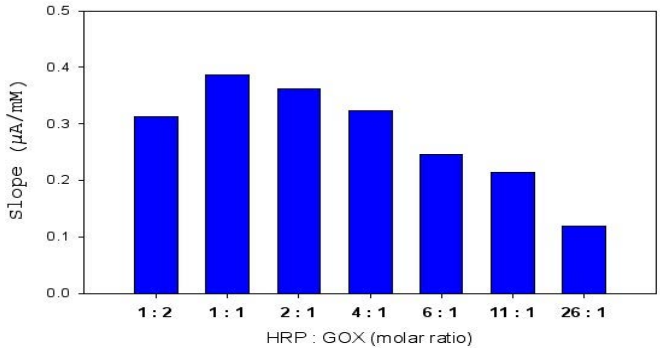

Figure 4.3 – Comparison of HRP/GOX ratio and sensitivity to glucose. The electrode prepared immobilizing HRP and GOX at the molar ratio 1:1 yields the highest catalytic signals and the highest sensitivity. The glucose concentration used in this experiment is 20 mM.

platform with GOX in excess with respect to HRP would be most efficient. The fact that the electrode with HRP and GOX present at molar ratio of 1:1 produced the highest signals is surprising and leads to the hypothesis that other phenomena might influence the response. For example, the activity of HRP may be reduced disproportionately as a consequence of its immobilization on the electrode surface, and its reliance on direct electron transfer.

A mathematical modelling strategy is sought which can describe the flow injection analysis of the bi-enzyme electrode. Numerical simulations could then be carried out in order to determine the ratio of the two enzymes which would lead to optimal biosensor performance and enable one to see how this ratio would respond to variations of the system parameters. The cascade reaction at the electrode represented by

(4.1)-(4.3) can be simplified to a pair of Michaelis-Menten reactions as follows

$$E_1 + S_1 \underset{k_{-1}}{\overset{k_1}{\rightleftarrows}} C_1 \xrightarrow{k_2} E_1 + S_2, \tag{4.4}$$

$$E_2 + S_2 \underset{k_{-3}}{\overset{k_3}{\rightleftarrows}} C_2 \xrightarrow{k_4} E_2 + P, \tag{4.5}$$

where we have used the following notation:

$E_1(t,x)$: first enzyme (Glucose Oxidase) concentration;

$E_2(t,x)$: second enzyme (Horseradish Peroxidase) concentration;

$S_1(t,x,y)$: first substrate (Glucose) concentration;

$S_2(t,x,y)$: second substrate (Hydrogen Peroxide) concentration;

$C_1(t,x)$: first complex concentration;

$C_2(t,x)$: second complex concentration;

$P(t,x,y)$: final product concentration.

This scheme has been used extensively for modelling glucose-glucose oxidase kinetics and it was also shown to be appropriate for the case of immobilized HRP in [21]. Moreover, we denote by K_M^1 and K_M^2 the Michaelis constants associated with the two reactions, that is

$$K_M^1 = \frac{k_{-1} + k_2}{k_1}; \quad K_M^2 = \frac{k_{-3} + k_4}{k_3}. \tag{4.6}$$

In attempting to construct a mathematical model for this problem, we make the following simplifying assumptions:

1. The immobilization mechanisms of the two enzymes are equally efficient on the sensor surface under the conditions employed.

2. Immobilization of HRP and GOX produces a geometrically close-packed spherical monolayer which is spatially homogeneous.

3. The distribution of immobilized HRP and GOX molecules on the surface of the electrode is equal in ratio to that of the solution used.

4. The electron transfer process is 100% efficient since this parameter only affects the magnitude of the signals and not their relative responses.

4.2 Previous Models and Results

Several modelling strategies have already been proposed by our team (see, for example, [30], [31] and [44]) to explain the behaviour of the bi-enzyme platform described in the introduction. We summarize these models below.

Model 1

This model was first proposed in [31] and then further analyzed in [44], where it was referred to as "the comprehensive model". It models the flow injection experiment as a one-dimensional diffusion problem on a domain given by $0 \leq x \leq L$, where convective transport effects are neglected and represented only by suitable boundary conditions at the top of the flow cell. The dimensional equations consist of diffusion equations for the two substrates, and are given by:

$$\frac{\partial S_1(x,t)}{\partial t} = D_1 \frac{\partial^2 S_1(x,t)}{\partial x^2}, \quad 0 \leq x \leq L, \quad t \geq 0,$$
$$\frac{\partial S_2(x,t)}{\partial t} = D_2 \frac{\partial^2 S_2(x,t)}{\partial x^2}, \quad 0 \leq x \leq L, \quad t \geq 0,$$

where D_1 and D_2 are the diffusion coefficients. At the top boundary, S_1 is in constant supply (due to the continuous glucose injection), and S_2 is assumed to be flushed away constantly, which gives the following boundary conditions:

$$S_1(L,t) = S_0, \quad t \geq 0,$$

$$S_2(L,t) = 0, \quad t \geq 0.$$

At the bottom boundary, the boundary conditions reflect the fact that the diffusive flux of each substrate is equal to the corresponding reaction rate as

$$D_1 \frac{\partial S_1(0,t)}{\partial x} = k_1 E_1(t) S_1(0,t) - k_{-1} C_1(t),$$

and

$$D_2 \frac{\partial S_2(0,t)}{\partial x} = k_3 E_2(t) S_2(0,t) - k_2 C_1(t) - k_{-3} C_2(t),$$

together with

$$\begin{aligned}
\frac{dE_1}{dt} &= -k_1 E_1(t) S_1(0,t) + (k_{-1} + k_2) C_1(t), \\
\frac{dE_2}{dt} &= -k_3 E_2(t) S_2(0,t) + (k_{-3} + k_4) C_2(t), \\
\frac{dC_1}{dt} &= k_1 E_1(t) S_1(0,t) - (k_{-1} + k_2) C_1(t), \\
\frac{dC_2}{dt} &= k_3 E_2(t) S_2(0,t) - (k_{-3} + k_4) C_2(t).
\end{aligned}$$

As before, the time evolution of the current is determined from the equation

$$\frac{dP}{dt} = k_4 C_2(t),$$

and the steady-state of this variable is used in future calculations as a model for the current amplitude. In accordance with the physical problem described above, the

following initial conditions are imposed:

$$E_1(0) = E_1^0, \quad E_2(0) = E_2^0, \quad C_1(0) = 0, \quad C_2(0) = 0, \quad P(0) = 0, \quad S_2(x,0) = 0,$$

$$S_1(x,0) = \begin{cases} S_0, & \text{if } x = L \\ 0, & \text{otherwise,} \end{cases}$$

where E_1^0, E_2^0 and S_0 are constants. We let

$$\zeta = \frac{E_1^0}{E_2^0},$$

which implies

$$E_1^0 = \frac{E\zeta}{1+\zeta}, \quad \text{and } E_2^0 = \frac{E}{1+\zeta}, \tag{4.7}$$

where E is the total amount of enzyme present on the electrode. We can assume that E is a constant which corresponds to full coverage of the electrode. This can be measured experimentally (see, for example, [30]).

Figure 4.4 in [31] shows the dependence of the (steady-state) current on the GOX:HRP ratio, ζ, for different concentrations of the first substrate, glucose (S_1). The optimal ζ values (the values which yield maximum signals) are then indicated on each curve. Also, in Figure 4.4, we note that at low glucose concentrations, varying the ratio of the immobilized enzymes has little effect on the electrode response. However, as the glucose concentration increases the optimal ratio value becomes more pronounced and converges to 1 (refer to [31]). The reason for this particular limiting value lies behind the choice of catalytic conversion constants, $k_2 = k_4$. By choosing $k_4/k_2 = 2$, a similar pattern can be observed, where $\zeta^* \to 2$ with increasing glucose concentrations.

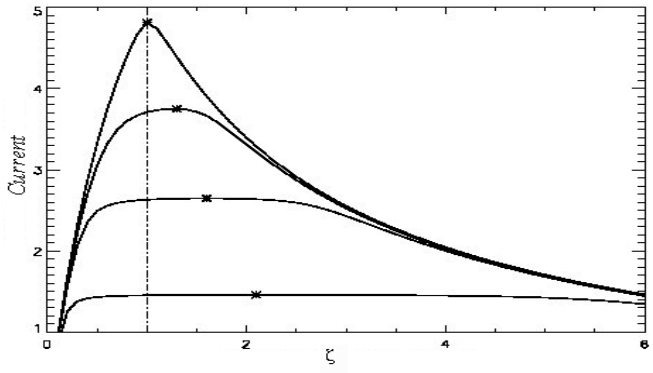

Figure 4.4 – Dependence of current on ζ (GOX:HRP) for different initial concentrations of glucose. The curves correspond to $S_0 = 1, 5, 10$ and 20 mM from bottom to top. The maximum value of current is indicated on each curve.

Figure 4.5 (also obtained in [31]) shows the dependence of the current on the GOX:HRP ratio when the relative speed of the two consecutive reactions k_4/k_2 is varied. Note again that, as the value of k_4/k_2 increases, there seems to be a wider range of values of ζ associated with an "optimal" biosensor response.

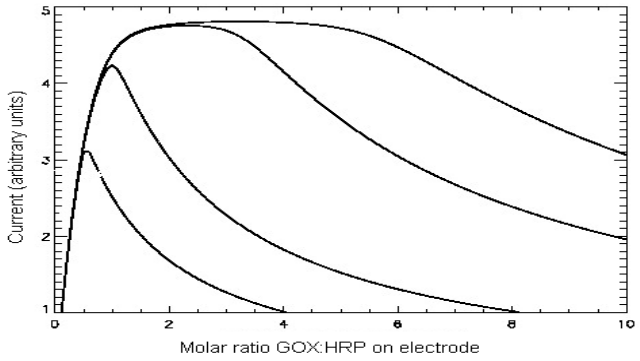

Figure 4.5 – Dependence of current on ζ (electrode GOX:HRP ratio) for different k_4/k_2 values. The lower curve corresponds to $k_4/k_2 = 0.5$ and the upper curve corresponds to $k_4/k_2 = 8$.

Model 2

This model was first proposed in [30] and a detailed analysis is provided in [44], where this model is referred to as "the simplified model". This is a "one-point" model which ignores all transport phenomena and concentrates only on the kinetic processes. The unknown functions we deal with have no spatial dependence and represent averaged quantities at generic points inside the flow cell. The model consists of three ordinary differential equations, as follows

$$\frac{dS_2}{dt} = k_2 C_1 - k_3(E_2^0 - C_2)S_2 + k_{-3}C_2, \tag{4.8}$$

$$\frac{dC_1}{dt} = k_1(E_1^0 - C_1)S_0 - (k_2 + k_{-1})C_1, \tag{4.9}$$

$$\frac{dC_2}{dt} = k_3(E_2^0 - C_2)S_2 - (k_4 + k_{-3})C_2, \tag{4.10}$$

with initial conditions

$$S_2(0) = 0, \quad C_1(0) = 0, \quad C_2(0) = 0,$$

where E_1^0 and E_2^0 are, again, given by (4.7). Due to the relative simplicity of the model, it was possible to carry out a detailed analytical study of the solutions [44]. It is shown that the long-term behaviour of the three concentrations is given by

$$\lim_{t\to\infty} C_1(t) = \frac{k_4\zeta}{k_2\zeta^*(1+\zeta)}, \quad \text{for all} \quad \zeta,$$

$$\lim_{t\to\infty} C_2(t) = \begin{cases} \dfrac{\zeta}{\zeta^*(1+\zeta)}, & \text{if } \zeta \le \zeta^* \\ \dfrac{1}{1+\zeta}, & \text{if } \zeta \ge \zeta^*, \end{cases}$$

$$\lim_{t\to\infty} S_2(t) = \begin{cases} \dfrac{\zeta K_M^2}{S_0(\zeta^* - \zeta)}, & \text{if } \zeta < \zeta^* \\ \infty, & \text{if } \zeta \ge \zeta^*. \end{cases}$$

These results are easy to interpret in the context of the cascade reactions. If $\zeta < \zeta^*$, there is a relatively small amount of E_1^0 compared to E_2^0 which means that the production of S_2 in the first reaction is somehow balanced by its consumption in the second reaction and an equilibrium state can be reached. On the other hand, if $\zeta \geq \zeta^*$, the relatively large amount of E_1^0 can facilitate the production of S_2 which is then not consumed fast enough in the second reaction so its concentration can grow indefinitely. Moreover, it is possible to deduce an explicit formula for the optimal GOX:HRP ratio in terms of the system parameters, given by

$$\zeta^* = \frac{k_4}{k_2}\left(1 + \frac{K_M^1}{S_0}\right). \tag{4.11}$$

This formula validates the observation made in the previous model, namely that the optimal ratio approaches 1 for high values of the glucose concentration S_0, when $k_4 = k_2$. More generally, this formula predicts that for high glucose concentrations the optimal enzyme ratio is equal to the inverse ratio of the catalytic conversion rates for the two consecutive reactions, which is close to the experimental intuition. (For example, a faster second reaction would necessitate a larger amount of the first enzyme, GOX, for maximum efficiency.) The plot of the current ($k_4 C_2^*$) versus ζ for different initial concentrations of glucose is as shown in Figure 4.6; if we vary k_4/k_2 instead, we obtain the graphs in Figure 4.7.

Model 3

This model was first proposed in [44], where it was called "the intermediate model", and represents a simplified version of the comprehensive model described above where

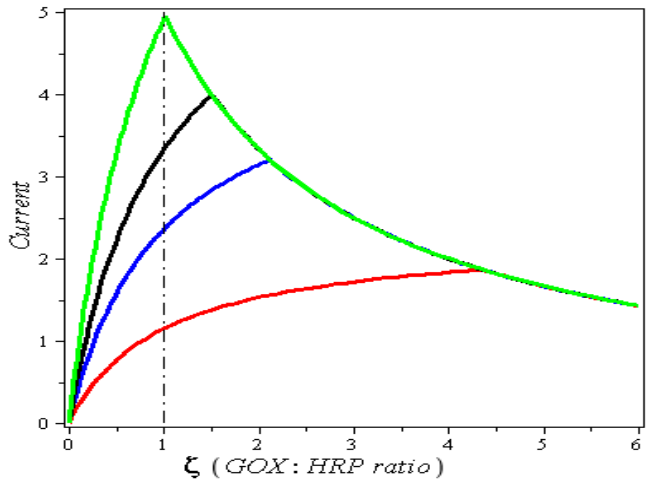

Figure 4.6 – Dependence of current on ζ for different initial concentrations of S_0. The curves correspond to $S_0 = 0.03, 0.09, 0.2$ and 5 mM from the bottom to top. Typical values for constants used in this simulation are: $k_1 = 10^2$, $k_{-1} = 10^{-1}$, $k_2 = 10$ and $k_4 = 10$.

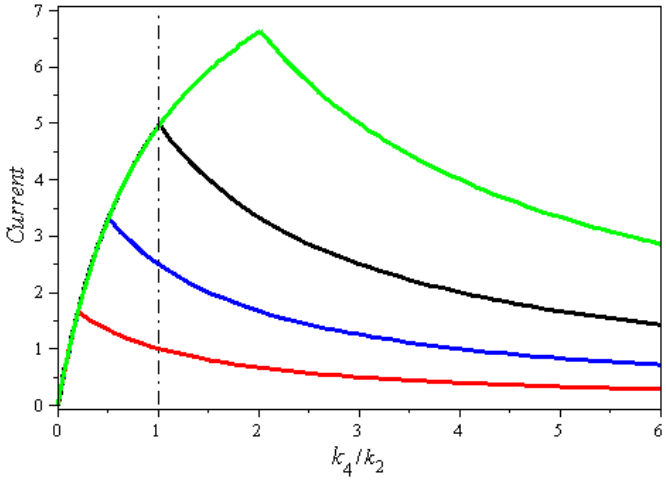

Figure 4.7 – Dependence of current on ζ for different values of k_4/k_2. The curves correspond to $k_4/k_2 = 0.2, 0.5, 1$ and 2 from the bottom to top. Typical values for constants used in this simulation are the same as in Figure 4.6.

only one substrate (hydrogen peroxide) diffuses while the other one (glucose) is assumed to be present only at the reaction point (the electrode). This leads to a simpler system consisting of one diffusion equation with the associated nonlinear boundary conditions which we do not reproduce here. This simplification was based on the expectation that the diffusion of glucose to the reaction place will not affect the value of the system steady-state, although it will affect the time taken to achieve it.

The plot of the current ($k_4 C_2^*$) versus ζ for different initial concentrations of glucose is shown in Figure 4.8. If we vary k_4/k_2 instead, we obtain the graphs in Figure 4.9. Note that the behaviour of the curves is very similar to that shown in Figure 4.4 and 4.5 for Model 1.

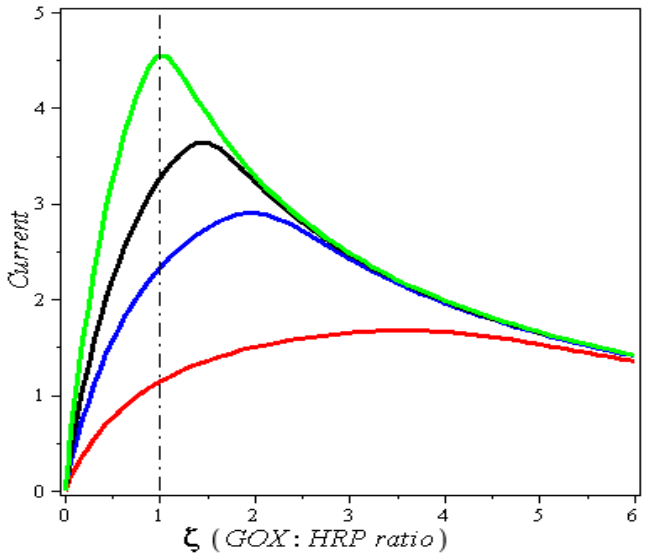

Figure 4.8 – Dependence of current on ζ for different initial concentrations of S_0. The curves correspond to $S_0 = 0.03, 0.09, 0.2$ and 5 mM from bottom to top.

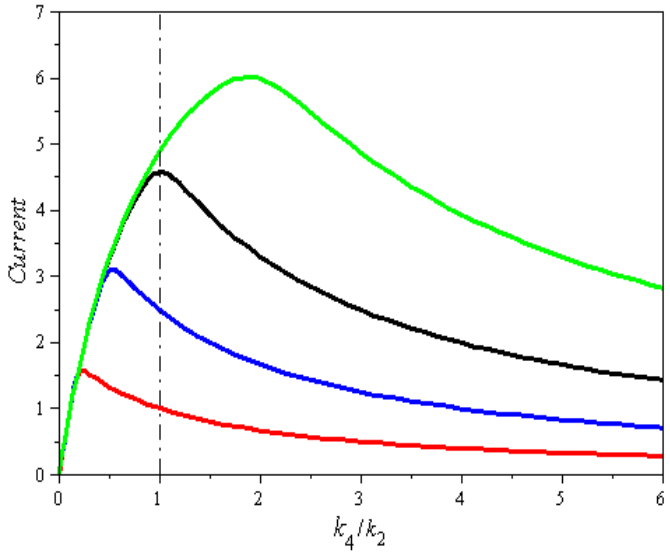

Figure 4.9 – Dependence of current on ζ for different values of k_4/k_2. The curves correspond to $k_4/k_2 = 0.2, 0.5, 1$ and 2 from bottom to top.

4.3 Convection-Diffusion Model

We now investigate a new modelling strategy which generalizes the models presented in the previous section, as it explicitly deals with the **convective and diffusive transport of species**. The flow cell is modelled as a rectangular spatial domain, $0 \leq x \leq L$, $0 \leq y \leq h$ where $y = 0$ describes the electrode at the bottom of the cell, $y = h$ is the (closed) top of the cell, and $x = 0$ represents the point where glucose is introduced into the system (see Figure 4.10). As in the BIACORE model (in Chapter 3) we assume the substrates are convected by a fully-formed Poiseuille flow, where the velocity profile across the channel height is parabolic. The evolution of the concentrations of the two substrates is governed by the following convection-diffusion

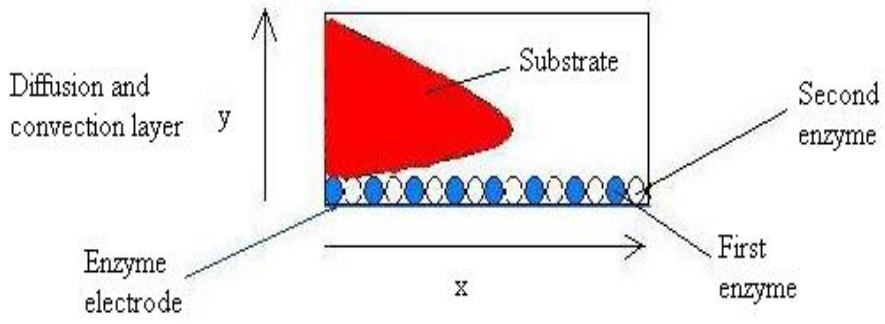

Figure 4.10 – Cascade reaction in a flow cell.

equations:

$$\frac{\partial S_1}{\partial t} = D_1(\frac{\partial^2 S_1}{\partial x^2} + \frac{\partial^2 S_1}{\partial y^2}) - 4v(\frac{y}{h})(1 - \frac{y}{h})\frac{\partial S_1}{\partial x}, \tag{4.12}$$

$$\frac{\partial S_2}{\partial t} = D_2(\frac{\partial^2 S_2}{\partial x^2} + \frac{\partial^2 S_2}{\partial y^2}) - 4v(\frac{y}{h})(1 - \frac{y}{h})\frac{\partial S_2}{\partial x}, \tag{4.13}$$

where D_1, D_2 represent diffusion rate constants, and v is the velocity of the flow. Note that a similar diffusion-convection equation holds for the product, P, but we do not write it here as it is not relevant to the numerical integration. The boundary conditions associated with these equations are explained below.

- At $x = 0$, the concentration of glucose is assumed constant as it is continuously pumped into the system, while hydrogen peroxide has not yet formed; this gives

$$S_1(t, 0, y) = S_0, \qquad S_2(t, 0, y) = 0, \qquad t \geq 0. \tag{4.14}$$

- At $x = l$, we assume uniform flow at the end of the channel, so the boundary conditions are:

$$\frac{\partial S_1(t, x, y)}{\partial x} = \frac{\partial S_2(t, x, y)}{\partial x} = 0. \tag{4.15}$$

- At $y = 0$ (the electrode surface), we have the reaction-type conditions

$$D_1 \frac{\partial S_1(t,x,0)}{\partial y} = k_1 S_1(t,x,0) E_1(t,x) - k_{-1} C_1(t,x), \tag{4.16}$$

$$D_2 \frac{\partial S_2(t,x,0)}{\partial y} = k_3 S_2(t,x,0) E_2(t,x) - k_{-3} C_2(t,x) - k_2 C_1(t,x), \tag{4.17}$$

which are supplemented by the following ordinary differential equations describing the boundary reactions (according to the Michaelis-Menten scheme)

$$\frac{\partial E_1(t,x)}{\partial t} = -k_1 E_1(t,x) S_1(t,x,0) + (k_{-1} + k_2)\, C_1(t,x), \tag{4.18}$$

$$\frac{\partial E_2(t,x)}{\partial t} = -k_3 E_2(t,x) S_2(t,x,0) + (k_4 + k_{-3})\, C_2(t,x), \tag{4.19}$$

$$\frac{\partial C_1(t,x)}{\partial t} = k_1 E_1(t,x) S_1(t,x,0) - (k_2 + k_{-1})\, C_1(t,x), \tag{4.20}$$

$$\frac{\partial C_2(t,x)}{\partial t} = k_3 E_2(t,x) S_2(t,x,0) - (k_4 + k_{-3})\, C_2(t,x), \tag{4.21}$$

$$\frac{\partial P(t,x,0)}{\partial t} = k_4 C_2(t,x). \tag{4.22}$$

- At $y = h$ (the top of the flow cell), we impose zero flux boundary conditions,

$$\frac{\partial S_1(t,x,h)}{\partial y} = \frac{\partial S_2(t,x,h)}{\partial y} = 0. \tag{4.23}$$

Finally, we specify the initial conditions:

$$S_1(0,x,y) = \begin{cases} S_0, & \text{if } x = 0 \qquad (4.24) \\ 0, & \text{otherwise,} \qquad (4.25) \end{cases}$$

$$S_2(0,x,y) = 0, \quad E_1(0,x) = E_1^0, \quad E_2(0,x) = E_2^0, \quad C_1(0,x) = C_2(0,x) = 0. \tag{4.26}$$

Note that the boundary and initial conditions closely resemble the ones presented in Chapter 3 for the BIACORE system and are typical for flow injection systems. As discussed in Section 4.2, we have the additional constraints

$$\zeta E_2^0 = E_1^0, \quad \text{and } E_1^0 + E_2^0 = E_0, \tag{4.27}$$

where E_0 is the total amount of enzyme present on the electrode. The parameter, ζ, which measures the ratio of the two enzymes on the electrode, will be investigated with the aim of determining the value which gives the highest current amplitude. The current measured at the electrode can be assumed proportional to the rate of formation of the final product, $\partial P/\partial t$, as given by equation (4.22).

We non-dimensionalise the system by introducing the following non-dimensional variables:

$$\bar{S}_i(\bar{t},\bar{x},\bar{y}) = \frac{S_i(t,x,y)}{S_0}, \quad \bar{E}_i(\bar{t},\bar{x}) = \frac{E_i(t,x)}{E_0}, \quad \bar{C}_i(\bar{t},\bar{x}) = \frac{C_i(t,x)}{E_0}, \quad i = 1,2.$$
$$\bar{P}(\bar{t},\bar{x},\bar{y}) = \frac{P(t,x,y)}{E_0}, \quad \bar{x} = \frac{x}{l}, \quad \bar{y} = \frac{y}{h}, \quad \bar{t} = \frac{D_1 t}{h^2}.$$

This yields the following equations

$$\frac{\partial \bar{S}_1}{\partial \bar{t}} = \varepsilon^2 \frac{\partial^2 \bar{S}_1}{\partial \bar{x}^2} + \frac{\partial^2 \bar{S}_1}{\partial \bar{y}^2} - \varepsilon\alpha\bar{y}(1-\bar{y})\frac{\partial \bar{S}_1}{\partial \bar{x}}, \tag{4.28}$$

$$\frac{\partial \bar{S}_2}{\partial \bar{t}} = \beta\left(\varepsilon^2 \frac{\partial^2 \bar{S}_2}{\partial \bar{x}^2} + \frac{\partial^2 \bar{S}_2}{\partial \bar{y}^2}\right) - \varepsilon\alpha\bar{y}(1-\bar{y})\frac{\partial \bar{S}_2}{\partial \bar{x}}, \tag{4.29}$$

with initial conditions

$$\bar{S}_1(0,\bar{x},\bar{y}) = \begin{cases} 1, & \text{if } \bar{x} = 0 \quad (4.30) \\ 0, & \text{otherwise,} \quad (4.31) \end{cases}$$

$$\bar{S}_2(0,\bar{x},\bar{y}) = 0, \quad \bar{E}_1(0,\bar{x},\bar{y}) = \frac{\zeta}{1+\zeta},$$
$$\bar{E}_2(0,\bar{x}) = \frac{1}{1+\zeta}, \quad \bar{C}_1(0,\bar{x}) = 0, \quad \bar{C}_2(0,\bar{x}) = 0,$$

where

$$\varepsilon = \frac{h}{l}, \quad \alpha = \frac{4vh}{D_1}, \quad \beta = \frac{D_2}{D_1}. \tag{4.32}$$

The non-dimensional boundary conditions are as follows: at $\bar{x} = 0$,

$$\bar{S}_1(\bar{t}, 0, \bar{y}) = 1, \quad \bar{S}_2(\bar{t}, 0, \bar{y}) = 0, \quad t \geq 0, \tag{4.33}$$

and at $\bar{x} = 1$,

$$\frac{\partial \bar{S}_1}{\partial \bar{x}} = \frac{\partial \bar{S}_2}{\partial \bar{x}} = 0. \tag{4.34}$$

At the electrode surface, $\bar{y} = 0$, we use the non-dimensional conservation laws

$$\bar{E}_1 + \bar{C}_1 = \frac{\zeta}{1+\zeta},$$
$$\bar{E}_2 + \bar{C}_2 = \frac{1}{1+\zeta},$$

and the boundary conditions (4.16) and (4.17) simplify to

$$\frac{\partial \bar{S}_1}{\partial \bar{y}} = k_a^1 \bar{S}_1 \bar{E}_1 - k_b^1 (\frac{\zeta}{1+\zeta} - \bar{E}_1), \tag{4.35}$$

$$\frac{\partial \bar{S}_2}{\partial \bar{y}} = k_a^2 \bar{S}_2 \bar{E}_2 - k_b^2 (\frac{1}{1+\zeta} - \bar{E}_2) - k_e (\frac{\zeta}{1+\zeta} - \bar{E}_1), \tag{4.36}$$

where we define

$$k_a^1 = \frac{k_1 E_0 h}{D_1}, \quad k_a^2 = \frac{k_3 E_0 h}{D_2},$$
$$k_b^1 = \frac{k_{-1} E_0 h}{D_1 S_0}, \quad k_b^2 = \frac{k_{-3} E_0 h}{D_2 S_0}, \quad k_e = \frac{k_2 E_0 h}{D_2 S_0}.$$

The equations (4.18)-(4.22) simplify to:

$$\frac{d\bar{E}_1}{d\bar{t}} = k_c^1 \bar{E}_1 \bar{S}_1 + k_d^1 (\frac{\zeta}{1+\zeta} - \bar{E}_1), \tag{4.37}$$

$$\frac{d\bar{E}_2}{d\bar{t}} = k_c^2 \bar{E}_2 \bar{S}_2 + k_d^2 (\frac{1}{1+\zeta} - \bar{E}_2), \tag{4.38}$$

$$\frac{d\bar{P}}{d\bar{t}} = k_f (\frac{1}{1+\zeta} - \bar{E}_2), \tag{4.39}$$

where we define

$$k_c^1 = \frac{-k_1 S_0 h^2}{D_1}, \quad k_c^2 = \frac{-k_3 S_0 h^2}{D_1},$$
$$k_d^1 = \frac{(k_{-1} + k_2) h^2}{D_1}, \quad k_d^2 = \frac{(k_{-3} + k_4) h^2}{D_1}, \quad k_f = \frac{k_4 h^2}{D_1}.$$

Finally, at $\bar{y} = 1$, we have

$$\frac{\partial \bar{S}_1}{\partial \bar{y}} = \frac{\partial \bar{S}_2}{\partial \bar{y}} = 0. \tag{4.40}$$

4.4 Numerical Simulations

A standard finite difference method (implemented in C) is used to solve the system of partial differential equations and boundary conditions (4.28)-(4.40). Table 4.1 summarizes the values of all physical constants used in the numerical simulations. Figures 4.11 and 4.12 show the time evolution of the non-dimensional current $d\bar{P}/d\bar{t}$ as given by equation (4.39) at various points along the electrode for two values of the flow velocity, $v = 2 \times 10^{-5}$ m/s and $v = 0$. It is seen that the profiles obtained are similar as they all tend to the same steady-state value as $t \to \infty$. We conclude that the x position at which the current is measured should not affect any of the future simulations and we therefore choose the non-dimensional value $\bar{x} = 0.25$ (corresponding to a physical value of $x = 0.5 \times 10^{-3}$ m). The equilibrium, or steady-state value is recorded as a measure of the current amplitude and used for future parameter iterations.

The first set of numerical simulations was carried out in order to assess the effect of varying the initial glucose concentration on the current response and the optimal GOX:HRP ratio. As described above, the equations (4.28)-(4.40) are integrated for different values of ζ, the molar enzyme ratio on the electrode, and the current ampli-

Description	***Constant***	***Value***
Flow cell length (m)	l	2×10^{-3}
Flow cell depth (m)	h	2×10^{-4}
Diffusion constants (m^2/s):		
First substrate	D_s	6.7×10^{-10}
Second substrate	D_p	8.8×10^{-10}
Reaction rate constants (m^3/mol·s)	k_1	10^2
	k_3	10^2
Reaction rate constants (s^{-1})	k_{-1}	10^{-1}
	k_{-3}	10^{-1}
	k_2	$0.2 - 10$
	k_4	1
Initial concentrations:		
Total enzyme (mol/m^2)	E_0	10^{-5}
Substrate (mol/m^3=mM)	S_0	$0.1 - 20$
Flow velocity (m/s)	v	$0 - 10^{-4}$

Table 4.1 – Typical values for constants.

tude recorded. This simulation is then repeated for different values of S_0, the initial glucose concentration, to produce the curves shown in Figure 4.13. This procedure is carried out twice, for $v = 0$ and $v = 2 \times 10^{-5}$ m/s in order to assess the effect of the flow on the simulations. The kinetic constants are assumed to be the same for both reactions, as given by Table 4.1, with $k_1 = k_3 = 10^2$ $m^3/mol \cdot s$ and $k_2 = k_4 = 1$ s^{-1}.

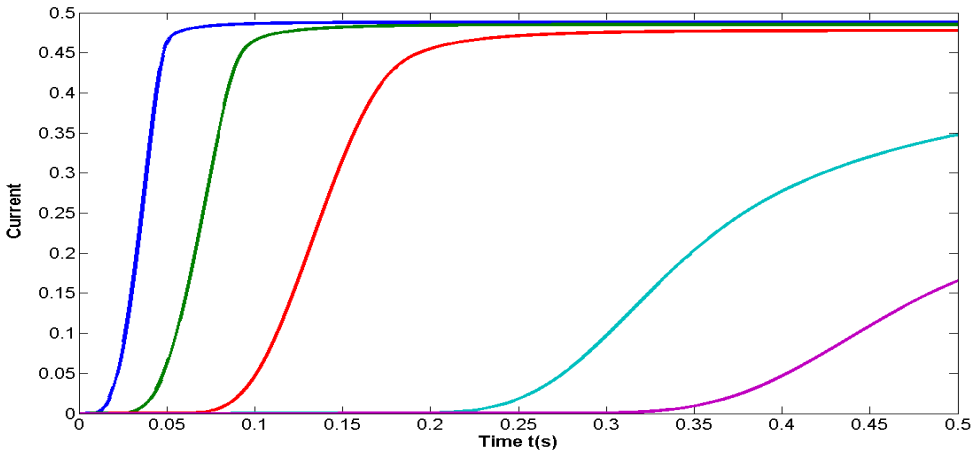

Figure 4.11 – Dependence of current on time for different position in the x direction (from top to bottom $x = 0.1, 0.2, 0.5, 1, 1.5 \times 10^{-3}$ m) at $v = 2 \times 10^{-5}$ m/s.

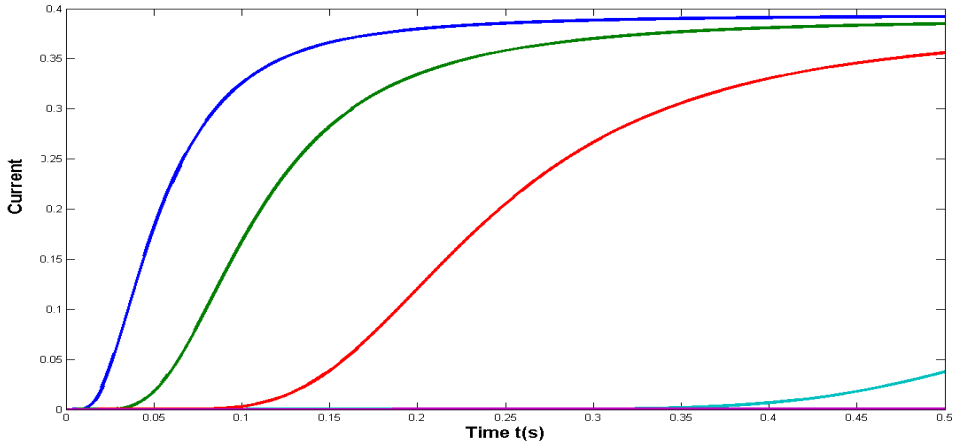

Figure 4.12 – Dependence of current on time for different position in the x direction (from top to bottom $x = 0.1, 0.2, 0.5, 1, 1.5 \times 10^{-3}$ m) at $v = 0$.

We use 50 values for the molar ratio, ζ, between 0 and 5, and values for the glucose concentration, S_0, between 0 and 20 mM. Note that the qualitative behaviour of the current as a function of the enzyme ratio is very similar to that obtained in the one

dimensional models reviewed in Section 4.2 and displayed in Figures 4.4 and 4.8.

For each of the curves in Figure 4.13 the optimal molar ratio, ζ, (the value which yields the highest current amplitude) is recorded and plotted in Figure 4.14 as a function of the glucose concentration S_0. Figure 4.14 shows that, as the glucose concentration S_0 increases, the optimal GOX:HRP ratio, ζ, approaches the value 1, a phenomenon also observed in the three models summarized in Section 4.2. Recall that, for these simulations, we chose $k_4 = k_2$. To test whether this result holds for other values of the ratio k_4/k_2, we repeat these simulations keeping $k_4 = 1$ s^{-1} constant and varying k_1 between 0 and 5 m^3/mol$\cdot$s. The results for the values $k_4/k_2 = 0.2, 0.6$ and 2 are displayed in Figures 4.15, 4.17 and 4.19. For each of these cases (and for many others we tested) it seems apparent that at high glucose concentrations, the optimal GOX:HRP ratio approaches the value k_4/k_2, which is the result predicted by equation (4.11). Moreover, Figures 4.13-4.20 show that the limiting value k_4/k_2 is approached for both $v = 0$ and $v = 2 \times 10^{-5}$ m/s.

The second set of numerical simulations is carried out to determine the dependence of the current and the optimal enzyme ratio on the ratio k_4/k_2 of the catalytic turnover numbers for the two consecutive reactions. The initial glucose concentration is kept constant at $S_0 = 1$ and again, we take $k_1 = k_3 = 10^2$ m^3/mol $\cdot$ s, $k_{-1} = k_{-3} = 10^{-1}$ s^{-1} as before, and the current steady-state is plotted as a function of the GOX:HRP ratio and the curves obtained for different k_4/k_2 values between 0.5 and 4 are shown in Figure 4.21. We note again the similarity between Figure 4.21 and the results from the one dimensional models shown in Section 4.2. The following set of numerical

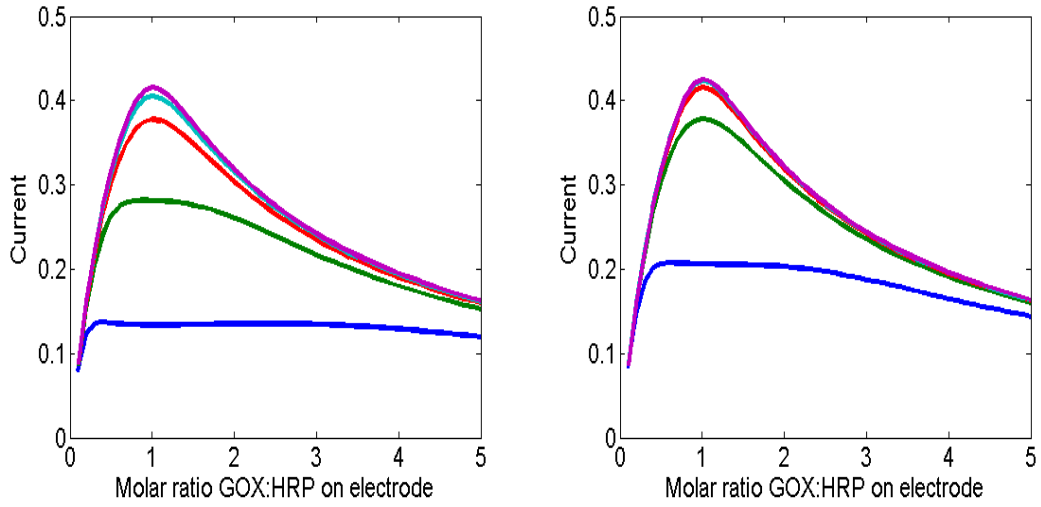

Figure 4.13 – Dependence of current on GOX:HRP ratio for different initial glucose concentration S_0 in the case $k_4/k_2 = 1$. From bottom to top the curves correspond to $S_0 = 0.1, \cdots, 1$ mM, for $v = 0$ (left) and $v = 2 \times 10^{-5}$ m/s (right).

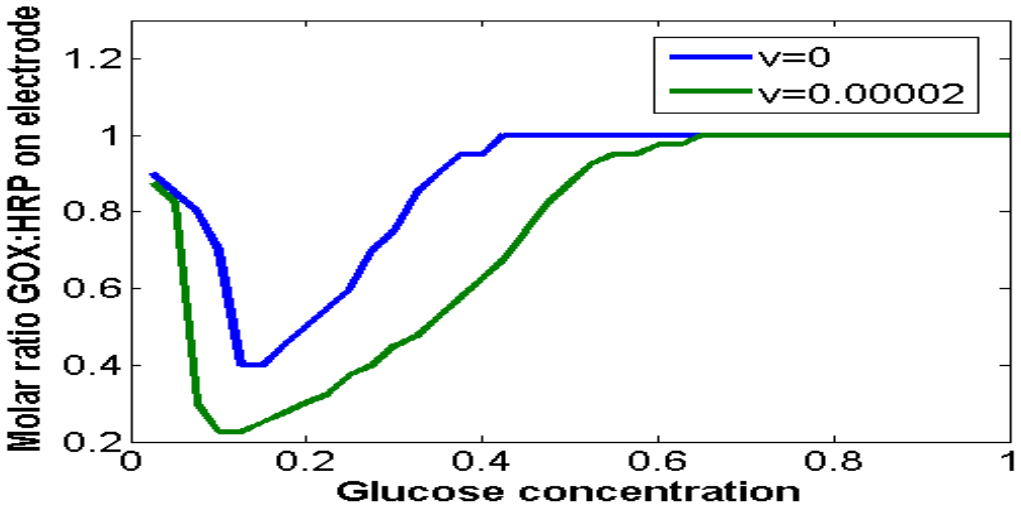

Figure 4.14 – Dependence of optimal GOX:HRP ratio on glucose concentration for $k_4/k_2 = 1$.

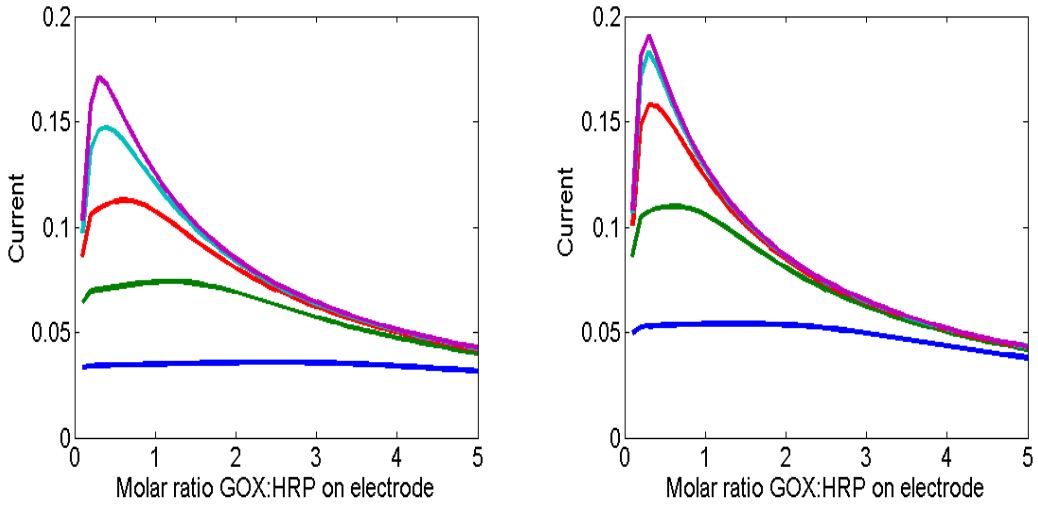

Figure 4.15 – Dependence of current on GOX:HRP ratio for different initial glucose concentration S_0 in the case $k_4/k_2 = 0.2$. From bottom to top the curves correspond to $S_0 = 0.1, \cdots, 1$ mM, for $v = 0$ (left) and $v = 2 \times 10^{-5}$ m/s (right).

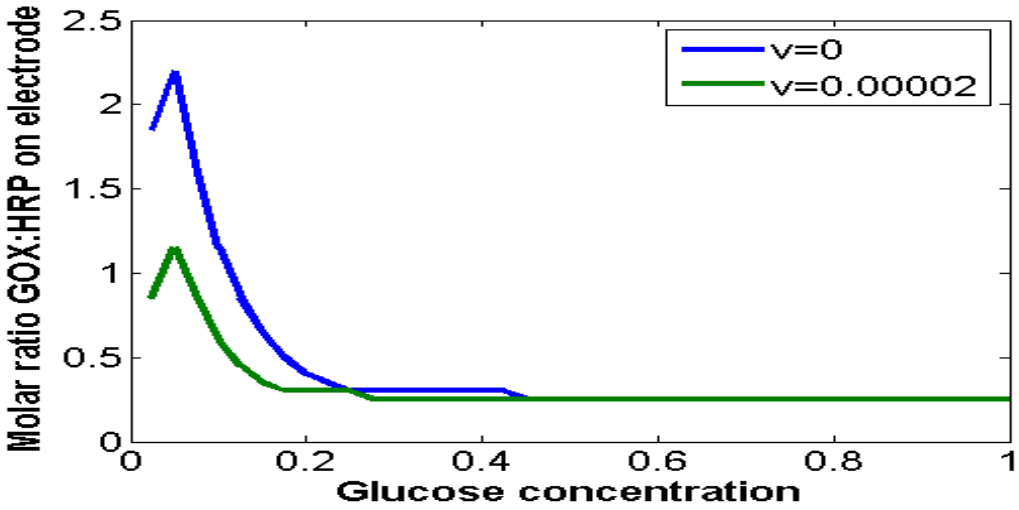

Figure 4.16 – Dependence of optimal GOX:HRP ratio on glucose concentration for $k_4/k_2 = 0.2$.

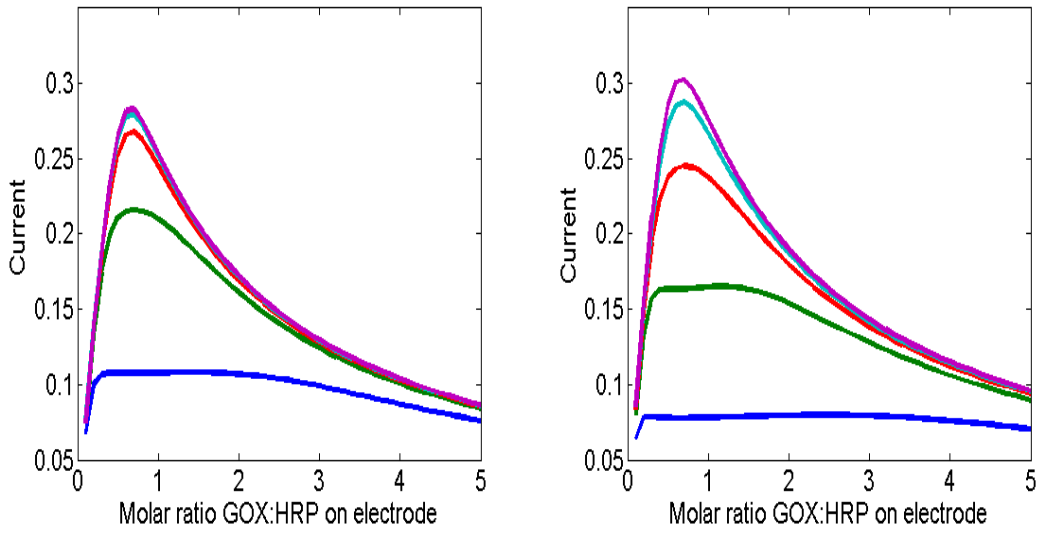

Figure 4.17 – Dependence of current on GOX:HRP ratio for different initial glucose concentration S_0 in the case $k_4/k_2 = 0.6$. From bottom to top the curves correspond to $S_0 = 0.1, \cdots, 1$ mM, for $v = 0$ (left) and $v = 2 \times 10^{-5}$ m/s (right).

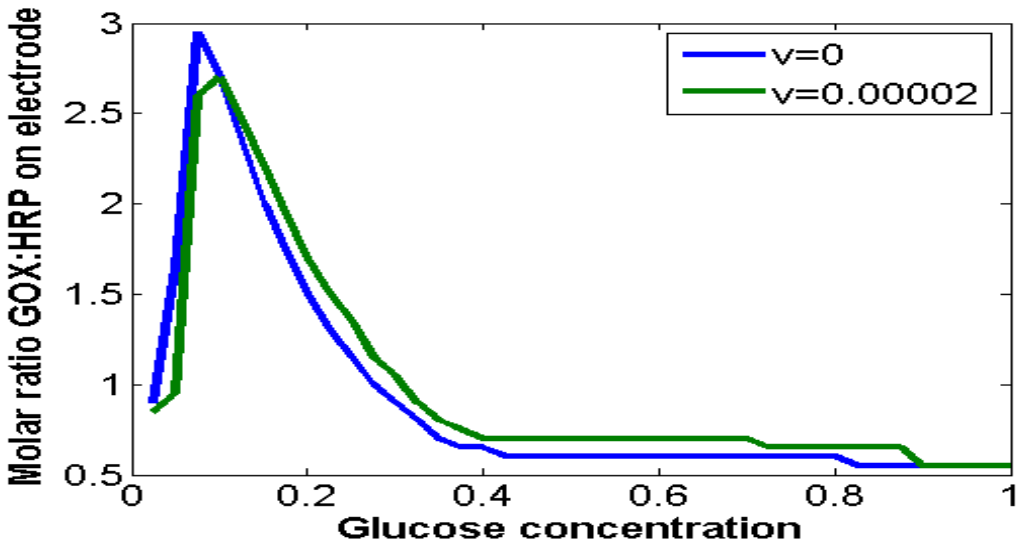

Figure 4.18 – Dependence of optimal GOX:HRP ratio on glucose concentration for $k_4/k_2 = 0.6$.

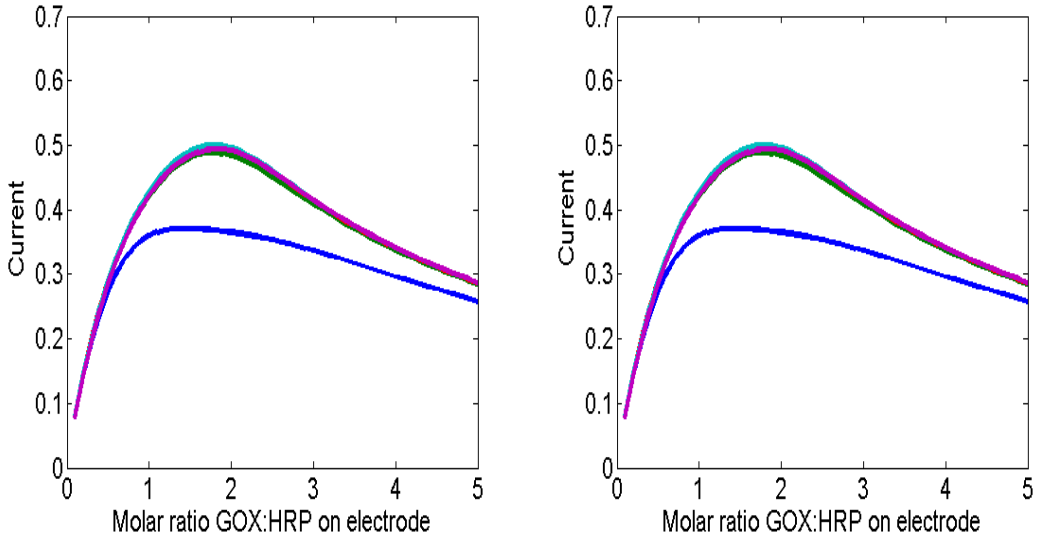

Figure 4.19 – Dependence of current on GOX:HRP ratio for different initial glucose concentration S_0 in the case $k_4/k_2 = 2$. From bottom to top the curves correspond to $S_0 = 0.1, \cdots, 1$ mM, for $v = 0$ (left) and $v = 2 \times 10^{-5}$ m/s (right).

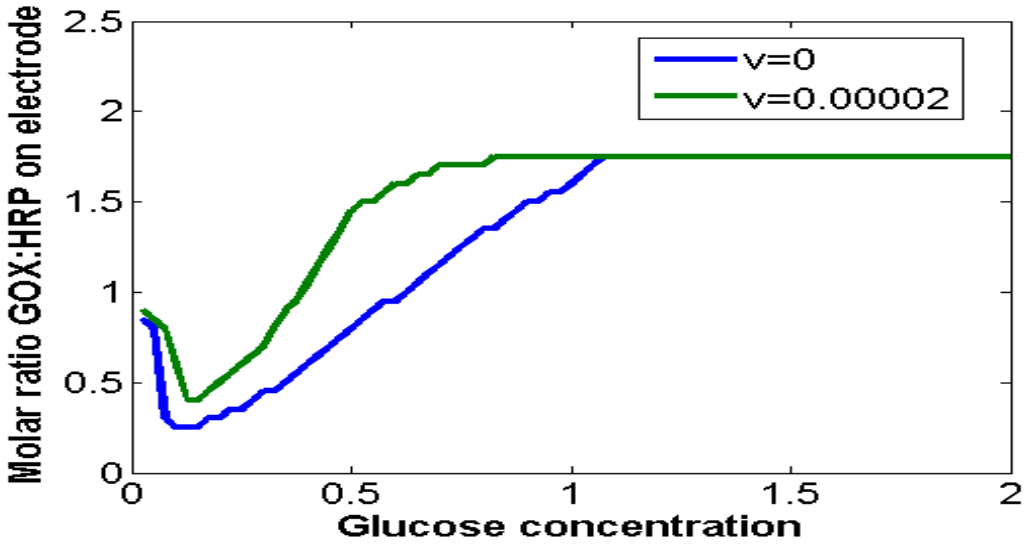

Figure 4.20 – Dependence of optimal GOX:HRP ratio on glucose concentration for $k_4/k_2 = 2$.

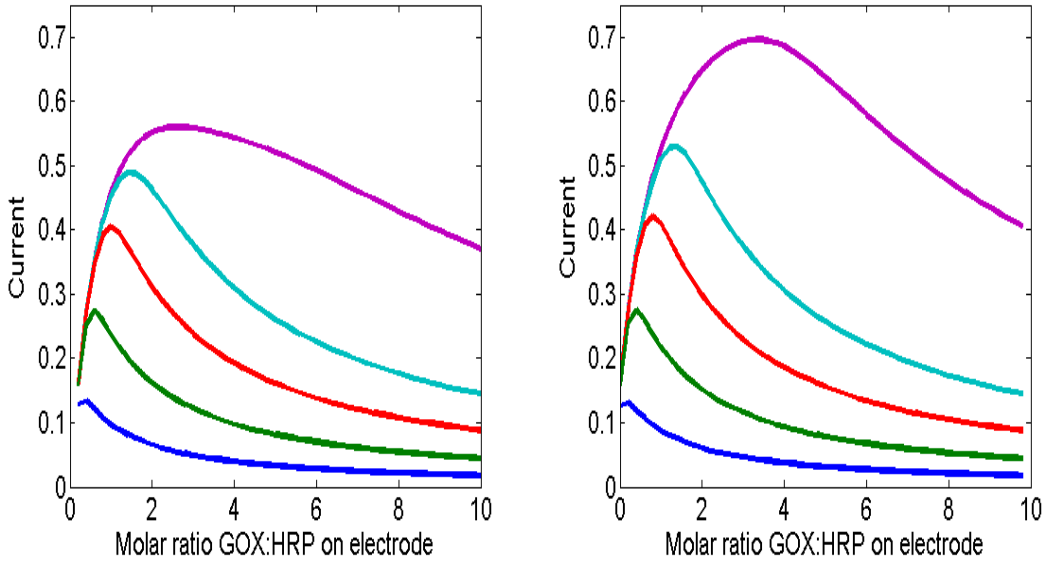

Figure 4.21 – Dependence of current on GOX:HRP ratio for different k_4/k_2. The lower curve corresponds to $k_4/k_2 = 0.5$ and the upper curve to $k_4/k_2 = 4$.

simulations is concerned with studying the effect of the flow rate v on the current amplitude and the optimal ζ ratio. As described in the previous set of simulations, we first obtain the equilibrium value of the current as a function of ζ whilst keeping all of the other parameters constant and this integration is then repeated for several values of v. Again, the parameter values are chosen according to Table 4.1, with $k_1 = k_3 = 10^2$ m^3/mol $\cdot$ s. We use 50 values for ζ ranging between 0 and 5, and 5 values for the flow rate v between 0 and 5×10^{-5} m/s. The resulting curves are shown in Figure 4.22, for $S_0 = 0.4$ mM (left) and $S_0 = 1$ mM (right). The optimal molar ratios are then plotted in Figure 4.23 as functions of the flow velocity v.

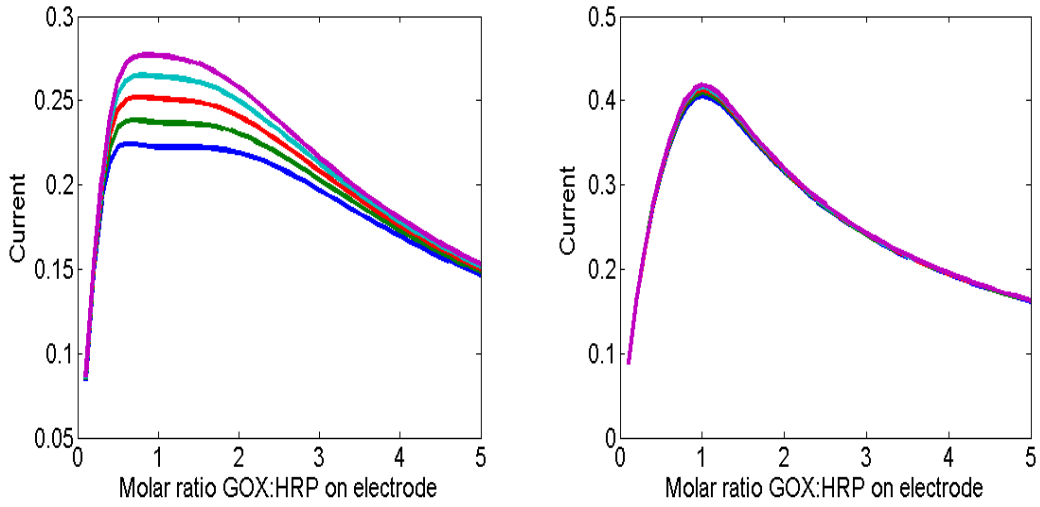

Figure 4.22 – Dependence of current on GOX:HRP ratio for different flow velocities v in the case $k_4/k_2 = 1$. From bottom to top the curves correspond to $v = 0, 2, 4, 6, 8 \times 10^{-5}$ m/s for $S_0 = 0.4$ mM (left) and $S_0 = 1$ mM (right).

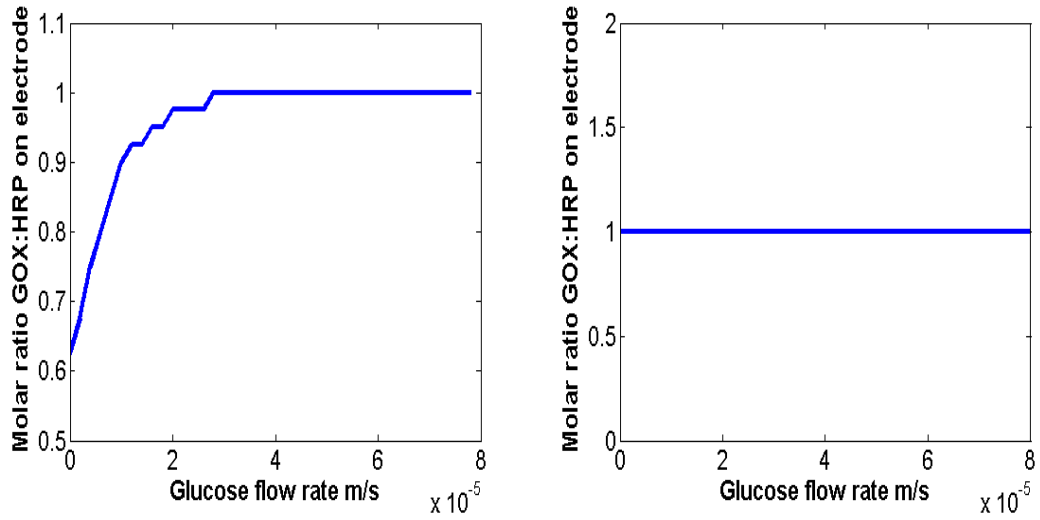

Figure 4.23 – Dependence of optimal GOX:HRP ratio on glucose flow rate in the case $k_4/k_2 = 1$ for $S_0 = 0.4$ mM (left) and $S_0 = 1$ mM (right).

4.5 Conclusions

In this chapter we presented a convection-diffusion model for a flow injection analysis of a bi-enzyme electrode with a view to further investigating the ratio of the two enzymes which maximizes signal amplitude. This model generalizes previous work by researchers in our team (see [30], [31] and [44]) by explicitly modelling the flow of the glucose solution over the electrode while the existing models (which are summarized in Section 4.2) greatly simplified (or even neglected) the transport of substrates in the analysis.

Extensive numerical simulations were carried out in order to assess the dependence of the signal amplitude (as measured by the rate of one of the reactions) and the optimal bi-enzyme ratio on three parameters: the initial concentration of glucose in the flow, the relative reaction speed k_4/k_2 and the velocity of the convective flow. The main result tested for is that the optimal ratio approaches the value k_4/k_2 in the limit of large glucose concentrations. This result is analytically proven in [44] for the case of the simple, one-point model and also observed in numerical simulations of all the other models reviewed in Section 5.2. It also reinforces the experimental intuition that the most efficient enzyme ratio is proportional to the inverse ratio of their catalytic turnover numbers. Analytic verifications have not yet been attempted for any of the one or two-dimensional spatially extended models and such proofs are likely to be extremely complicated. Here, we have merely provided a check based on the behaviour of the numerical solution.

The experimental results, reviewed in Section 4.1, showed that an electrode with equal molar ratios of the two immobilized enzymes yields the optimal sensor response, which seemed to contradict the knowledge that HRP has a higher activity than GOX (in solution). By contrast, numerical simulations (as well as some theoretical results) of all four models studied in this chapter indicate that an optimal ratio of 1 occurs when the two consecutive reactions are equally fast ($k_2 = k_4$). This seems to suggest that the activity of HRP is disproportionately reduced during the immobilization process, probably because of its reliance on direct electron transfer.

The comprehensive model presented in [31] assumed a one-dimensional geometry for the experimental configuration where substrate diffuses from the cell surface to the electrode and the flow injection analysis is approximated by appropriate boundary conditions at the top of the cell. By contrast, the model presented here uses two spatial variables (accounting for the cell length and depth) and the flow is explicitly modelled by including convection terms in the system. Also recall that, in our model, diffusion of substrate takes place in both x and y directions, while convection occurs only in the x direction. Given the complexity of the experimental configuration, it is not clear which of these modelling strategies offers a better geometrical description of the pump shown in Figure 4.1. On comparing the time evolution of glucose gradients across the cell, the one and two-dimensional models yield quite different patterns. The diffusion-only model produces a linear gradient for the glucose concentration across the cell depth (see Figure 4.26) while the new convection-diffusion model studied here yields a parabolic profile (Figures 4.24 and 4.25).

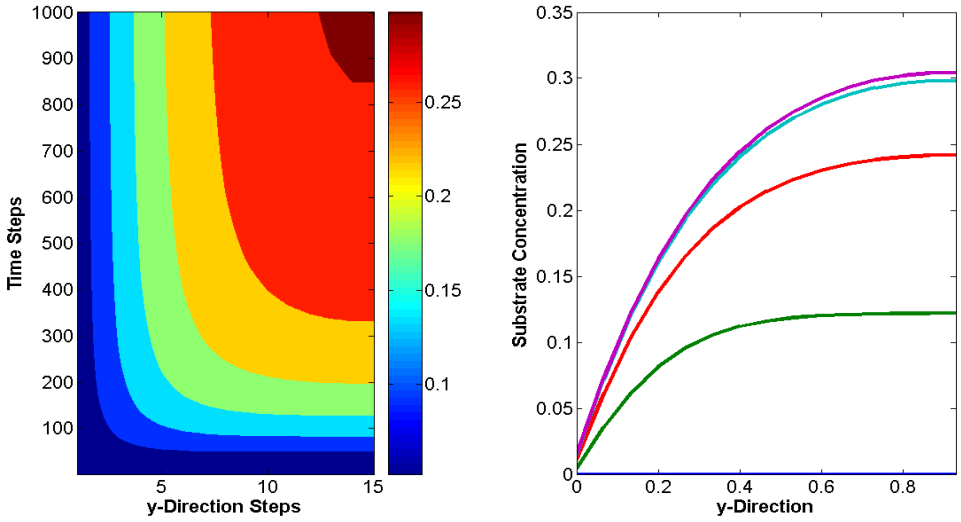

Figure 4.24 – Glucose concentration gradient across channel height ($v = 0$). The curves in the right diagram correspond to $t = 1, 2, 5, 15, 20$ s).

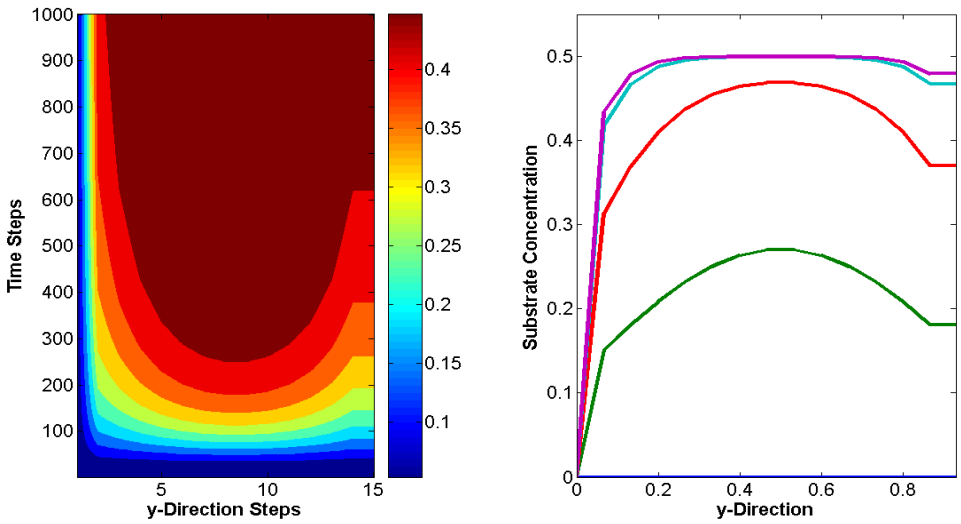

Figure 4.25 – Glucose concentration gradient across channel height ($v = 2\times10^{-5}$ m/s). The curves in the right diagram correspond to $t = 1, 2, 5, 15, 20$ s).

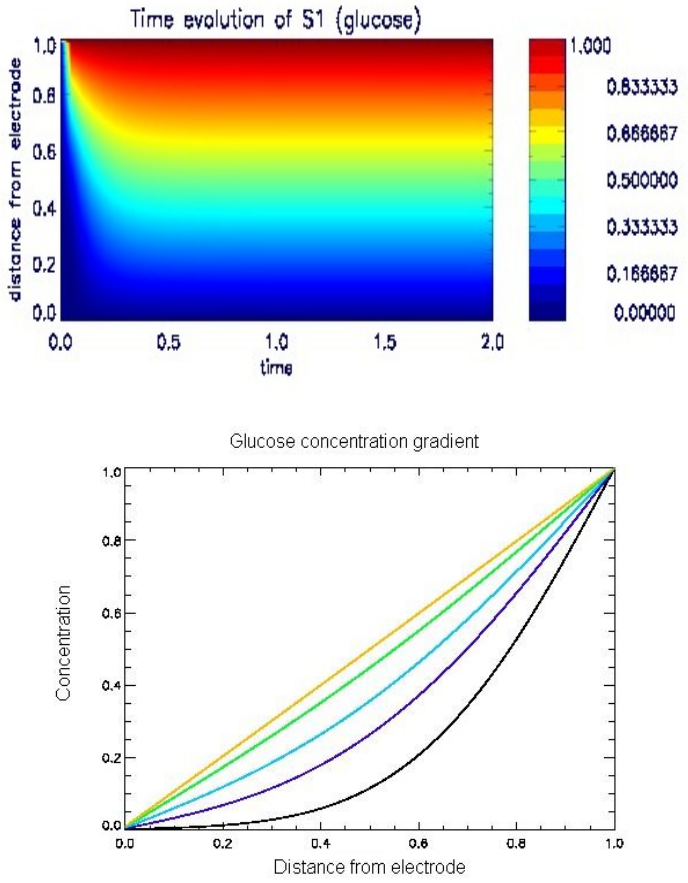

Figure 4.26 – Time evolution of S_1 (glucose) and the glucose concentration gradient. (These graphs are obtained from numerical integration of the equations in Model 1 of Section 4.2.)

Despite the apparent differences in substrate concentrations across the cell, the four models investigated yield surprisingly similar results. This could be explained by the observation that since the optimization problem we are trying to solve involves equilibrium states, the transport processes that supply glucose to the reaction site are less important than the subsequent reactions, especially for large concentrations when all enzymes are optimally engaged.

Chapter 5

Competition Immunoassay Based on a Bi-enzyme Electrode

The performance of the bi-enzyme electrode was investigated in Chapter 4 where we determined which ratio of GOX to HRP resulted in the highest signal amplitude. In this chapter we construct a model for a biosensor based on the same enzyme coupling in order to detect the immunological reaction between avidin and biotin. This time we consider a combination of avidin and HRP immobilized on an electrode and a fluid sample containing biotin and GOX-labelled biotin. The specific avidin-biotin interaction brings the biotin-GOX conjugate close to the immobilized HRP on the electrode surface and the same cascade reaction as in the previous chapter is initiated. Using a constant biotin-GOX concentration and increasing the concentration of free biotin, we can construct theoretical calibration curves for biotin determination.

5.1 Introduction

Electrochemical immunosensing is a potential strategy for the development of next generation diagnostic devices. To achieve the simplicity and low cost required for high volume point-of-care and self-use devices, strategies must be formulated which make these devices as basic as possible. For instance, developing an immunosensor device that is as quick and simple to use as a glucose biosensor is a challenging but commercially beneficial goal.

Some studies have succeeded in reducing the immunoassay to a single step on an electrode surface. However, for this to occur, fluid movement is still required by external devices (pumps) to introduce the assay components to the electrode surface. Removal of any external physical force would make the device simpler and cheaper. Any such device would have to rely predominantly on diffusional processes to bring about the interactions of the assay components on the electrode surface as occurs with glucose biosensors. Such a principle has not yet been extended to electrochemical immunosensors.

A theoretical platform, proposed by researchers in the NCSR, is described in the following paragraphs. This also illustrates the general principle of competition assays. Briefly, the platform consists of an electrode surface held at a suitable potential, modified with a conducting polymer and immobilized antibody (B). In a real-world application, the analyte or antigen to be measured (A) would be introduced with the sample liquid (blood, urine etc.) to the vicinity of the electrode. An analogue of this

antigen connected to an enzyme glucose oxidase (E) and an enzyme substrate (S) would have been present in an inactive form in the vicinity of the electrode prior to sample introduction. Following sample introduction, antigen, analogue and substrate will all be present near the electrode and will all interact with one another in various ways. E will consume S in the bulk solution; while E and A will diffuse to the electrode surface and interact with B forming the complex P^E and product P, respectively. When P^E is formed, the enzyme is brought close to the electrode surface, and when it interacts with substrate, its consumption is linked to electron transfer at the electrode surface and a current measurement is made. The current generated is dependent on the number of interactions of E with B (which is in turn inversely proportional to the number of interactions of A and B) and also the concentration of substrate at the electrode surface.

An argument is made in [2] for improving this platform so that the enzyme label is catalytically linked to another enzyme so it produces a cascade reaction. The disadvantage of the first approach is that the specific signal, obtained from labelled analogue binding to antibody, is very small compared to the nonspecific signal (the noise) which arises from the conjugate in the bulk solution. The use of an enzyme-channelling system is known to improve this situation.

As in the previous chapter, the experimental situation we model is that of a three-dimensional tank where the electrode is placed at the bottom (coated with a monolayer of HRP and avidin) and the surface is a free boundary. Since the diffusion process is assumed to be one-dimensional (in the vertical direction only) the shape

of the tank is irrelevant for the modelling process. The experiment is started with uniform substrate concentration in the solution and uniform concentration of avidin and HRP on the electrode. The biotin and GOX-labelled analogue are then released into the solution at a point near the surface, see Figure 5.1 for a schematic representation of this biosensing platform. As an additional simplification we also assume that convection effects are negligible so that transport of species to the electrode occurs mainly by diffusion. This is similar to the approach we took when we modelled the flow injection analysis in Section 2.2.3 (Experiment 3). This simplifying assumption is now justified by the results of Chapter 4 which shows that the dependence of the optimal enzyme ratio on the system parameters is very similar across the wide range of models discussed.

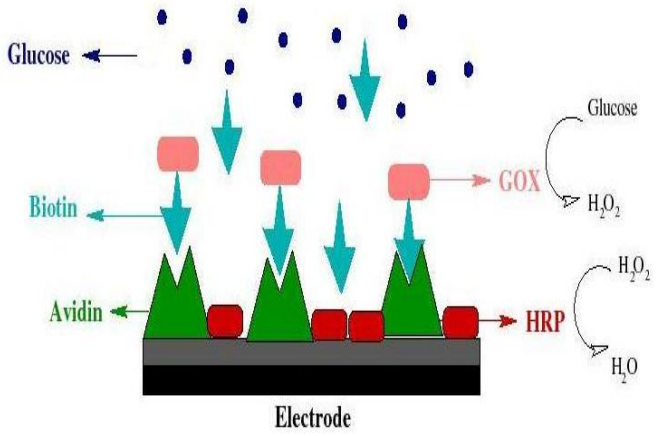

Figure 5.1 – Enzyme channeling immunoassay.

The notation we use for this slightly more complicated platform closely resembles

the notation used in Chapter 4 in the study of the bi-enzyme electrode. Thus, we let

A : immobilized avidin;

B : free biotin;

E_1^B : first enzyme (GOX-labelled biotin);

E_2 : second enzyme (Immobilized HRP);

S_1 : first substrate (Glucose);

S_2 : second substrate (Hydrogen Peroxide);

C_1^B : first complex;

C_2 : second complex;

P : compound formed by avidin and biotin;

P^{E_1} : compound formed by avidin and biotin-GOX (E_1^B);

P^{C_1} : compound formed by avidin and complexed biotin (C_1^B);

P_f : final product formed by reduction of H_2O_2.

As it diffuses through the solution, the enzyme label reacts with its substrate (glucose), where the reaction scheme is expressed by

$$E_1^B + S_1 \underset{K_{-1}}{\overset{K_1}{\rightleftarrows}} C_1^B \xrightarrow{K_2} E_1^B + S_2. \tag{5.1}$$

The following reactions take place at the electrode surface

$$E_1^B + A \xrightarrow{K_b^*} P^{E_1}, \tag{5.2}$$

$$B + A \xrightarrow{K_b} P, \tag{5.3}$$

$$P^{E_1} + S_1 \underset{K_{-1}}{\overset{K_1}{\rightleftarrows}} P^{C_1} \xrightarrow{K_2} P^{E_1} + S_2, \tag{5.4}$$

$$C_1^B + A \xrightarrow{K_b^*} P^{C_1} \xrightarrow{K_2} P^{E_1} + S_2, \tag{5.5}$$

$$S_2 + E_2 \underset{K_{-3}}{\overset{K_3}{\rightleftarrows}} C_2 \xrightarrow{K_4} E_2 + P_f. \tag{5.6}$$

5.2 Mathematical Model

As explained in the introduction, we will construct a mathematical model to describe the behaviour of a large number of chemical species, which are subject to diffusion and chemical reactions in the spatial domain [0, L], where $X = 0$ denotes the position of the electrode and $X = L$ is the free surface of the flow cell. As we have chosen to neglect convection for this problem, the system can now be modelled by the following reaction-diffusion equations, for $X \in [0, L], T > 0$

$$\frac{\partial [B]}{\partial T} = D \frac{\partial^2 [B]}{\partial X^2}, \tag{5.7}$$

$$\frac{\partial [E_1^B]}{\partial T} = D \frac{\partial^2 [E_1^B]}{\partial X^2} + (K_{-1} + K_2)[C_1^B] - K_1 [E_1^B][S_1], \tag{5.8}$$

$$\frac{\partial [S_1]}{\partial T} = D \frac{\partial^2 [S_1]}{\partial X^2} + K_{-1}[C_1^B] - K_1 [E_1^B][S_1], \tag{5.9}$$

$$\frac{\partial [C_1^B]}{\partial T} = D \frac{\partial^2 [C_1^B]}{\partial X^2} - (K_{-1} + K_2)[C_1^B] + K_1 [E_1^B][S_1], \tag{5.10}$$

$$\frac{\partial [S_2]}{\partial T} = D \frac{\partial^2 [S_2]}{\partial X^2} + K_2 [C_1^B], \tag{5.11}$$

$$\frac{\partial [P_f]}{\partial T} = D \frac{\partial^2 [P_f]}{\partial X^2}, \tag{5.12}$$

where [ ] denotes the concentration of the species. Given the large number of diffusing species and the difficulty in obtaining precise diffusion constants for all of them, we have assumed all these constants to be the same and have denoted this number by D.

On the free surface (where $X = L$) we impose zero-flux boundary conditions, namely;

$$\frac{\partial[B]}{\partial X}(L,T) = \frac{\partial[E_1^B]}{\partial X}(L,T) = \frac{\partial[S_1]}{\partial X}(L,T) = 0,$$
$$\frac{\partial[C_1^B]}{\partial X}(L,T) = \frac{\partial[S_2]}{\partial X}(L,T) = \frac{\partial[P_f]}{\partial X}(L,T) = 0.$$

At the electrode (where $X = 0$) we have the reaction boundary conditions,

$$D\frac{\partial[B]}{\partial X}(0,T) = K_b[B][A], \tag{5.13}$$
$$D\frac{\partial[E_1^B]}{\partial X}(0,T) = K_b^*[E_1^B][A], \tag{5.14}$$
$$D\frac{\partial[S_1]}{\partial X}(0,T) = K_1[P^{E_1}][S_1] - K_{-1}[P^{C_1}], \tag{5.15}$$
$$D\frac{\partial[C_1^B]}{\partial X}(0,T) = K_b^*[C_1^B][A], \tag{5.16}$$
$$D\frac{\partial[S_2]}{\partial X}(0,T) = K_3[S_2][E_2] - K_2[P^{C_1}] - K_{-3}[C_2], \tag{5.17}$$
$$D\frac{\partial[P_f]}{\partial X}(0,T) = -K_4[C_2]. \tag{5.18}$$

In addition, the following evolution equations hold on the boundary;

$$\frac{d[A]}{dT} = -K_b^*([E_1^B] + [C_1^B])[A] - K_b[B][A], \tag{5.19}$$

$$\frac{d[C_2]}{dT} = K_3[E_2][S_2] - (K_4 + K_{-3})[C_2], \tag{5.20}$$

$$\frac{d[P^{E_1}]}{dT} = K_b^*[E_1^B][A] - K_1[S_1][P^{E_1}] + (K_{-1} + K_2)[P^{C_1}], \tag{5.21}$$

$$\frac{d[P^{C_1}]}{dT} = K_b^*[C_1^B][A] + K_1[S_1][P^{E_1}] - (K_{-1} + K_2)[P^{C_1}], \tag{5.22}$$

$$\frac{d[P]}{dT} = K_b[B][A], \tag{5.23}$$

and the current is calculated as

$$\frac{\partial[P_f]}{\partial T} = K_4[C_2]. \tag{5.24}$$

The initial values are;

$$[S_1](X,0) = S_0, \quad [S_2](X,0) = 0, \quad [C_1^B](X,0) = 0,$$

$$[E_2](0) = E_2^0, \quad [A](0) = A_0, \quad [P](X,0) = 0,$$

$$[P^{E_1}](X,0) = 0, \quad [P^{C_1}](X,0) = 0, \quad [P_f](X,0) = 0,$$

$$[E_1^B](X,0) = \begin{cases} B_0^*, & \text{if } X = L \\ 0, & \text{otherwise,} \end{cases}$$

$$[B](X,0) = \begin{cases} B_0, & \text{if } X = L \\ 0, & \text{otherwise.} \end{cases}$$

As stated at the beginning of this section, the initial concentration of glucose is uniform throughout the domain while finite amounts of biotin and biotin-GOX are injected at a point near the surface. Although experimental observations and the results of Chapter 4 indicate that, in the case of the bi-enzyme electrode, a HRP/GOX

ratio of 1 leads to the highest signal, we will re-examine this ratio when avidin and HRP are concerned. In a manner similar to Chapter 4, we let

$$\zeta E_2^0 = A_0, \tag{5.25}$$

and, if we denote by E_0 the total concentration corresponding to full electrode coverage, we have

$$E_2^0 + A_0 = E_0, \tag{5.26}$$

which gives

$$E_2^0 = \frac{E_0}{1+\zeta}, \quad A_0 = \frac{\zeta E_0}{1+\zeta}. \tag{5.27}$$

The following variables are used to non-dimensionalise the system,

$$\begin{aligned}
x &= \frac{X}{L}, \quad t = \frac{D}{L^2}T, \\
a &= \frac{[A]}{E_0}, \quad b = \frac{[B]}{B_0^*}, \\
c_1 &= \frac{[C_1^B]}{B_0^*}, \quad c_2 = \frac{[C_2]}{E_0}, \\
e_1 &= \frac{[E_1^B]}{B_0^*}, \quad e_2 = \frac{[E_2]}{E_0}, \\
s_1 &= \frac{[S_1]}{S_0}, \quad s_2 = \frac{[S_2]}{S_0}, \\
p &= \frac{[P]}{E_0}, \quad p_1 = \frac{[P^{E_1}]}{E_0}, \\
p_2 &= \frac{[P^{C_1}]}{E_0}, \quad p_f = \frac{[P_f]L}{E_0}.
\end{aligned}$$

Note that we used B_0^*, the initial concentration of labelled biotin, to non-dimensionalise certain species as this concentration is usually kept constant during experiments while B_0, the initial biotin concentration, is allowed to vary. The non-dimensional reaction-

diffusion equations are:

$$\frac{\partial b}{\partial t} = \frac{\partial^2 b}{\partial x^2}, \tag{5.28}$$

$$\frac{\partial e_1}{\partial t} = \frac{\partial^2 e_1}{\partial x^2} + (k_{-1} + k_2)c_1 - k_1 e_1 s_1, \tag{5.29}$$

$$\frac{\partial s_1}{\partial t} = \frac{\partial^2 s_1}{\partial x^2} + \eta k_{-1} c_1 - \eta k_1 e_1 s_1, \tag{5.30}$$

$$\frac{\partial c_1}{\partial t} = \frac{\partial^2 c_1}{\partial x^2} + k_1 e_1 s_1 - (k_{-1} + k_2)c_1, \tag{5.31}$$

$$\frac{\partial s_2}{\partial t} = \frac{\partial^2 s_2}{\partial x^2} + \eta k_2 c_1, \tag{5.32}$$

$$\frac{\partial p_f}{\partial t} = \frac{\partial^2 p_f}{\partial x^2}, \tag{5.33}$$

where

$$k_1 = \frac{K_1 S_0 L^2}{D}, \quad k_{-1} = \frac{K_{-1} L^2}{D}, \quad k_2 = \frac{K_2 L^2}{D}, \quad \eta = \frac{B_0^*}{S_0}.$$

The non-dimensional form of the boundary conditions on $x = 0$ is

$$\frac{\partial b}{\partial x} = k_b a b, \tag{5.34}$$

$$\frac{\partial e_1}{\partial x} = k_b^* a e_1, \tag{5.35}$$

$$\frac{\partial s_1}{\partial x} = k_1 \varphi p_1 s_1 - k_{-1} \varphi p_2, \tag{5.36}$$

$$\frac{\partial c_1}{\partial x} = k_b^* a c_1, \tag{5.37}$$

$$\frac{\partial s_2}{\partial x} = k_3 e_2 s_2 - k_2 \varphi p_2 - k_{-3} c_2, \tag{5.38}$$

$$\frac{\partial p_f}{\partial x} = -k_4 c_2, \tag{5.39}$$

where

$$k_b = \frac{L K_b E_0}{D}, \quad k_b^* = \frac{L K_b^* E_0}{D}, \quad \varphi = \frac{E_0}{S_0 L},$$
$$k_3 = \frac{L K_3 E_0}{D}, \quad k_{-3} = \frac{L K_{-3} E_0}{D S_0}, \quad k_4 = \frac{L^2 K_4}{D},$$

and the evolution equations become

$$\frac{da}{dt} = -\frac{k_b^*\eta}{\varphi}(e_1 + c_1)a - \frac{k_b\eta}{\varphi}ab, \tag{5.40}$$

$$\frac{dc_2}{dt} = \frac{k_3}{\varphi}e_2 s_2 - (\frac{k_{-3}}{\varphi} + k_4)c_2, \tag{5.41}$$

$$\frac{dp_1}{dt} = \frac{k_b^*\eta}{\varphi}ae_1 - k_1 s_1 p_1 + (k_{-1} + k_2)p_2, \tag{5.42}$$

$$\frac{dp_2}{dt} = \frac{k_b^*\eta}{\varphi}ac_1 + k_1 s_1 p_1 - (k_{-1} + k_2)p_2, \tag{5.43}$$

$$\frac{dp}{dt} = \frac{k_b\eta}{\varphi}ab. \tag{5.44}$$

The remaining boundary conditions are:

$$\frac{\partial b}{\partial x}(1,t) = \frac{\partial e_1}{\partial x}(1,t) = \frac{\partial s_1}{\partial x}(1,t) = \frac{\partial c_1}{\partial x}(1,t) = \frac{\partial s_2}{\partial x}(1,t) = \frac{\partial p_f}{\partial x}(1,t) = 0.$$

Finally, the initial conditions can be written as

$$a(x,0) = \frac{\zeta}{1+\zeta}, \quad s_1(x,0) = 1, \quad e_2(x,0) = \frac{1}{1+\zeta},$$

$$c_1(x,0) = s_2(x,0) = p(0) = p_1(0) = p_2(0) = p_f(0) = 0,$$

$$e_1(x,0) = \begin{cases} 1, & \text{if } x = 1 \\ \\ 0, & \text{otherwise,} \end{cases}$$

$$b(x,0) = \begin{cases} \beta, & \text{if } x = 1 \\ \\ 0, & \text{otherwise,} \end{cases}$$

where we let

$$\beta = \frac{B_0}{B_0^*}$$

denote the ratio of biotin to labelled biotin.

The system of differential equations (5.28)-(5.33), together with its boundary and initial conditions, is integrated numerically, using a standard finite difference scheme.

Figures 5.2 and 5.3 show the time evolution across the flow cell for some of the diffusing reactants. Figures 5.4 and 5.5 show the time evolution of the current dp/dt for different initial biotin to labelled biotin concentration ratios (β). The initial concentrations used for our numerical simulations are shown in Table 5.1; where values for reaction rate constants are, again, taken from Table 4.1. The "universal" diffusion constant for all free species was taken as $D = 6.7 \times 10^{-10}$ m^2/s. Note that, as a consequence of starting with a finite amount of glucose, the shape of the signal is different from that in Chapter 4 (Figure 4.11) where the flow injection analysis involves a continuous supply of glucose. In this case, the current peaks and then decays and we use the maximum value of this function as the signal amplitude for all future calculations. For example, the information contained in Figures 5.4 or 5.5 can be more compactly presented as one of the curves in Figure 5.6 which shows the dependence of the current peak response on the biotin-analogue ratios.

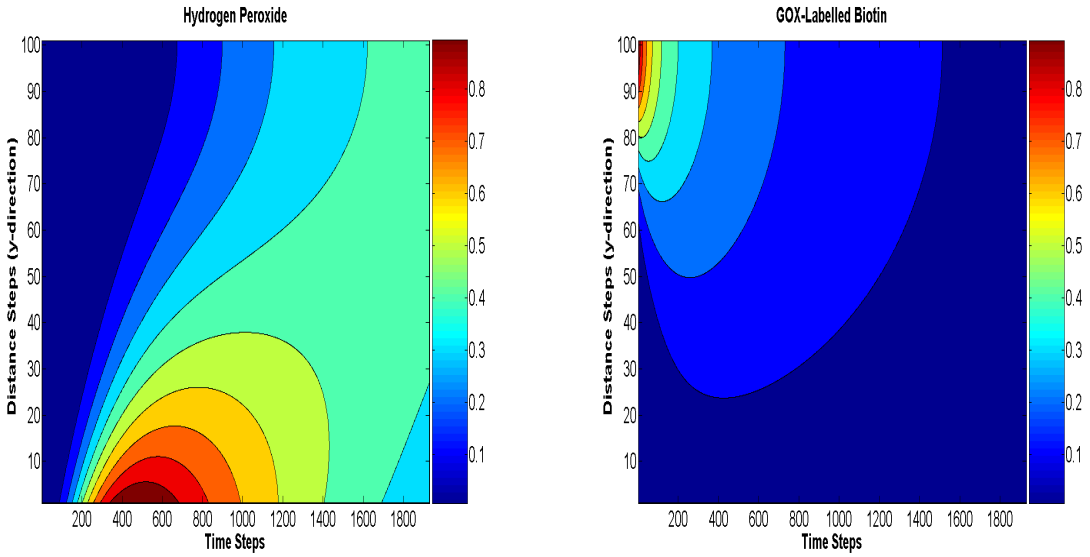

Figure 5.2 – Time evolution of substrates.

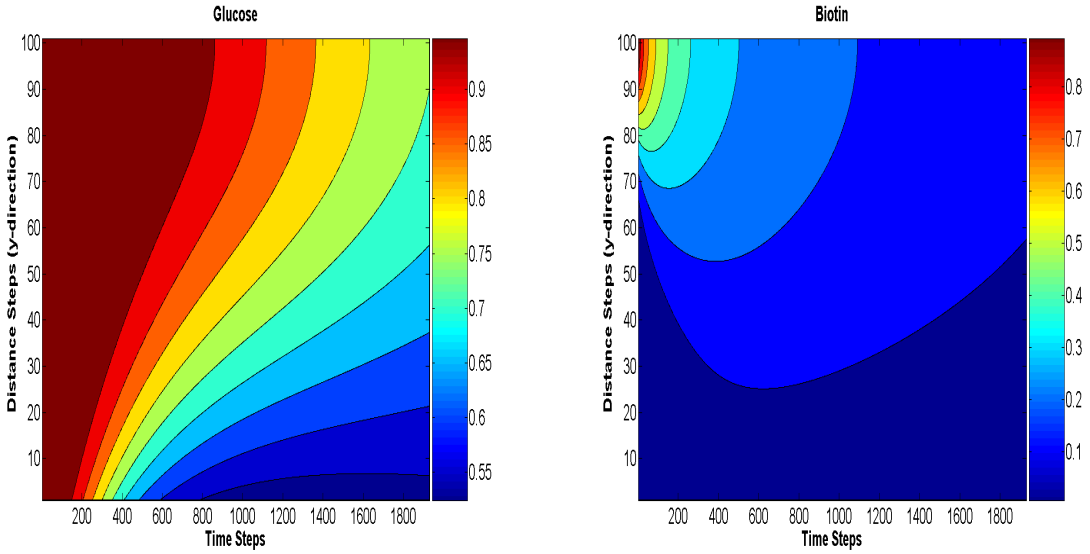

Figure 5.3 – Time evolution of added analytes.

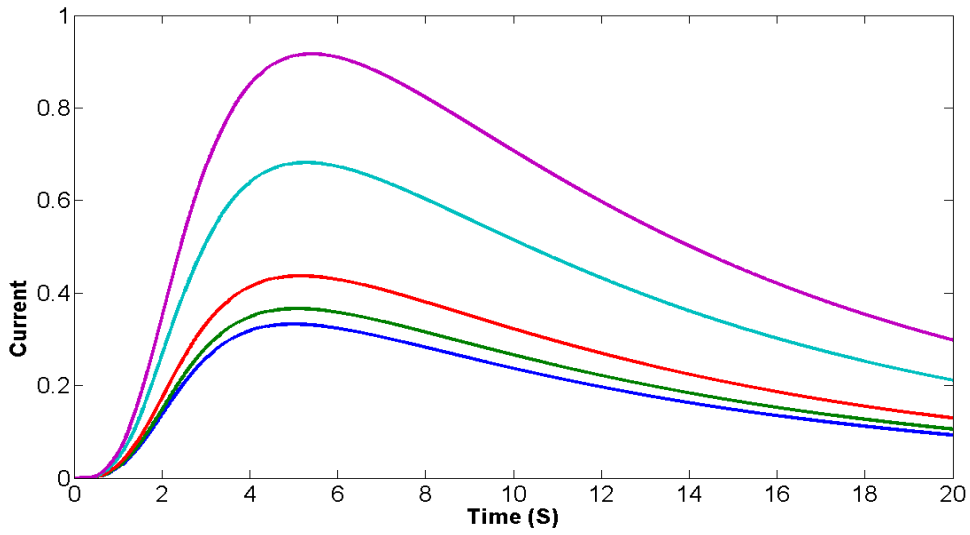

Figure 5.4 – Dependence of current on time for different biotin to labelled biotin ratios, β. The ratio of avidin to HRP is 1:1. From bottom to top the curves correspond to $\beta = 100, 20, 5, 1, 0$.

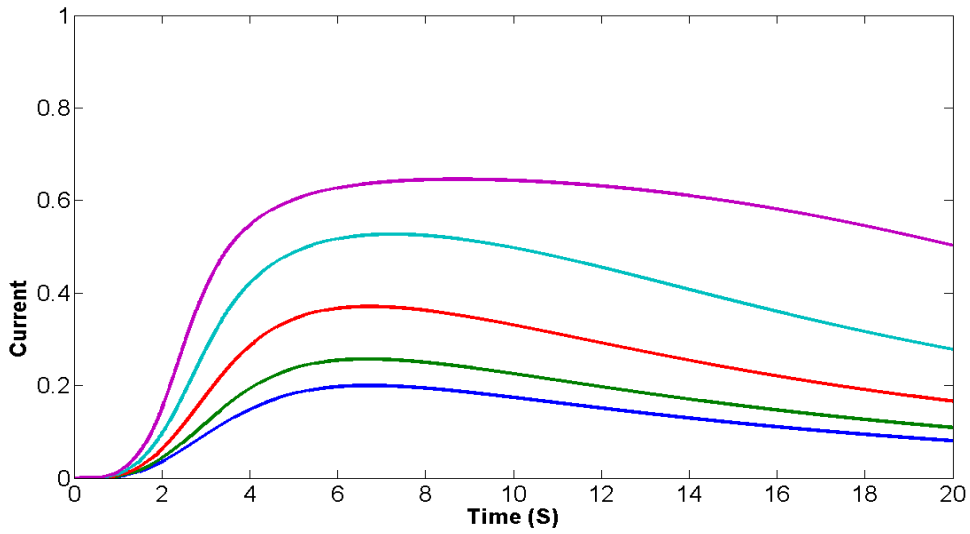

Figure 5.5 – Dependence of current on time for different biotin to labelled biotin ratios, β. The ratio of avidin to HRP is 3:1. From bottom to top the curves correspond to $\beta = 100, 20, 5, 1, 0$.

Description	***Constant***	***Value***
Total enzyme (mol/m^2)	E_0	10^{-5}
Glucose (mol/m^3=mM)	S_0	1
Biotin (mol/m^3=mM)	B_0	$0 - 0.75 \times 10^{-5}$
Labelled biotin (mol/m^3=mM)	B_0^*	0.25×10^{-7}

Table 5.1 – Typical values for initial concentrations of reactants.

These type of curves are known as **calibration curves** (or **dose-response curves**) and are generally constructed by measuring and plotting the biosensor responses against a wide range of initial analyte concentrations. Calibration curves can then be used for future estimations of the "dose" once the "response" is known. Note that, in

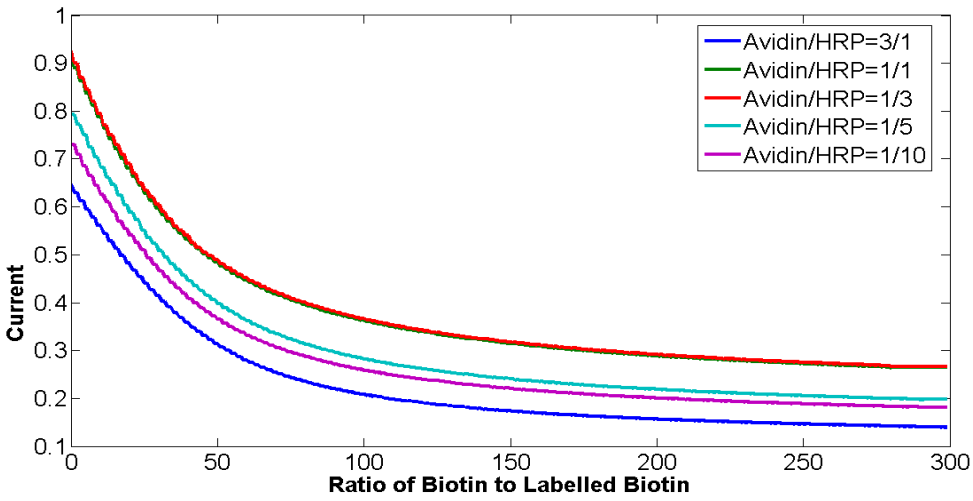

Figure 5.6 – Dependence of maximum current on β, the ratio of biotin to labelled biotin.

a competitive assay, the analyte (in this case, biotin) competes with a labelled analogue (biotin-GOX) for a limited number of antibody (avidin) binding sites. Since the signal is generated by the labelled species, it follows that the biosensor response is inversely proportional to the amount of analyte present. Hence the calibration curve for a competitive system is always decreasing. Note from Figure 5.6 that the highest signals are obtained for an avidin/HRP ratio (ζ) of between 1/3 and 1, which is a close approximation to the result obtained in Chapter 4. A theoretical and computational optimization study for ζ in the more complex setting of the avidin/HRP platform, which combines a cascade reaction with a competitive assay, could be attempted, in the manner of Chapter 4 and the work presented in [44], but is outside the scope of this thesis and will form the subject of future work. For the time being, we are treating ζ as a variable so as to allow for different results which may arise from the

influence of the additional reactants and also because a further optimization issue will arise in the next section when we consider signal to noise ratio.

5.3 Specific and nonspecific Signals

The performance of a biosensor is often affected by the presence of a nonspecific, or noisy, component of the recorded signal. In the configuration studied in this section, the specific signal is generated when biotin-GOX binds to the immobilized avidin and the enzymatic cascade reaction is initiated close to the electrode. In this instance, the current is proportional to the catalytic conversion of H_2O_2 in the second reaction and is clearly related to the binding between avidin and labelled biotin. However, hydrogen peroxide can also be generated throughout the cell when the GOX label reacts with the glucose present in solution. This "stray" hydrogen peroxide reaches the electrode and reacts with the immobilized HRP thus completing the second step of the cascade reaction and generating an electrical signal. Clearly, this current arises in the absence of any relevant binding of avidin and biotin and can therefore be described as a noisy (and useless) component of the signal.

It is obviously very difficult to distinguish between specific and nonspecific signals during the experimentation phase. The experimental method presented in [2] suggests that the nonspecific signal can be obtained by passing a GOX solution (without the attached biotin) over the electrode. This is then compared with the total signal which is recorded for the usual biotin-GOX flow injection system. The assumption that the signal generated from GOX can mimic the nonspecific interactions associated with

biotin-GOX could be challenged with the observation that the two enzymes (with and without biotin) may display different activities.

The modelling approach has the advantage that the evolution of all concentrations can be precisely monitored and hence, in this section, we propose a method for separating the noise from the good signal. This method is based on the simple observation that the "good" and "bad" currents can be traced back to the H_2O_2 generated at the electrode surface or in the bulk solution. We therefore treat hydrogen peroxide generated in these different contexts as **two different species** and keep track of each of them separately. We denote the H_2O_2 generated at the electrode (in the presence of avidin-biotin binding) by S_2 as before, while the solution H_2O_2, which will ultimately lead to the noisy signal, is denoted by S_n. The reactions (5.1)-(5.6) are rewritten below.

The reaction taking place in the bulk solution is

$$E_1^B + S_1 \underset{K_{-1}}{\overset{K_1}{\rightleftarrows}} C_1^B \xrightarrow{K_2} E_1^B + S_n, \tag{5.45}$$

and the following reactions take place at the electrode surface

$$E_1^B + A \xrightarrow{K_b^*} P^{E_1}, \tag{5.46}$$

$$B + A \xrightarrow{K_b} P, \tag{5.47}$$

$$P^{E_1} + S_1 \underset{K_{-1}}{\overset{K_1}{\rightleftarrows}} P^{C_1} \xrightarrow{K_2} P^{E_1} + S_2, \tag{5.48}$$

$$C_1^B + A \xrightarrow{K_b^*} P^{C_1} \xrightarrow{K_2} P^{E_1} + S_2, \tag{5.49}$$

$$S_2 + E_2 \underset{K_{-3}}{\overset{K_3}{\rightleftarrows}} C_2 \xrightarrow{K_4} E_2 + P_f, \tag{5.50}$$

$$S_n + E_2 \underset{K_{-3}}{\overset{K_3}{\rightleftarrows}} C_n \xrightarrow{K_4} E_2 + P_n, \tag{5.51}$$

where C_2, C_n denote the second enzyme bound to specific and noisy substrate respectively, while P_f, P_n denote the final products of the system. As before, this scheme can be expressed as a system of reaction-diffusion equations, for $X \in (0, L)$ and $T > 0$,

$$\frac{\partial [B]}{\partial T} = D \frac{\partial^2 [B]}{\partial X^2}, \tag{5.52}$$

$$\frac{\partial [E_1^B]}{\partial T} = D \frac{\partial^2 [E_1^B]}{\partial X^2} + (K_{-1} + K_2)[C_1^B] - K_1 [E_1^B][S_1], \tag{5.53}$$

$$\frac{\partial [S_1]}{\partial T} = D \frac{\partial^2 [S_1]}{\partial X^2} + K_{-1}[C_1^B] - K_1 [E_1^B][S_1], \tag{5.54}$$

$$\frac{\partial [C_1^B]}{\partial T} = D \frac{\partial^2 [C_1^B]}{\partial X^2} - (K_{-1} + K_2)[C_1^B] + K_1 [E_1^B][S_1], \tag{5.55}$$

$$\frac{\partial [S_2]}{\partial T} = D \frac{\partial^2 [S_2]}{\partial X^2} + K_2 [C_1^B], \tag{5.56}$$

$$\frac{\partial [S_n]}{\partial T} = D \frac{\partial^2 [S_n]}{\partial X^2} + K_2 [C_1^B], \tag{5.57}$$

$$\frac{\partial [P_f]}{\partial T} = D \frac{\partial^2 [P_f]}{\partial X^2}, \tag{5.58}$$

$$\frac{\partial [P_n]}{\partial T} = D \frac{\partial^2 [P_n]}{\partial X^2}, \tag{5.59}$$

where [ ] denotes the concentration of the species. On the free surface (where $X = L$)

we impose zero-flux boundary conditions

$$\frac{\partial[B]}{\partial X}(L,T) = \frac{\partial[E_1^B]}{\partial X}(L,T) = \frac{\partial[S_1]}{\partial X}(L,T) = \frac{\partial[C_1^B]}{\partial X}(L,T) = 0,$$
$$\frac{\partial[S_2]}{\partial X}(L,T) = \frac{\partial[S_n]}{\partial X}(L,T) = \frac{\partial[P_f]}{\partial X}(L,T) = \frac{\partial[P_n]}{\partial X}(L,T) = 0.$$

At the electrode (where $X = 0$) we have reaction boundary conditions

$$D\frac{\partial[B]}{\partial X}(0,T) = K_b[B][A], \tag{5.60}$$
$$D\frac{\partial[E_1^B]}{\partial X}(0,T) = K_b^*[E_1^B][A], \tag{5.61}$$
$$D\frac{\partial[S_1]}{\partial X}(0,T) = K_1[P^{E_1}][S_1] - K_{-1}[P^{C_1}], \tag{5.62}$$
$$D\frac{\partial[C_1^B]}{\partial X}(0,T) = K_b^*[C_1^B][A], \tag{5.63}$$
$$D\frac{\partial[S_2]}{\partial X}(0,T) = K_3[S_2][E_2] - K_2[P^{C_1}] - K_{-3}[C_2], \tag{5.64}$$
$$D\frac{\partial[S_n]}{\partial X}(0,T) = K_3[S_n][E_2] - K_{-3}[C_n], \tag{5.65}$$
$$D\frac{\partial[P_f]}{\partial X}(0,T) = -K_4[C_2], \tag{5.66}$$
$$D\frac{\partial[P_n]}{\partial X}(0,T) = -K_4[C_2]. \tag{5.67}$$

In addition, the following evolution equations hold on the boundary

$$\frac{d[A]}{dT} = -K_b^*([E_1^B] + [C_1^B])[A] - K_b[B][A], \tag{5.68}$$
$$\frac{d[C_2]}{dT} = K_3[E_2][S_2] - (K_4 + K_{-3})[C_2], \tag{5.69}$$
$$\frac{d[P^{E_1}]}{dT} = K_b^*[E_1^B][A] - K_1[S_1][P^{E_1}] + (K_{-1} + K_2)[P^{C_1}], \tag{5.70}$$
$$\frac{d[P^{C_1}]}{dT} = K_b^*[C_1^B][A] + K_1[S_1][P^{E_1}] - (K_{-1} + K_2)[P^{C_1}], \tag{5.71}$$
$$\frac{d[C_n]}{dT} = K_3[E_2][S_n] - (K_4 + K_{-3})[C_n], \tag{5.72}$$
$$\frac{d[P]}{dT} = K_b[B][A], \tag{5.73}$$

while the specific and nonspecific currents, I_s and I_n, are calculated as

$$I_s = \frac{d[P_f]}{dT} = K_4[C_2], \tag{5.74}$$

$$I_n = \frac{d[P_n]}{dT} = K_4[C_n]. \tag{5.75}$$

The initial values are:

$$[S_1](X,0) = S_0, \quad [S_2](X,0) = 0, \quad [S_n](X,0) = 0, \quad [C_1^B](X,0) = 0,$$

$$[E_2](0) = E_2^0, \quad [A](0) = A_0, \quad [P](X,0) = 0, \quad [P^{E_1}](X,0) = 0,$$

$$[P^{C_1}](X,0) = 0, \quad [P_f](X,0) = 0, \quad [P_n](X,0) = 0.$$

$$[E_1^B](X,0) = \begin{cases} B_0^*, & \text{if } X = L \\ \\ 0, & \text{otherwise,} \end{cases}$$

$$[B](X,0) = \begin{cases} B_0, & \text{if } X = L \\ \\ 0, & \text{otherwise.} \end{cases}$$

By using the same non-dimensional variables as in Section 5.2, together with the following variables

$$c_n = \frac{[C_n]}{E_0}, \quad s_n = \frac{[S_n]}{S_0}, \quad p_n = \frac{[P_n]L}{E_0},$$

the non-dimensional form of equations (5.52)-(5.73) are the same as the non-dimensional equations (5.28)-(5.44) plus the following non-dimensional reaction boundary conditions for S_n, P_n, and the evolution equation for C_n on the boundary:

$$\frac{\partial s_n}{\partial x} = k_3 e_2 s_n - k_{-3} c_n, \tag{5.76}$$

$$\frac{\partial p_n}{\partial x} = -k_4 c_2, \tag{5.77}$$

$$\frac{dc_n}{dt} = \frac{k_3}{\varphi} e_2 s_n - (\frac{k_{-3}}{\varphi} + k_4) c_n, \tag{5.78}$$

$$\tag{5.79}$$

with additional zero-flux boundary conditions:

$$\frac{\partial s_n}{\partial x}(1,t) = \frac{\partial p_n}{\partial x}(1,t) = 0,$$

and initial conditions:

$$s_2(x,0) = p_n(0) = 0.$$

As before, the system of non-dimensional equations can be integrated numerically and the specific and nonspecific signals given by (5.74) and (5.75), are plotted in Figure 5.7 (when the ratio of avidin to HRP is 1:1) and Figure 5.8 (when the ratio is 3:1). The total signal is then obtained as the sum of the specific and noisy components, that is;

$$I_{tot} = I_s + I_n. \tag{5.80}$$

It is easily seen from this simulation result that for the choice of system parameters corresponding to Figure 5.7 ($S_0 = 1$ mM, B_0 (biotin) $= 0$, ζ (avidin/HRP) $= 1$, B_0^* (labelled biotin) $= 0.25 \times 10^{-7}$ mM), the noisy component seems to be approximately half the size of the specific current and so, approximately one third of the recorded signal is due to nonspecific causes. The question now arises whether this platform can be further optimized where the design parameters are chosen so as to maximize the specific current to noise ratio. We first investigated how this ratio responds to changes in the biotin concentration; Figures 5.9 and 5.10 show the time evolution of the total current to noise ratio for values of β ranging between 0 and 100. (The two figures correspond to avidin/HRP ratios of 1 and 3.) It is clearly seen that the best results are obtained in the absence of biotin ($\beta = 0$) which is not surprising given the competitive nature of the system (large amounts of biotin would prevent the binding

of labelled biotin to avidin, thus decreasing the specific current component of the signal).

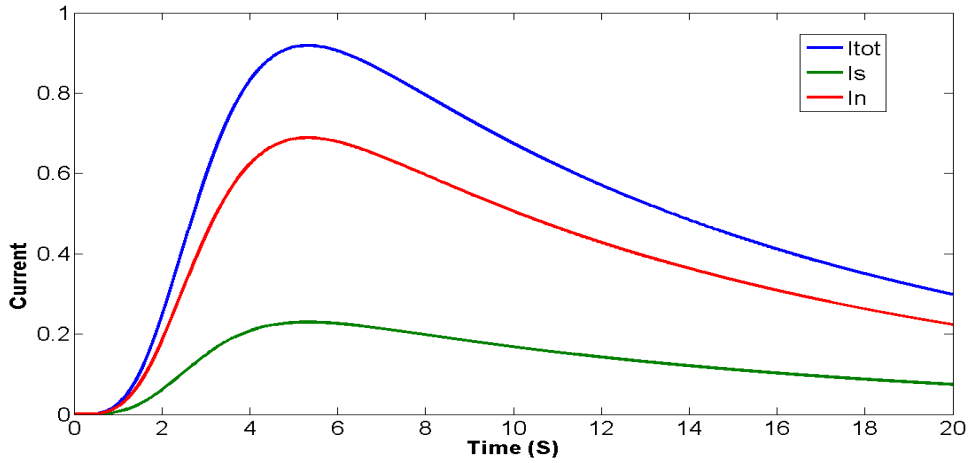

Figure 5.7 – Dependence of current on time:total, specific and nonspecific signals. (The ratio of avidin to HRP is 1:1.)

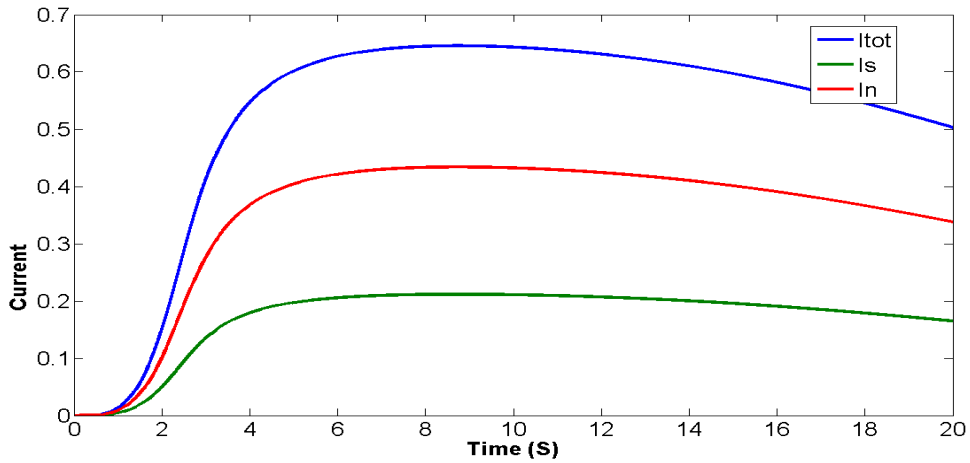

Figure 5.8 – Dependence of current on time:total, specific and nonspecific signals. (The ratio of avidin to HRP is 3:1.)

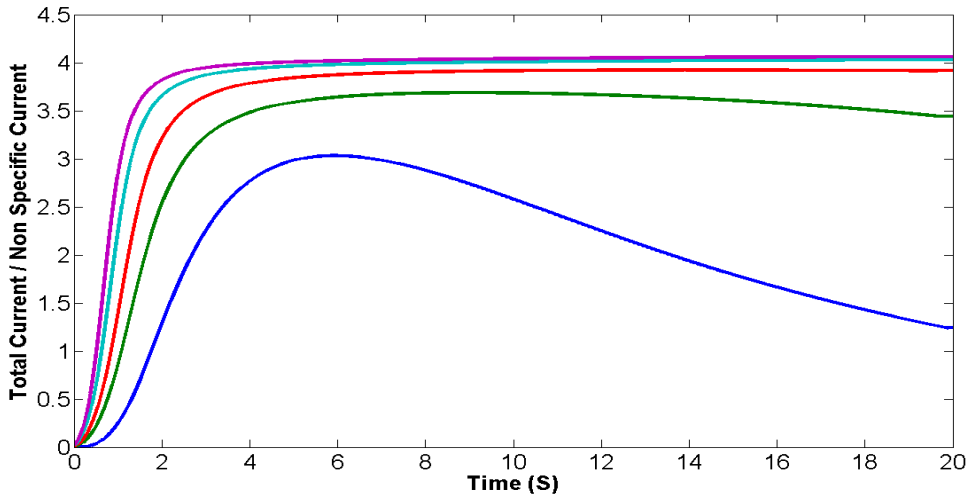

Figure 5.9 – Dependence of ratio of total current to nonspecific current on time for different ratios of biotin to labelled biotin, β. The ratio of avidin to HRP is 1:1. From bottom to top the curves correspond to $\beta = 100, 20, 5, 1, 0$.

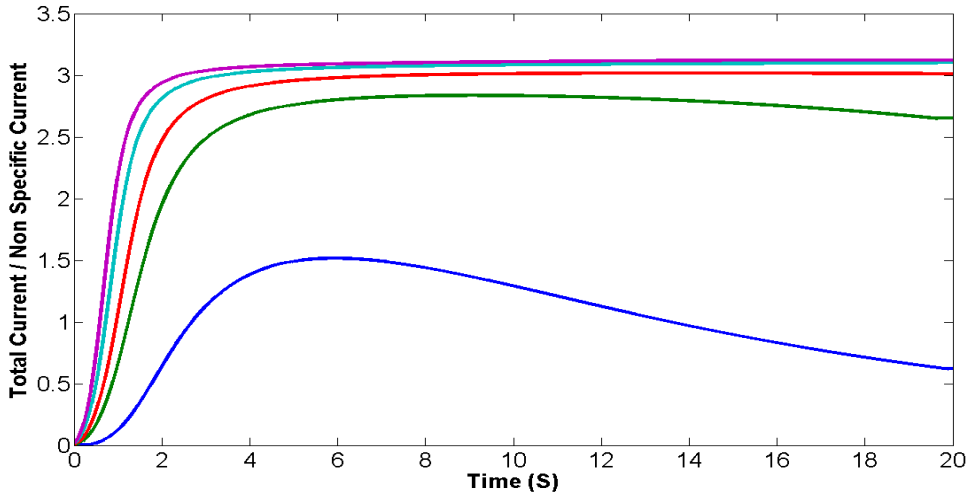

Figure 5.10 – Dependence of ratio of total current to nonspecific current on time for different ratios of biotin to labelled biotin, β. The ratio of avidin to HRP is 3:1. From bottom to top the curves correspond to $\beta = 100, 20, 5, 1, 0$.

We therefore keep $\beta = 0$ (no free biotin) and study the effect of modifying the avidin/HRP ratio on the electrode. Figure 5.11 shows the time evolution of the total current to noise ratio for several values of ζ ranging between 0.1 and 10. The best results, according to these simulations, seem to be achieved for $\zeta = 1/3$, while $\zeta = 1$ still gives a good signal to noise response.

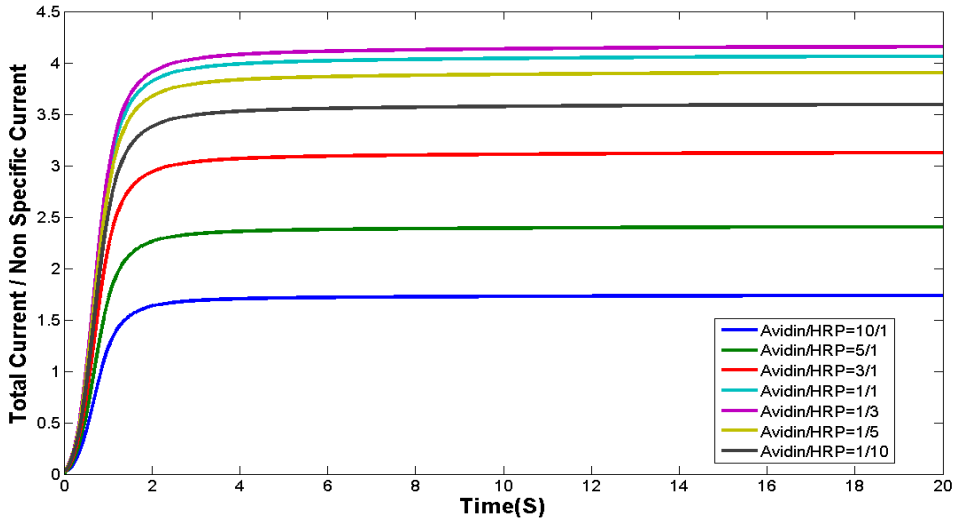

Figure 5.11 – Dependence of ratio of total current to nonspecific current on time for different ratios of avidin to HRP.

5.4 Conclusions

The optimized avidin/HRP platform studied in Chapter 4 was now tested for a real-time biotin determination using a competition assay system, where solutions with free biotin at different concentrations and biotin-GOX were introduced. A mathematical

model was constructed which illustrates the competition between biotin and biotin-GOX for binding with avidin, coupled with an enzymatic cascade reaction at the electrode. Using numerical simulations we were able to plot the biosensor response (the maximum current) as a function of the free biotin concentration. We anticipate that this procedure could be used more widely in biosensor modelling in order to generate theoretical calibration curves.

A necessary preliminary step before the calculation of a satisfactory calibration curve is the optimization of the biosensing platform. The problem of maximizing signal amplitude was approached in Chapter 4 where we analyzed the optimal GOX:HRP ratio. A similar question regarding the avidin/HRP ratio in the competitive assay context remains to be investigated. Numerical simulations were performed in order to assess the effect of the avidin/HRP ratio on the nonspecific interactions, which are unavoidable in such systems. It was concluded in [2] that the nonspecific signal which resulted from their experimental assessment of this platform, was unacceptably high and that a sensitive evaluation in real time of the immunological interaction for avidin-biotin was not practical. Perhaps, if a mathematical and computational feasibility study is attempted before the experimentation stage in future problems, this could lead to shorter design times and smaller costs.

Conclusions and Future Work

The motivation for this thesis was provided by a collaboration with the National Centre for Sensor Research (NCSR) and the Biomedical Diagnostics Institute (BDI) at Dublin City University involving mathematical and computational modelling of biosensors. Several experimental problems relevant to ongoing research in these centres were presented which were mostly concerned with optimizing design parameters for biosensing devices. We modelled these problems mathematically, used numerical techniques to solve them, and described the behaviour of the solutions, with a view to providing recommendations for improving experimental practice.

A brief summary of this thesis is given below, together with recommendations for future work. After reviewing the Michaelis-Menten kinetics scheme for enzyme-substrate interactions (together with other useful Biochemistry and Mathematics concepts) in Chapter 1. Chapter 2 presented a novel experimental and computational method for calculating relevant kinetic rate constants in the case of an immobilized enzyme. (This method was submitted for publication as [24].) Michaelis numbers and catalytic constants are well known for enzymes in solution, but the difficulty associated with surface-bound species is that the immobilized mass needs to be pre-

cisely calculated first. Three simple problems involving immobilized enzymes were then modelled and the experiments were executed in parallel with the numerical simulations, both using the kinetic values observed just determined and good agreement was observed. It would be interesting to investigate whether mathematical, statistical and computational methods could be employed for studying surface deposition of particles and estimating immobilized concentrations. Extensive experimental data performed at NCSR for immobilized HRP (see, for example, [34]) would allow verification of any such theoretical results.

Chapter 3 reviews mathematical models for biomolecular interactions. Diffusion of an analyte in a small cell is studied (in the context of a simplified model for a pregnancy testing device) and fluid convection in a flow channel is introduced while discussing the BIACORE device.

Chapter 4 investigates the problem of optimizing the design of a bi-enzyme biosensor by finding the ratio of two immobilized enzymes which maximizes signal amplitude. A new convection-diffusion model is proposed which generalizes modelling strategies already proposed by our team. This model reinforces the result that the optimal enzyme ratio is inversely proportional to the ratio of their catalytic turnover numbers.

This represents, however, only a first step towards modelling the theoretical and experimental platform studied by NCSR researchers which provided the initial motivation. The original experimental setting involves a combination of avidin and enzyme

(HRP) immobilized on an electrode and a fluid sample containing biotin and biotin-GOX. The substrate of the enzyme label (i.e., glucose) is also introduced into the system and the same cascade reaction as in Chapter 4 is initiated. The main problem to be addressed in this context is to determine initial concentration of pure antigen in the sample, given the amount of enzyme-labelled antigen and the signal recorded at the electrode. This competitive immunosensor was studied experimentally in [2] where it was argued that there are many advantages of coupling the immunological reaction to an enzyme-channelling scheme such as, for example, increasing the amplitude of the specific signal (obtained from labelled antigen binding to antibody) relative to the noise (given by reactions in the bulk solution). A mathematical model for this complex system was proposed in Chapter 5 and some preliminary numerical simulations were performed. We were able to plot the biosensor response as a function of the free biotin concentration and we also introduced a method for separating the noise from the total current signal. Constructing analytical and numerical techniques for tracking specific and nonspecific signals in a wider set of problems could also be attempted, which should lead to improved design parameter choices and device optimization.

At our collaborators' suggestion, the computational codes established in this thesis could be combined into a user-friendly computational platform for simulating enzyme-substrate and biomolecular interactions under several fluid dynamics and transduction conditions. The ultimate goal envisaged is to develop a flexible, modular mathematical model which can be used towards a software platform capable of predicting the behaviour of a wide range of electrochemical and optical biosensors. Each module

represents a discrete, definable device subsystem capable of isolated characterisation. The design process would involve selecting a set of modules from which to simulate a system with a specific set of characteristics (such as fluidic or transduction processes, chemical species and labels involved, etc.) Ideally, this simulation would be executed on a personal computer and controlled by the development scientist via a suitable user interface. The design of biosensing devices offers a rich source of mathematical modelling problems and we hope to continue our interdisciplinary collaboration with NCSR/BDI.

Bibliography

[1] E. C. Alocilja, S. M. Radke, *Market analysis of biosensors for food safety.* Biosensors and Bioelectronics Vol 18, Issues 5, pp841-846, 2003.

[2] A. Ambrosi, *The application of nanomaterials in electrochemical sensors and biosensors.* PhD. thesis, Dublin City University, 2007.

[3] R. A. Badley, R. A. L. Drake, I. A. Shanks, A. M. Smith and P. R. Stephenson, *Optical biosensors for immunoassays, the fluorescence capillary-fill device Philos.* Trans. R. Soc. Lond. Ser. B 316, 143-160, 1987.

[4] A. J. Bard and L. R. Faulkner, *Electrochemical methods: fundamentals and applications.* Wiley, New York, 2001.

[5] E. Benjamini, R. Coico and G. Sunshine, *Immunology: a short course.* Published by Wiley, 2000.

[6] J. M. Berg, J. L. Tymoczko and L. Stryer, *Biochemistry.* W.H. Freeman and Company, New York, 2002.

[7] G. E. Briggs and J.B.S. Haldane, *A note on the kinetics of enzyme action.* Biochem. J., 1925.

[8] D. Britz, *Digital simulation in electrochemistry.* Springer-Verlag, New York, 1988.

[9] J. Bowen, A. Acrivos and A. Oppenheim, *Singular perturbation refinement to quasi-steady state approximation in chemical kinetics.* Chem. Engrg. Sci., 18 (1963), pp. 177-188.

[10] T. M. Canh, *Biosensors.* Published by Chapman & Hall and Masson, 1993.

[11] R. Chang, *Physical Chemistry for the biosciences.* University Science Books, 2005.

[12] Edited by J. Cooper and T. Cass, *Biosensors (Practical Approach).* Oxford University Press, 2004.

[13] P. V. Danckwerts, *Continuous flow systems; distribution of residence times.* Chemical Engineering Science, 2(1953), pp, 2-3, 1953.

[14] H. B. Dunford, *Heme Peroxidases.* Wiley-VCH, 1999.

[15] D. A. Edwards, *Estimating rate constants in a convection - diffusion system with a boundary reaction.* IMA Journal of Applied Mathematics (199) 63, 89-112.

[16] D. A. Edwards, *Refining the measurement of rate constants in the BIACORE.* J. Math. Biol. 49, 272-292, 2004.

[17] A. Fersht, *Enzyme Structure and Mechanism.* Published by W.H.Freeman, New York, 1985.

[18] A.C. Fowler, *Mathematical Models in the Applied Sciences.* Published by Cambridge University Press, 1997.

[19] L. Gorton, *Biosensors and Modern Biospecific Analytical Techniques.* Published by Elsevier B.V., 2005.

[20] E.Henry and P. David, *Elementary Differential Equations with Boundary Value Problems.* 4th ed., Prentice Hall, 1999.)

[21] E. I. Iwuoha, M. R. Smyth and M. E. G. Lyons, *Organic phase enzyme electrodes: kinetics and analytical applications.* Biosensors and Bioelectronics Vol 12, No. 1, pp 53-75, 1997.

[22] S. Jones, B. Jumarhon, S. McKee and J.A. Scott, *A mathematical model of a biosensor.* Journal of Engineering Mathematics 30: 321-337, 1996.

[23] B. Jumarhon and S. McKee, *On the Heat Equation with Nonlinear and Nonlocal Boundary Conditions.* Journal of Mathematical Analysis and Applications 190, 806-820 (1995).

[24] K. Karagianni, Y. Liu, A. J. Killard, D. Mackey and M. R. Smyth. *The determination of improved rate constants for enzymes immobilized at an electrochemical sensor interface.*

[25] J. Keener, J. Sneyd, *Mathematical Physiology.* Published by Springer-Verlag, New York, Inc., 1998.

[26] A. J. Killard, S. Zhang, R. Zhao, R. John, E. I. Iwuoha, M. R. Smyth, *Development of an electrochemical flow-injection immunoassay(FIIA) for the real-time monitoring of biospecific interactions.* Anal. Chim.Acta 400 109-119, 1999.

[27] A. Lehninger, *Principles of Biochemistry.* Published by Worth, New York, 1982.

[28] V. Leskovac, *Comprehensive enzyme kinetics.* Published by Kluwer Academic/Plenum Publishers, New York, 2003.

[29] C. C. Lin and L. A. Segel, *Mathematics Applied to Deterministic Problems in the Natural Sciences.* Published by SIAM, 1988.

[30] D. Mackey and A. J. Killard, *Optimizing design parameters of enzyme-channelling biosensors.* Progress in Industrial Mathematics at ECMI 2006, pp. 853–857, Springer, R. Mattheij et al. (editors), 2008.

[31] D. Mackey, A. J. Killard, A. Ambrosi, M. R. Smyth, *Optimizing the ratio of horseradish peroxidase and glucose oxidase on a bi-enzyme electrode: Comparison of a theoretical and experimental approach.* Sensors and Actuators B122 395-402, 2007.

[32] T. Mason, A. R. Pineda, C. Wofsy, B. Goldstein, *Effective rate models for the analysis of transport-dependent biosensor data.* Mathematical Biosciences 159 123-144, 1999.

[33] L. Michaelis and M. Menten, *Die Kinetik der Invertinwirkung.* Biochem. Z., 49(1913), pp. 333.

[34] A. Morrin, A. Guzman, A. Killard, J. Pingarron and M. Smyth, *Characterisation of horseradish peroxidase immobilization on an electrochemical biosensor by colorimetric and amperometric techniques.* Biosensors and Bioelectronics 18(5-6), 715-720, 2003.

[35] H. Motulsky *Analyzing Data with GraphPad Prism.* GraphPad Software, Inc.

[36] A. Rutherford, *Mathematical Modeling: A chemical engineer's perspective.* by Acdemic Press, 1999.

[37] L. A. Segel, *Simplification and Scaling.* SIAM Rev., 14 (1972), pp. 547-571.

[38] P. A. Serra, *Biosensors for Health, Environment and Biosecurity.* Published by InTech, ISBN 978-953-307-443-6, 2011.

[39] V. Sikavitsas, J. M. Nitsche, and T. J. Mountziaris, *Transport and Kinetic Processes Underlying Biomolecular Interactions in the BIACORE Optical Biosensor.* Biotechnol. Prog. 18, 885-897, 2002.

[40] F. Scheller and F. Schubert, *Biosensors.* Published by Akademie Verlag licensed edition for Elsevier Science Publishers B.V., 1992.

[41] J. W. Thomas, *Numerical Partial Differential Equations: Finite Difference Methods.* Spinger-Verlag New York, Inc, 1995.

[42] A. P. F. Turner, I. Karube and G. S. Wilson, *Biosensors: Fundamentals and Applications.* Oxford University Press, Oxford, 1987.

[43] J. Wang, *Analytical Electrochemistry.* Second Edition, Wiley-VCH, 2000.

[44] Q. Wang, *Mathematical methods for Biosensor models.* PhD. thesis, Dublin Institute of Technology, 2011.

[45] L. F. Whiting and P. W. Carr, *J. Electroanal.* 1977.

[46] D. Wild, *The Immunoassay Handbook.* Published by Elsevier, 2005.

[47] J. S. Wilson, *Sensor technology handbook, Volume 1.* Published by Elsevier Inc., 2005.

[48] M. Wright and A Chorin, *Mathematics and Science.* National Science Foundation, USA, 1999.